# Self-assembled styrene based alternating copolymer nanotubes: modeling and experiment

by Thomas Dominic Lazzara

*A thesis submitted to the Faculty of Graduate Studies and Research of McGill University in partial fulfillment of the requirements of the degree of Master of Science.*

August 2007
Department of Chemistry, McGill University
Montreal, Quebec, Canada

Library and
Archives Canada

Published Heritage
Branch

395 Wellington Street
Ottawa ON K1A 0N4
Canada

Bibliothèque et
Archives Canada

Direction du
Patrimoine de l'édition

395, rue Wellington
Ottawa ON K1A 0N4
Canada

*Your file Votre référence*
*ISBN: 978-0-494-51299-9*
*Our file Notre référence*
*ISBN: 978-0-494-51299-9*

NOTICE:
The author has granted a non-exclusive license allowing Library and Archives Canada to reproduce, publish, archive, preserve, conserve, communicate to the public by telecommunication or on the Internet, loan, distribute and sell theses worldwide, for commercial or non-commercial purposes, in microform, paper, electronic and/or any other formats.

The author retains copyright ownership and moral rights in this thesis. Neither the thesis nor substantial extracts from it may be printed or otherwise reproduced without the author's permission.

AVIS:
L'auteur a accordé une licence non exclusive permettant à la Bibliothèque et Archives Canada de reproduire, publier, archiver, sauvegarder, conserver, transmettre au public par télécommunication ou par l'Internet, prêter, distribuer et vendre des thèses partout dans le monde, à des fins commerciales ou autres, sur support microforme, papier, électronique et/ou autres formats.

L'auteur conserve la propriété du droit d'auteur et des droits moraux qui protège cette thèse. Ni la thèse ni des extraits substantiels de celle-ci ne doivent être imprimés ou autrement reproduits sans son autorisation.

In compliance with the Canadian Privacy Act some supporting forms may have been removed from this thesis.

While these forms may be included in the document page count, their removal does not represent any loss of content from the thesis.

Conformément à la loi canadienne sur la protection de la vie privée, quelques formulaires secondaires ont été enlevés de cette thèse.

Bien que ces formulaires aient inclus dans la pagination, il n'y aura aucun contenu manquant.

Canada

Two roads diverged in a wood, and I-
I took the one less traveled by,
and that has made all the difference.
*Robert Frost*

# Thesis abstract
# Résumé de la thèse

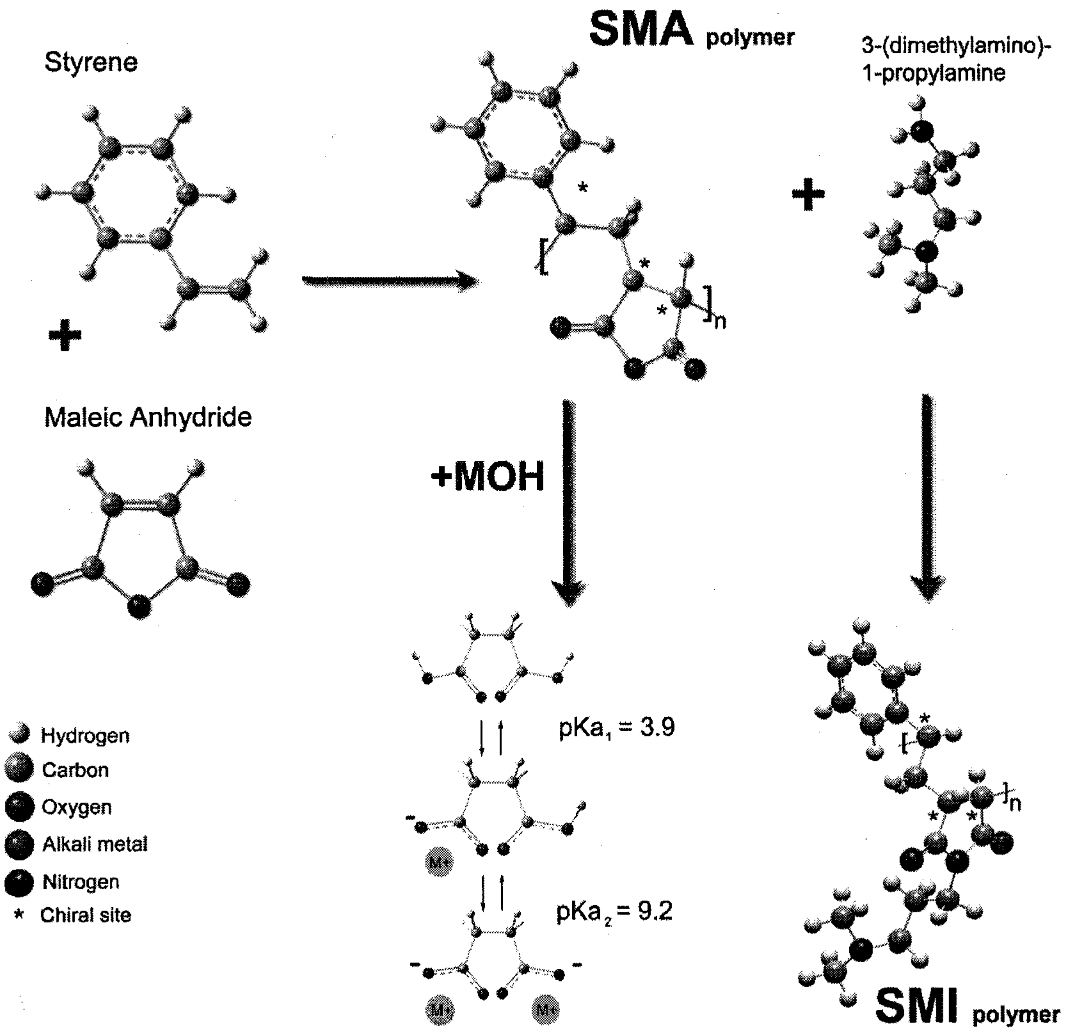

## Self-assembled styrene based alternating copolymer nanotubes: modeling and experiment

The structure and association behaviour of poly(styrene-alt-maleic anhydride) (SMA) and poly(styrene-alt-N,N-dimethylpropylamide) (SMI) polymers were studied using molecular modeling. The conformational studies were carried out at a semi-empirical PM3 level. SMA and SMI polymers were found to associate into nanotubes. These nanotubes have primary, secondary and tertiary structures. The primary structure is the conformation the polymer takes depending on the degree of protonation and its chirality. The secondary structure is the association of many polymers to form a nanotube structure. The tertiary structure is a higher order aggregation between the nanotubes.

These nanotubes are formed from a minimum of 8 polymers and have lengths varying from one to many polymer contour lengths. The shape and the size of the nanotubes vary with the choice of styrene based alternating copolymer. These structures were observed experimentally in aqueous solution. The degree of protonation was controlled using dialysis. The nanostructures were experimentally observed and the sizes measured agreed with the theoretically predicted secondary and tertiary structures.

## Nanotubes par l'entremise de l'association entre polymères alternés à base de styrène : théorie et expérimentation

La structure et le mécanisme d'association entre les polymères poly(styrène-alt-anhydride maléique) (SMA) et poly(styrène-alt-N,N-diméthylpropylamide) (SMI) ont été étudiés par l'entremise de la modélisation moléculaire. L'étude de la conformation des polymères a été effectuée au niveau semi-empirique avec la méthode PM3. Il a été déterminé que les polymères SMA et SMI sont capables de s'associer pour former des nanotubes. Ces nanotubes ont une structure primaire, secondaire et tertiaire. La structure primaire est définie comme étant la conformation du polymère qui varie selon son degré de protonation et de sa chiralité. La structure secondaire représente l'association de plusieurs polymères pour former des nanotubes. Finalement, la structure tertiaire est définie comme étant l'agrégation entre plusieurs nanotubes de polymère.

Les nanotubes sont formés d'un minimum de 8 polymères et peuvent croître de façon linéaire par l'addition de polymères aux extrémités. La longueur des nanotubes peut varier de un a plusieurs multiples de la longueur d'un polymère. La taille et la forme des nanotubes varient en fonction du choix du polymère alterné contenant le co-monomère de styrène. Ces nanotubes ont été observés expérimentalement en solution aqueuse. Le degré de protonation a été contrôlé par l'utilisation de la dialyse. Des techniques expérimentales ont permis d'observer ces nanostructures et les dimensions mesurées correspondent aux tailles prédites théoriquement pour les structures secondaires et tertiaires.

# Acknowledgements

*The author gratefully acknowledges the assistance*
*provided by the following contributors:*

I would like to express my gratitude to Prof. M.A. Whitehead and Prof. Theo G.M. van de Ven for their supervision, guidance and dedication to this research effort.

Dr. Jurek Petlicki, (Pulp and Paper Research Centre, McGill University) for his help with light scattering studies, titration experiments and for his scientific advice, criticism, valuable ideas and discussions.
Marta Kocun, Dr. Rolf Schmidt and Dr. Louis Cuccia, (Department of Chemistry and Biochemistry, Concordia University) for their help with atomic force microscopy studies.
Renata Vyhnalkova, (Department of Chemistry, McGill University) for her help with electron microscopy studies.
Dr. Tony Azzam, (Department of Chemistry, McGill University) for his help in polymer synthesis and transmission electron microscopy studies.
Gilles Bourret and Dr. Bruce R. Lennox, (Department of Chemistry, McGill University) for their help with gold chemistry experiments and valuable scientific discussions.
Dr. Grazyna Wilczek for giving me the opportunity and challenge of a teaching assistantship in the instrumental analysis course.
Sigma Xi, The Scientific Research Society, for their Grand-in-Aid of Research, which was used to purchase a new sample vat for the light scattering instrument.
Rami Hourani for his moral support during the last years, which helped me trough rough times.

Finally, I would like to thank Prof. M.A. Whitehead and Prof. Theo G.M. van de Ven for believing in me and helping me believe in myself. These Professors put their trust in me, when others didn't and for this, I shall always remember them.

To all those who did not believe in me, well that's alright, its now water under the bridge and I am moving on to better things. I also thank all my Otto Maass and Pulp and Paper friends, for those days that their presence cheered me up and made it all worthwhile.

I would also like to thank my parents and my sister for their support, their unconditional love and for teaching me that life is not about personal gain.

And, above all, I wish to thank Marta Kocun for faithfully standing by me through good times and bad times, for her encouragement, her patience with my moody attitude and for all those times she pushed me to go beyond what I though I was capable of. Thanks!

# Table of contents

Section page

# Table of contents

# List of symbols and abbreviations

## List of symbols and variables

| | |
|---|---|
| 2D | Two dimensional |
| 3D | Three dimensional |
| $\alpha$ | polarizability |
| $\mathbf{C}$ | Atomic orbital coefficient matrix |
| $\chi$ | Flory-Huggins parameter |
| $C_{ij}$ | Matrix element of the molecular orbital coefficient matrix |
| $d$ | distance between electrostatic elements |
| $D$ | Optimizable parameter in AM1 method |
| $D_R$ | Rotational diffusion coefficient |
| $D_T$ | Translational diffusion coefficient |
| $\Delta G$ | Change in Gibbs Free Energy |
| $\Delta H$ | Change in Enthalpy |
| $\Delta S$ | Change in Entropy |
| $\nabla$ | Laplace Operator |
| $dV$ | Space element (dx dy dz) |
| $e$ | Elementary charge |
| $E$ | Optimizable parameter in AM1 method |
| $\varepsilon_0$ | dielectric constant of vacuum |
| $\mathbf{E}$ | Energy eigenvalue matrix |
| $E_{AA}$ | Interaction energy between block A and A of AB block copolymers |
| $E_{AB}$ | Interaction energy between block A and B of AB block copolymers |
| $E_{BB}$ | Interaction energy between block B and B of AB block copolymers |
| $E_{electronic}^{HF}$ | Hartee Fock electronic energy |
| $E_{electronic}^{Roothaan}$ | Roothaan electronic energy |
| $E_{experimental}$ | Experimental energy |
| $E_{I\text{-}I}$ | Ion-Ion interaction energy |
| $E_{I\text{-}Pd}$ | Ion-Permanent dipole interaction energy |
| $E_{Id\text{-}Id}$ | Induced dipole – Induced dipole interaction energy |
| $E_{Pd\text{-}Pd}$ | Permanent dipole – Permanent dipole interaction energy |
| $E(r)$ | Energy of polymer association at inter-polymer distance $r$ |
| $E(r \rightarrow \infty)$ | Energy of polymer association at a separation beyond interaction |
| $E_{stabilization}$ | Stabilization energy |
| $\xi$ | Electronic energy |

# List of symbols and abbreviations

| | |
|---|---|
| eV | Electronvolt |
| $\mathbf{F}$ | Fock matrix |
| $\mathbf{F}_{ts}$ | Fock matrix element |
| $G_{\underline{assoc}}$ | Gibbs free energy of associated polymer dimer |
| $G_{opt}$ | Gibbs free energy of unassociated polymer |
| $g^1(q,\tau)$ | First order auto-correlation function |
| $g^2(q,\tau)$ | Second order auto-correlation function |
| $\Gamma$ | Force fitted decay frequency |
| $h$ | Planck's constant |
| $\eta$ | Viscosity |
| $H_{\underline{assoc}}$ | Enthalpy of associated polymer dimer |
| $H_{opt}$ | Enthalpy of unassociated polymer |
| $\hat{H}_{eff}$ | Effective electronic Hamiltonian |
| $\hat{H}_{electronic}$ | Electronic Hamiltonian |
| $\hat{H}_{total}$ | Total Hamiltonian |
| $\mathbf{H}_{\mu v}$ | 1-electron integral |
| $I\ (t)$ | Ensemble average of the light scattering intensity at time $t$ |
| $I\ (t+\tau)$ | Ensemble average of the light scattering intensity delayed by a time $\tau$ |
| $\hat{J}_{ij}$ | Coulomb operator |
| $k$ | Boltzmann constant |
| $\hat{K}_{ij}$ | Exchange operator |
| kJ | Kilojoule |
| kV | Kilovolt |
| $\zeta$ | Orbital exponent in STO |
| L | Litre |
| $\mu$ | Dipole moment |
| $M_w$ | Molecular Weight |
| $m'$ | Mass of electron |
| $m$ | Number of dimension in atomic orbitals |
| mL | Millilitre |
| mW | MilliWatt |
| µL | Microlitre |
| mol | Mole |
| N | Number of Nuclei |
| n | Number of electrons |
| nm | Nanometer |

# List of symbols and abbreviations

| | |
|---|---|
| r | Racemic |
| $r$ | inter-polymer distance |
| $r'$ | inter-phenyl distance |
| $R_H$ | Hydrodynamic radius |
| $\rho$ | Atomic orbital ($m$-dimensional) |
| q | Scattering vector |
| s | Meso |
| **S** | Overlap matrix |
| $\mathbf{S}'_{\mu v}$ | Overlap integral |
| $\tau$ | Time delay |
| W | Watt |
| $\lvert\psi\rangle$ | Wavefunction for $N$ nuclei and $n$ electrons |
| $\lvert\psi_{electrons}\rangle$ | Electronic wavefunction |
| Z | Valency |
| $Z_\alpha$ | Nuclear charge |

## List of abbreviations

| | |
|---|---|
| AFM | Atomic Force Microscopy |
| AM1 | Austin Model 1, analogue of MNDO |
| BNNT | Boron Nitride Nanotube |
| CVD | Chemical Vapour Deposition |
| DFT | Density Functional Theory |
| DLMO | Delocalized Molecular Orbital |
| DLS | Dynamic Light Scattering |
| FEMR | Facilities for Electron Microscopy Research |
| GTO | Gaussian Type Orbital |
| H-bond | Hydrogen Bond |
| HF | Hartree-Fock |
| INDO | intermediate neglect of differential overlap model |
| MINDO/3 | modified INDO |
| MNDO | modified neglect of diatomic overlap |
| MWNT | Multi-Wall Carbon Nanotube |
| NDDO | neglect of diatomic differential overlap model |
| NDO | complete neglect of differential overlap |

# List of symbols and abbreviations

| | |
|---|---|
| PM3 | Third Parametrization of MNDO and AM1 |
| RAFT | Radical Addition Fragment Transfer |
| SCF | Self-Consistent Field |
| SMA | poly(styrene-alt-maleic anhydride) |
| SMI | poly(styrene-alt-N,N-dimethylpropyl amide) |
| STO | Slater Type Orbital |
| SWNT | Single Wall Carbon Nanotbue |
| TEM | Transmission Electron Microscopy |
| ZDO | zero differential overlap |

# Introduction to polymer self-assembly, polymer nanotubes, and experimental methods

# Chapter I

## 1. Scope of the thesis

This thesis describes the preparation and characterization of polymeric nanotubes from poly(styrene-alt-maleic anhydride) (SMA) and poly(styrene-alt-N,N dimethyl propyl amide) (SMI).

Chapter I introduces polymer self-assembly and reviews organic nanotube systems in the literature, followed by the theoretical and experimental tools used to characterize polymer nanotubes. Chapter II extends the theoretical modeling of the association properties of SMA in solution, initiated by Malardier[1]. Chapter III covers the synthesis of a highly alternating SMA polymer and describes an improved method to prepare SMA nanotubes, which provides a higher yield of SMA nanotubes. Different factors governing nanotube formation were investigated: the type of base used, the molecular weight of SMA used and the ionic strength of the solution.

Thiol chemistry with the noble metals silver and gold is described in Chapter IV. The synthesized SMA polymer was modified so as to be thiol terminated. Gold and silver nanoparticles stabilized with SMA were prepared. The possibility to prepare metal nanowires was investigated and preliminary results are discussed.

The theoretical investigation of an SMA derivative, where the maleic anhydride is functionalized to a maleimide (SMI) is presented in chapter V. The effect of polymer chirality becomes crucial when studying the association of maleimide polymers. Chiralities that lead to linear structures were determined and the association between SMI polymers investigated. In Chapter VI, a mechanism of association between SMI polymers, which leads to nanotubes was suggested and the predicted nanostructures experimentally observed. The sizes and the yield agree with the results from the theoretical investigation. In Chapter VII, general conclusions are presented. Ideas for future work are presented along with potential applications for these polymer nanotube systems.

## 2. Introduction to polymers

Staudinger introduced the term *Macromolecüle* in 1924 to describe molecules of high molecular weight, which he considered to be giant chainlike molecules. A *polymer* is a large molecule (*macromolecule*) built from many (poly = many) smaller covalently bonded molecules called *monomers* (meros = parts).

Polymers are present in biological systems; cellulose, starch, DNA and proteins are natural polymers. However, the first true synthetic polymer was created in 1907 from phenol and formaldehyde by Baekeland, which he named Bakelite[2]. The science of synthetic polymer making has since developed to control the properties of the polymers synthesized by designing the monomer composition, the polymer length and its stereo-regularity. These macromolecules can be made of one repeating monomer, in which case the polymer is called a *homopolymer*, or they can be composed of two or more types of monomers, in which case the polymer is called a *copolymer*.

Homopolymers do not vary in composition, only in chain length, and the chiralities of the atoms involved in the covalent bonds between monomers, are variable. The length of the polymer chain is given by the molecular weight ($M_w$) of the polymer. The distribution of chiralities along the polymer chain usually varies randomly unless it is controlled and such polymers are called atactic polymers. If the polymerization is controlled, such as by polymerization methods introduced by Ziegler and Natta[3-6], the polymer can be isotactic when the chiralities are all identical or syndiotactic when the chiral sites alternate regularly (Figure 1).

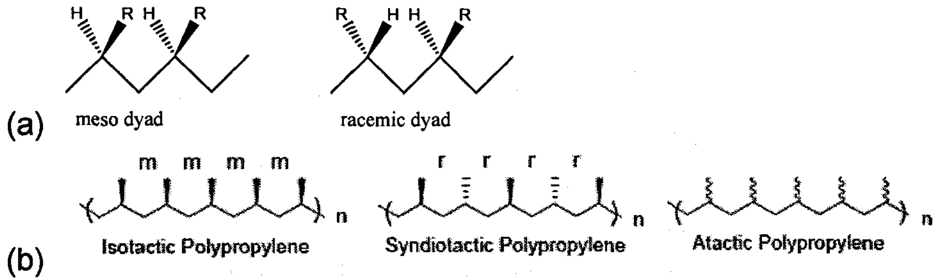

Figure 1: (a) illustration of meso (m) and racemic (r) dyads (b) Structure of stereoregular polymer and non-stereoregular.

Copolymers[7,8] on the other hand, when prepared from bifunctional monomers, can be further subdivided into four main categories. These categories depend on the monomer distribution of the polymer. When the monomer distribution is essentially regulated by the individual monomer reactivities, which are not very different, the distribution is random and the polymer is called a *statistical copolymer*. When the reactivity ratios are very different, the monomer distribution is alternating and the polymer is called an *alternating copolymer*. Modifications of the monomers of a polymer, by covalently bonding other molecules to the polymer, as branches create polymers called *graft copolymers*. The last type of monomer distribution is composed from substantial sequences of each repeat unit and is called a *block copolymer*. If a specific number (x) of monomer sequences are present in segregated parts, the polymer is called a *x-block copolymer*. Figure 2 shows a schematic representation of the types of copolymers described above. Copolymers also have the same varying properties as homopolymers: they vary in molecular weight and stereoregularity[9,10].

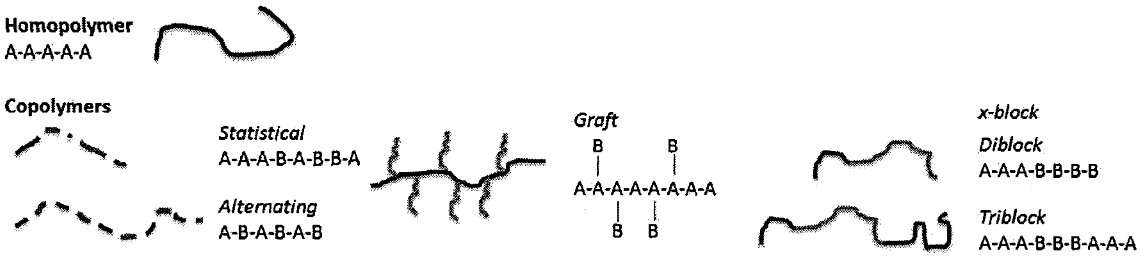

Figure 2: Schematic representation of the different classes of polymers according to their monomer sequences.

## 3. Introduction to Self-assembly

In recent years nanotechnology has generated interest in self-assembled structures. Self-assembly is essentially the fabrication of nanostructures from ordered weak, non-covalent interactions, between molecules. Large, well defined systems result from these weak interactions between molecules. Self-assembly occurs because of attractive and repulsive interactions, which can be divided into three classes:

(a) **Hydrogen bonding**: *electronic exchange between Hydrogen and negatively charged atoms*
(b) **Coulomb interactions**: *between electrostatic charges, permanent dipoles, quadrupoles*
(c) **Van der Waals interactions**: *from induced polarization by neighbouring molecules*

### 3.1. Hydrogen bonding

Covalently bonded Hydrogen atoms to electronegative atoms such as N-F, N-H or O-H systems are electron deficient and will interact with the lone electron pairs on other electronegative atoms (N, O, F). The group providing the H atom is termed the *H-bond donor* and the atom providing the lone pair is a *H-bond acceptor.* Hydrogen bonds energies are typically between 5-60 kJ/mol[11,12] and are strongest between a strong donor such as HF and a strong acceptor such as $NH_3$. Hydrogen bonds are also directional[11] and occur at either 0° or 60° (Figure 3). The typical distance for a Hydrogen bond varies between 2.5 Å for strong H-bonds to 5 Å for weak ones. The strength of a Hydrogen bond is also dependent on the solvent used because polar solvents tend to decrease the bond strength. The directionality of these interactions provides a method to fabricate well defined structures by controlling the structure of interacting molecules.

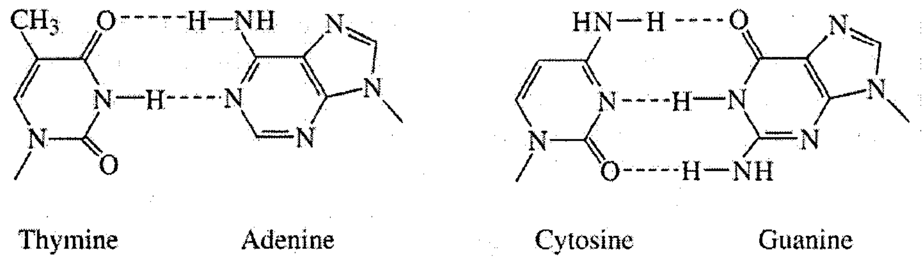

Figure 3: Hydrogen bond interactions in DNA nucleotide bases.

### 3.2. Coulomb interactions

Coulomb interactions originate from the interaction between static molecular charges and are either repulsive or attractive. Static molecular charges can be either ions (*I*) or permanent dipoles (*Pd*).

The electrostatic interaction between two ions (1,2) can be described by Eq. (1), where *E* is the electrostatic energy, *Z* is the valency, $e$ is the elementary charge, $\varepsilon_0$ is the dielectric constant in vacuum and *d* is the separation between charges.

$$E_{I-I} = \frac{(Z_1e)(Z_2e)}{4\pi\varepsilon_0 d} \qquad (1)$$

The ion – permanent dipole (*I-Pd*) interaction energy is given in Eq. (2), where $cos\theta$ is the angle between the two centres and the axis of the dipole and $\mu$ is the dipole moment.

$$E_{I-Pd} = \frac{(Ze)\,\mu cos\theta}{4\pi\varepsilon_0 d^2} \qquad (2)$$

The permanent dipole – permanent dipole (*Pd-Pd*) interaction energy is given in Eq. (3), where *C* is a constant that depends on the relative orientation between the two dipoles.

$$E_{Pd-Pd} = \frac{C\,\mu_1\mu_2}{4\pi\varepsilon_0 d^3} \qquad (3)$$

Ion – ion interactions in self-assembled systems can be observed in polyelectrolyte multilayers obtained by electrostatic layer-by-layer deposition techniques. A charged polymer, a polyelectrolyte, is dissolved in solution and an oppositely charged surface is dipped into the solution. The polyelectrolyte covered surface is rinsed and dipped in another oppositely charged polyelectrolyte solution. Well defined alternating charged polymer layers can be achieved by this technique. The multilayer systems are then sensitive to pH and ionic strength.

In some case, the dipole moment is null, but a quadrupole moment is present. Interactions between quadrupole moments can cause molecules to form ordered complexes. These interactions are usually between aromatic molecules and are often encountered in self-assembled systems and referred to as π-stacking[13-19] but are coulombic in origin[20]. Hexafluorobenzene interacts with benzene to form a stabilized parallel stacked complex because the quadrupole moment of $C_6F_6$ is roughly equal to that of $C_6H_6$ but of opposite sign, while benzene can form dimers of different stabilizing geometries such as displaced parallel, T-shaped and staggered (Figure 5). Benzene derivativatized with a long alkyl chain can self-assemble on graphite surfaces and form ordered monolayers of uniformly stacked molecules consequently the interaction of the aromatic moiety with the aromatic groups of the graphite[21]. This is also the reason why polycyclic aromatic hydrocarbons are considered as potential materials for electronics: these large disk shaped molecules can form ordered stacks by π-stacking of aromatic groups, and can be patterned onto surfaces[22]. π-stacking complexes have stabilization energies ranging from 7.5 – 25 kJ/mol, depending on the type of functional groups present on the aromatic molecules [13,15,16,23].

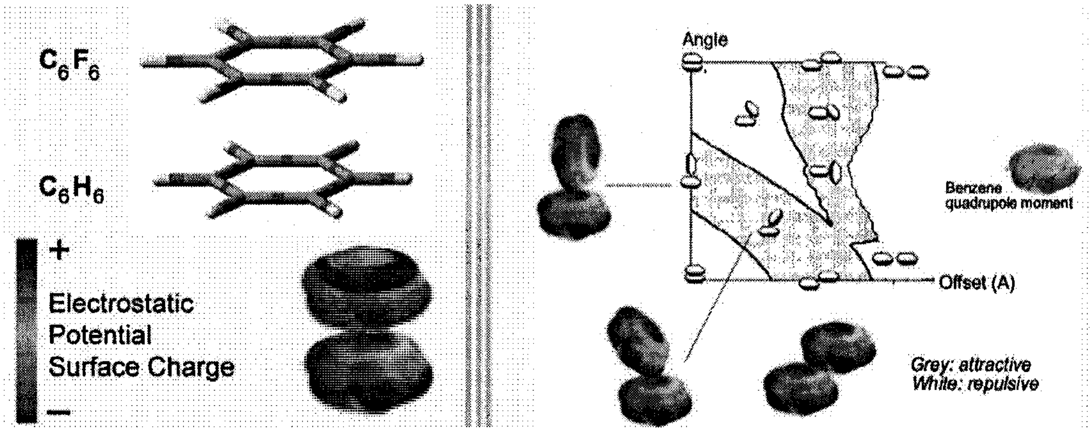

Figure 5: Coulomb interactions in aromatic systems due to quadrupole moments. Interaction of hexafluorobenzene with benzene where regions of positive and negative electrostatic potential are of opposite signs (left) and benzene dimer conformations (right) from x-ray crystallography of phenylalanine[13,15,16]. These interactions are commonly referred to as π-stacking.

### 3.3. Van der Waals interactions

Van der Waals interactions between molecules arise from an instantaneous polarization induced by neighbouring molecules. Two different interactions are possible: permanent dipole – induced dipole (*Pd-Id*) and induced dipole – induced dipole (*Id-Id*).

The permanent dipole – induced dipole interaction energy is described by Eq. (4), where $\alpha$ is the polarizability of the two dipoles (1,2).

$$E_{Pd-Id} = \frac{\alpha_1 \mu_2^2}{(4\pi\varepsilon_0)^2 d^6} \tag{4}$$

The induced dipole – induced dipole interaction is also known as London dispersion force and its energy is described by Eq. (5), where $h$ is Planck's constant, $v$ is the characteristic vibration frequency of the electrons.

$$E_{Id-Id\ attractive} = -\frac{2h}{3}\left(\frac{v_1 v_2}{v_1+v_2}\right)\frac{\alpha_1\alpha_2}{(4\pi\varepsilon_0)^2 d^6} \tag{5}$$

The attractive terms given in Eq. 4 and 5 are also accompanied by a repulsive term that accounts for strong steric repulsion between molecules at close distances. This term is given in Eq. (6), where $\in$ is a pre-exponent.

$$E_{Id-Id\ repulsive} = \in d^{-12} \tag{6}$$

The combination of the two *Id-Id* terms leads to the familiar Lennard-Jones (6-12) potential used to model van der Waals forces.

## 4. Self-assembly of block copolymers

The most common polymeric self-assembled systems encountered are from block copolymers self-association. Diblock copolymer self-assembly are well studied systems[7]. These are typically designed to have a short hydrophilic block compared to the hydrophobic block segment. The two blocks interact differently with the choice of a polar or non-polar solvent. Self-association in organic solvents is usually exothermic, and therefore enthalpy driven ($\Delta H$), while the association in aqueous environments is endothermic and entropy driven ($\Delta S$). Self-assembly of these systems tends to increase the favourable solvent-polymer interactions and decrease the unfavourable ones. This leads to hydrophobic phase segration in aqueous solvents, and the reverse in organic solvents, and explains the formation of diblock copolymer micelles in solution. However, by controlling the organic/water mixture used to dissolve diblock copolymers, the shape of the association can be modified, similar as for surfactants (Figure 6). Parameters such as temperature, salts and ionic strength can modify the curvature of polymer morphologies. The phase separation is determined by the Flory-Huggins ($\chi$) thermodynamic parameter that describes the segment-segment interaction: Eq. (7), where $E_{AA}$, $E_{BB}$ and $E_{AB}$ are interaction energies between the blocks A and B [24].

$$\chi = \frac{\left[E_{AB} - \frac{1}{2}(E_{AA} + E_{BB})\right]}{k_b T} \tag{7}$$

The Flory-Huggins parameter is directly related to the Gibbs Free Energy of mixing. If the term is negative, phase separation does not occur and the system is homogeneous. When $\chi > ½$, phase separation is observed and different morphologies are possible (Figure 6). Triblock copolymer have a greater morphological complexity and can form vesicles and hollow nanotubes[25] which are not possible with diblock copolymers. Triblock copolymer self-association is not as well understood as diblock copolymers[26].

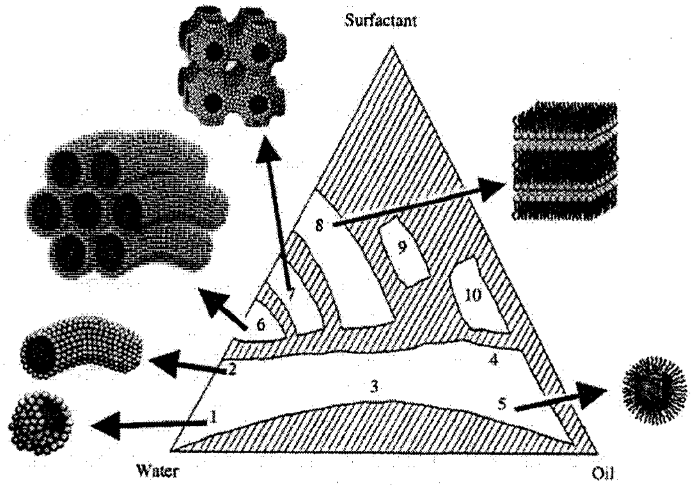

Figure 6: Schematics of a surfactant-water-oil phase diagram [27]; diblock copolymers exhibit similar self-assembly. 1.Spherical micelles 2.Rod-like micelles 3.Irregular bicontinuous phase 4.Reverse cylindrical micelles 5.Reverse micelles 6.Hexagonal phase 7.Cubic phase 8.Lamellar phase 9.Reverse cubic phase 10.Reverse hexagonal phase

Homopolymers do not self-assemble spontaneously into ordered structures, because their structure does not have dissimilar segments, which would allow ordered phase segregation, as in diblock copolymer nanostructures. However, when tailored with functional end-groups such as thiols, carboxylic acids or aromatic substituents, the polymers can organize into ordered monolayers on functional surfaces. Thiol–gold interactions for example can guide the ordered deposition of polymers onto a surface to form Self-Assembled Monolayers (SAM) of alkyl chain polymers[28-30]. Carbolylic acids are known to stabilize gold, silver and copper nanoparticles[31]. Aromatic substituents can interact between each other through coulomb interactions and order the polymers into patterns on surfaces[32].

Other copolymers such as alternating, statistical and graft copolymers behave similarly to homopolymers in their ability to self-assemble by tailoring the end groups, but do not phase segregate as block copolymers do.

## 5. Self-assembled nanotubes

The general description of nanotube structures is a hollow curved architecture with a diameter in the nanometer range with unbound length. Nanotubes have generated much interest because of their nanometer sizes, elongated shape and hollow interior. These properties have been a research subject in a diversity of fields, which try to develop new structures or modify and apply these structures to improve current technology. Doping the inside of a semi-conducting nanotube can lead to conductive nanowires. Drug delivery has been investigated using carbon nanotubes as carriers for drugs and the targeted delivery of these compounds. Similar to

Tinkertoys of molecular size, nanotubes can be used as a frame for the addition of chemicals, molecules or even metals[33] that can provide specific property structures or direct the structures towards selected targets. This tailoring of nanostructures allows the development of high performance materials and new diagnostic tools to treat diseases.

The first type of nanotubes were produced by Radushkevich and Lukyanovich who published, in the Russian Journal of Physical Chemistry, images of 50 nm diameter carbon tubes[34]. Most people however, associate their discovery to Sumio Iijima of NEC in 1991[35] and since then, their discovery resulted in many publications in this area. Carbon nanotubes are cylindrical molecules with a diameter as small as 1 nm and lengths that can exceed one μm. They are composed of carbon atoms only and can be thought of as a sheet of graphite that has been wrapped into a cylinder. Single wall carbon nanotubes (SWNT) are of similar size to zeolites, about 1 nm in diameter, and exist in single nanotubes or multi-walled carbon nanotubes (MWNT), which are different diameter nanotubes concentrically wrapped around each other. Their diameter varies from 1 – 50 nm. They can be described by the folding of a graphite sheet, one carbon atom thick, into a nanotube [36]. SWNT have electrical conducting properties not observed in MWNT. Depending on how the graphite sheet is folded along the **$C$** axis, Figure 7, where **T** is the nanotube axis and $\boldsymbol{a_1}$ and $\boldsymbol{a_2}$ are the unit vectors of the graphene sheet in real space. Variations in the folding $C_h$ axis leads to metallic conducting or semi-conducting nanotubes; only nanotubes with $(n,m) \rightarrow n-m=3i$ with $i$ as an integer are metallic.

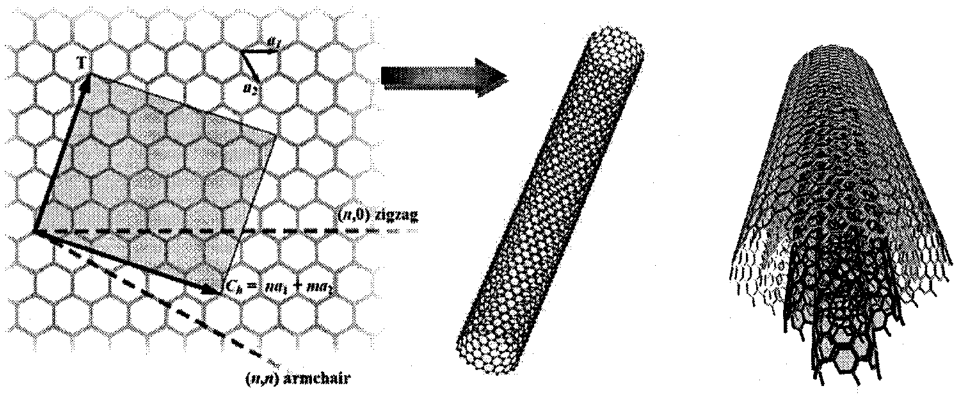

Figure 7: Schematic[36] of a graphene sheet folding to form SWNT (left). Also shown, are multi-walled[37] carbon nanotubes (right).

Single walled Carbon nanotubes are the smallest size individual tubes known. Recently, metal catalysis has been used to synthesize SWNT by chemical vapour deposition (CVD). At high temperatures, 500-1000°C, hydrocarbon gas flows through a reactor tube where the transition metal catalytic species ($Fe_2O_3$ nanoparticles) are supported on large surface area alumina materials, from which the nanotubes grow[38]. CVD methods can control the growth direction relying on the van der Waals forces between growing tubes and applied electrical fields, which also controls the diameter of the SWNT fabricated.

Boron nitrite nanotubes (BNNT) are structurally similar to carbon nanotubes and the bonds have ionic character. A number of studies predicted BNNT bandgaps that are independent of chirality, number of shells, diameter and similar mechanical properties to carbon nanotubes[39-46], but BNNTs also to exhibit piezoelectricity. BNNT can therefore be used in applications requiring uniform electronic properties. Multi-walled boron nitrite nanotubes, about 50 nm in diameter, were found to reversibly change from insulators to semi-conductors through bending deformations[47]. These nanotubes may find applications such as nanoscale sensors and actuators.

Naturally occurring nanotubes are present in living organisms and help fulfill a range of different tasks, from being building block for larger organized structure to being used as transport devices for molecules. Microtubules are rigid rods of approximately 25 nm diameter with a hollow core[48]. These naturally occurring nanotubes are the third principle component of the cytoskeleton in living cells. These structures are composed of a single type of globular protein, called tubulin. Tubulin is formed from two poly(peptides) of 55,000 Da molecular weight: α-tubulin and β-tubulin. Tubulin dimers polymerize to form a microtubule made from 13 linear protofilaments, which are composed of head-to-tail tubulin dimer arrays and arrange in parallel. The protofilaments then assemble around a hollow core forming a peptide nanotube (microtubule, Figure 8). The microtubules are also self-assembled systems because they continually assemble and disassemble in the cellular environment. Other biological components also this type of microtubules as part of their structure such as the flagellum of bacteria[49-51]: *E.coli* and *Salmonella* for example. The structure is a complex arrangement of microtubules held together by different proteins (Figure 8).

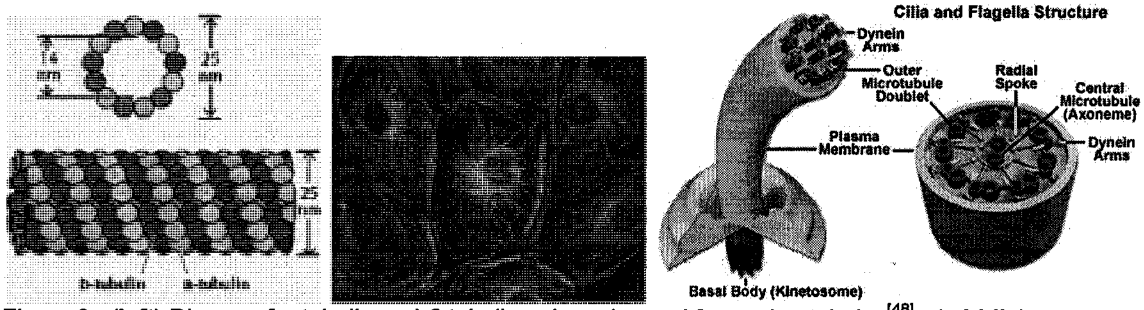

Figure 8: **(left)** Dimers of $\alpha$-tubulin and $\beta$-tubulin polymerize and form microtubules[48]. **(middle)** Microtubules radiate (green staining) within the cytoplasm of living cells[52]. **(right)** Bacteria flagellum microstructure showing a complex arrangement of microtubules[53].

Lower molecular weight peptides have also been shown to self-assemble into smaller diameter ordered nanotube structures[54-66] by two general association paths. For cyclic polypeptides (Figure 9), the association occurs by stacking of the cyclic molecules, which are held together by Hydrogen bonds between the urea groups and the amide ones. The cyclic peptides have an equivalent amount of chiral L and D amino acids, which adopt a flat ring-shaped conformation, and are composed of 6, or more, amino acids because the steric strain prevents smaller units. The alternating between D and L chiralities, provides complementary Hydrogen bond donor and acceptors on each face of macrocyle. The size depends on the number of amino acids present, and their sequence. The Hydrogen bonding in these systems is strongest when the cyclic peptides are stacked anti-parallel. The nanotubes formed from these vary between 5 and 15 nm in diameter, and can reach a µm in length. These nanotubes are usually observed as stacks of closely packed nanotubes. The arrays are held together by inter-tube Hydrogen bonds and van der Waals forces. Cyclic peptides[57] such as c-[(Gln-D-Ala)$_4$-], c-[(Gln-D-Val)$_4$-], c-[(Gln-D-Leu)$_4$-], c-[(Gln-D-Phe)$_4$-] were shown to form nanotubes, Figure 9, and the ensembles of nanotubes were observed as 200 nm x 10 µm needles. Other cyclic peptides such as c-[(L-Trp-D-Leu)$_3$-L-Gln-D-Leu][59], c-[L-Gln-D-Ala-L-Gln-D-Ala)$_2$-][67] and c-[(D-Ala-Gln-D-Ala-Gln)$_2$-][54] also have been shown to form nanotube structures of similar sizes. The smallest diameter peptide nanotubes measured has an outer radius of approximately 0.8 nm and an inner diameter of 0.5 nm, and is self-assembled from a peptide macrocycle incorporating 1,2,3-triazole $\epsilon$-amino acids[58]. Assembling of different peptides, with specific functional groups, that extend from the macrocycle, can allow additional attractive interaction between the cyclic peptides of a same tube, or between tubes. Designing a cyclic peptide with phenyl substituents allows a stronger binding of the top and bottom cycles because of a $\pi$-stacking interaction (T-shape: edge-to-face). Complementary Hydrogen bond donors and acceptors allow nanotubes to stack parallel to each other and form bundles.

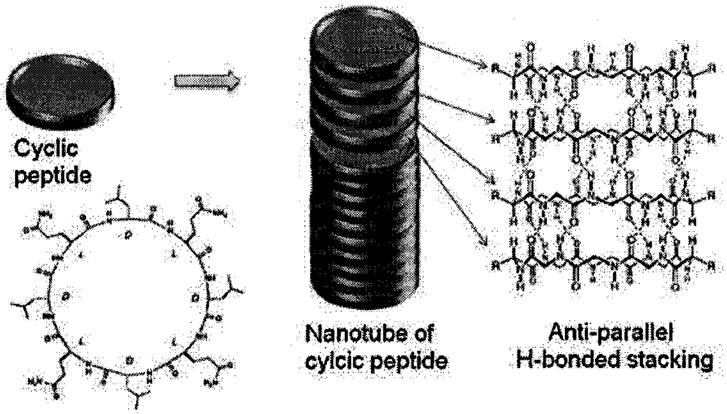

Figure 9: General mechanism of association observed in cyclic peptide nanotubes. *Structures reproduced from* [57]

Non-cyclic peptides have also been shown to form nanotubes[55,60-62] through equilibrium between the gain in enthalpy of forming Hydrogen bonds and the gain in entropy from associating linear peptides, similar to the micellization process. Aromatic short di-peptides, such as $NH_2$-Phg-Phg-COOH. can interact by parallel displaced π-stacking to form stacks, which can further interact by Hydrogen bonding of the $NH_2$ – COOH ends to form a sheet structure (Figure 10 left). The sheet can fold onto itself to minimize unfavourable solvent-peptide interactions to form a closed tubular structure when the end groups are thiolated, to prevent further Hydrogen bonding, or a hollow shell structure, when the sheet ends Hydrogen bond to each other. Other sheet structures made from linear peptides, such as bis-(N-α-amido-glycylglycine)-1.7-heptane dicarboxylate, may also form by Hydrogen bonding only, which occur between COOH-COOH and amide-amide dimers. This peptide sheet folds into tubes with diameters varying from 40 to 140 nm, and it was shown that nanotube bundles can form by chelation with $M^{2+}$ ions. Amphiphile peptide conjugates, such as peptides conjugated with hydrophobic alkyl tails, and bolaamphiphiles peptides, can form nanotubes because of poor solvent-peptide interactions, which promote the ordered aggregation of the peptides. Surfactant-like peptides (Figure 10 right) can also associate similarly, minimize their solvent contact and form closed peptide rings that further grow linearly to form a nanotube. Ionic complementary peptides, such as complementary Hydrogen bonding groups, can form sheets[60,68], which fold for similar reasons. These small diameter peptide nanotubes may find future application as model ion channels in lipid bilayer systems, biocompatible drug delivery systems, and functionalization can be of interest in the field of material science and biosensors[28].

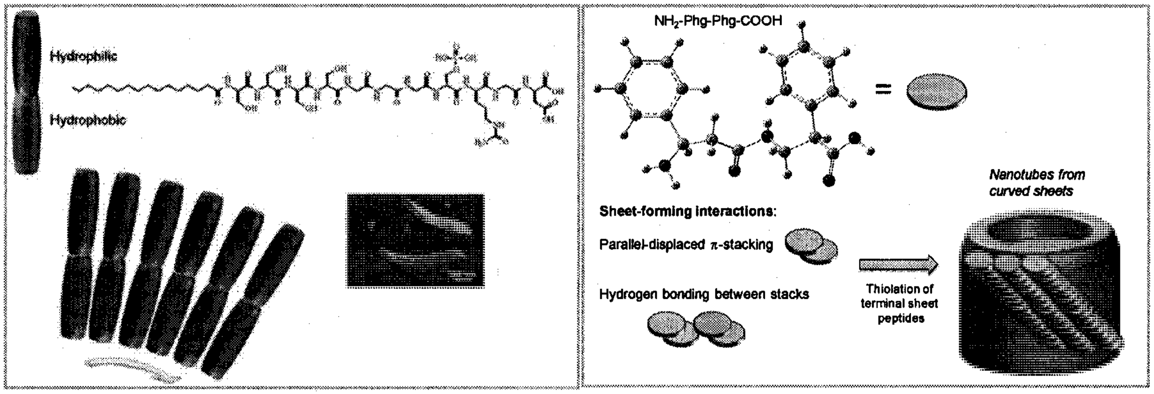

Figure 10: nanotube formation from sheet structures made of non-cyclic peptides. **(left)**: amphiphilic peptides stacking to minimize unfavourable solvent interactions and form flexible circular sheets in the arrow direction and can then grow linearly into a tube **(right)**: aromatic peptides with complementary Hydrogen bonding ends. They stack because of π-stacking interactions and the stacks associate by H-bonding. Thiolation of the terminal groups of a sheet prevent the sheet from forming a closed shell and therefore forms a nanotube. *Molecular structure and TEM reproduced from* [61]

Nanotubes obtained with linear peptide self-assemblies have a greater diameter than the cyclic peptide nanotubes, because of the large strain imposed on the small diameter curved sheet structure. The outer diameter of these peptide nanotubes range from approximately 40 nm to over 500 nm. These larger peptide nanotubes can be used to fabricate metal wires, ~50 nm diameter, by reducing metal ions on the inside or outside walls of the peptide nanotubes[69-78].

Nanotubes can be made from other organic molecules using self-assembly with diameters ranging from 3-20 nm. Hydrogen bonded molecules can self-assemble to form nanotubes to feature complementary H-bonding arrays of DNA nucleotides such as guanine and cytosine terminated blocks. These blocks self-assemble into a supermacrocycle, maintained by 18 H-bonds, and which can then $\pi$-stack up to several millimeters in length. They have outer diameters of 3-10 nm and interior diameters on the order of 1 nm[79-81] (Figure 11). The outer part of the blocks can be modified to give crown ethers which can be used as ion channels[80], to phenyl groups that can further stabilize the complex through $\pi$-stacking, and these modifications vary the effective outer diameter[81] of the organic nanotubes. Naphtalenediimide derivatives were shown to self-assemble by a similar mechanism[82-84], involving Hydrogen bonding between the derivatives, and a helical growth of the hollow nanotube. These 3 nm diameter nanotubes were shown to be capable of encapsulating $C_{60}$ fullerene molecules[84] within the hollow cavity measuring 1.2 nm, rendering them soluble in chloroform.

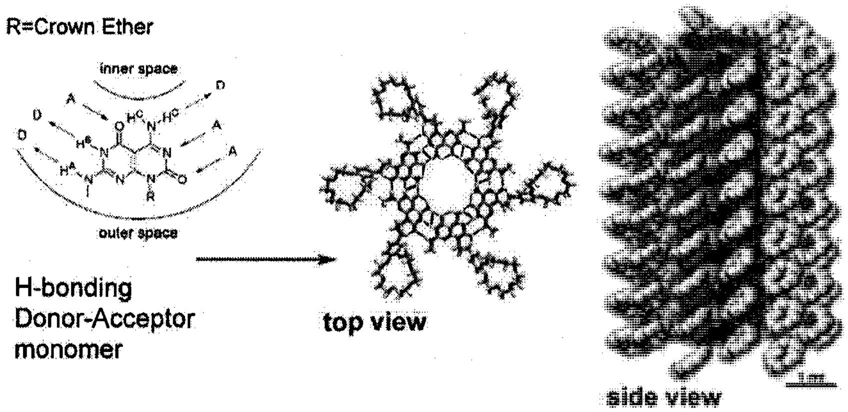

Figure 11: Rosette type nanotubes made from monomers with complementary Hydrogen bonding sites. They form macrocycles that can stack vertically.

Self-assembly can be used to fabricate block copolymers nanotubes[85-92]. These structures are better described as elongated vesicles. These nanotubes are usually observed in the presence of vesicles. The formation of tubules versus the formation of vesicles is a function of the relative lengths of the hydrophilic and hydrophobic blocks. Block copolymer nanotubes are usually monodisperse in diameter, while the vesicles formed from these are more polydisperse. For the triblock copolymer poly(2-methyloxazoline-block-dimethylsiloxane-block-2-methyloxazoline), in aqueous solution, the yield of nanotubes[85] was best for hydrophilic blocks being about 15% of the size of the hydrophobic middle block. Increase of the hydrophobic block to about 30% in size, decreased the nanotube yield from 90% to 10%. The close packing of the block copolymers gave nanotubes with monodisperse diameters of 40 nm with length over 1 μm. the triblock copolymer, poly(butyl methacrylate)-block-poly(2-cinnamoyloxyethyl methacrylate)-block-poly(tert-butyl acrylate) self-assembles to produce nanotubes of ~35 nm in diameter[92].

Phospholipids also self-assemble into nanotube structures[93-98]. These molecules are the building blocks of living cell membranes and can be viewed as a micrometer size vesicle. Nanotubes self-assembled from these phospholipid molecules are essentially elongated vesicles. Control of the solvent composition and cooling process allows formation of these structures. To obtain nanotubes from a bilayer membrane, the stacking of the phospholipids must be unsymmetrical and this is achieved by using bolaamphiphiles, which are phospholipids having two hydrophilic head groups of different size with a long hydrophobic block in between[93-95] (Figure 12). These preferentially stack with the similar head groups on each side of a bilayer membrane, which forces curvature. The nanotubes obtained vary in diameter from 30-500 nm. Chiral phospholipids also assemble into supramolecular tubular structures. The self-association takes place as with the bolaamphiphiles, but because the molecules have a unique chirality, the self-assemble bilayer has a tilt and grows into a nanotube because of the chiral preference[96-98]. Recent advances in nanotechnology have made it possible to mechanically form a nanotube from a lipid bilayer membrane of polymersomes using optical tweezers. Capturing the membrane in the optical tweezers and stretching it creates a hollow lipid nanotubes and the process is reversible. In addition, networks of these stretched membranes can be produced by pulling an additional nanotube from the junction of the first nanotube with the membrane. Overall, these lipid bilayer nanotubes are not very stable, but they can be made rigid using a cross-linking reagent that effectively immobilizes the membrane in its nanotube conformation, and allows an improved processing of the nanostructures. Lipid nanotubes vary in diameter from 30-100 nm in diameter.

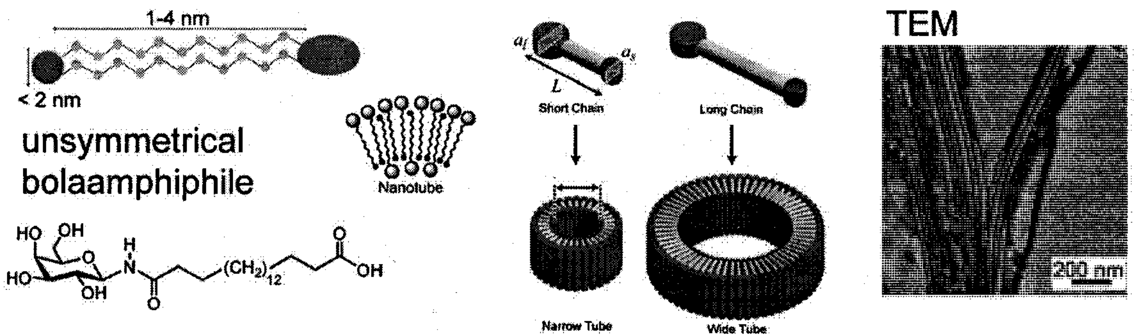

Figure 12: Schematic representation of a bolaamphiphile and the mechanism of assembly leading to hollow tubular structures. The molecule shown is a bolaamphiphile and assembled in nanotubes with diameters of about 30-50 nm, shown in the TEM micrograph on the right. *TEM and schematics of lipid association reproduced from* [95].

Nanotubes can be fabricated from polymer melts using a template, which is typically a membrane of porous $Al_2O_3$ grown electrochemically referred to as template wetting[88,99-103]. The polymers used are typically polystyrene (PS) or polymethyl-methacrylate (PMMA) This membrane has cylindrical pores ranging from 100-500 nm in diameter, depending on the method of fabrication. The pore depth can reach up to 100 μm. The technique used is simply to wet the porous membrane with the polymer melt and let the melt cool or the solvent evaporate. This induces crystallization or vitrification of the polymer along the pore walls, while the interior of the pore remains hollow. The aluminium membrane is etched away using a concentrated basic aqueous solution in which the polymer is insoluble. The polymer structures obtained are cylindrical hollow tubes with lengths over 1 μm, diameters of 100-500 nm, and with a wall thickness of about 10-20 nm. The membranes used for this type of nanotube synthesis must have high surface energy, to interact with the low surface energy polymer melt, and good monodisperse pore size distribution, characteristic of macroporous silicon and porous aluminium oxide membranes. This method can produce biocompatible or chemically inert polymer nanotubes from polymers that are difficult to dissolve in common solvents, which makes them very difficult to nanostructure by conventional methods. Polymers such as polyether ketone (PEEK), polyamide 66 and fluorinated polymers such as polytetrafluoroethylene (PTFE) have desired properties but are difficult to process and can be moulded in required nanotube structures using this template wetting technique. This method also has the advantage of low cost production of nanotubes; a 100 $cm^2$ membrane can produce over 100 billion polymer nanotubes. There is also the possibility of creating hybrid polymer nanotubes by selectively flowing one polymer followed by another that can covalently bind to the first. This was performed with polyethyleneimide and poly(styrene-alt-maleic anhydride) [104]. Metal functionalization is also possible by chemical evaporation of metals onto the membrane before wetting. The resulting polymer nanotubes have a core-shell structure with an outer metal shell [105].

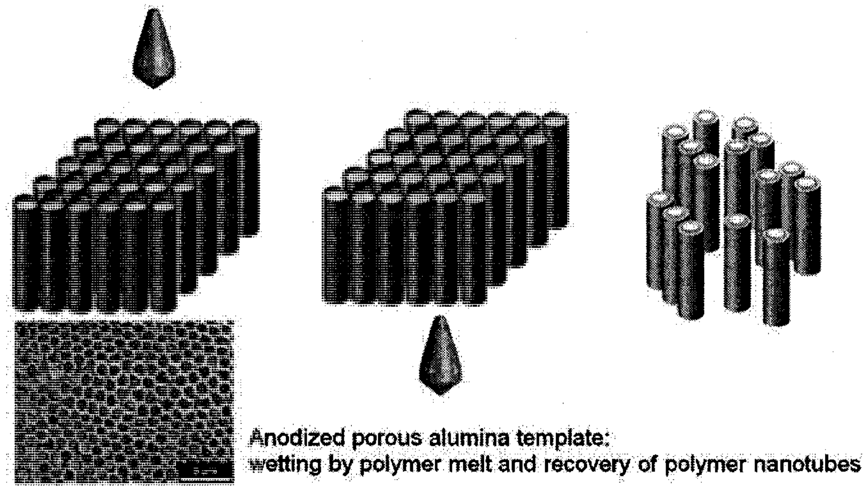

Figure 13: Schematic representation of the template wetting technique described. The polymer melt (green) is filtered through an anodized aluminium template (SEM [101]) and is thereafter dissolved away leaving polymer nanotubes.

Typical experiments to study the presence of nanotubes involve direct imaging at the nanometer scale paired with spectroscopic methods to confirm the inter-molecular interactions involved in the nanotube structure. Transmission Electron Microscopy (TEM)[106], Atomic Force Microscopy (AFM)[107] and Scanning Electron Microscopy (SEM)[108] are used to probe the shape, size and composition of the nanotubes. AFM gives accurate nanotube dimensions while the electron microscopy techniques give information on sample density, composition and dimensions. However, it is always useful to probe the interactions between the molecules that compose the nanotube to understand the self-assembly mechanism. For H-bonds in nanotubes, NMR was used to probe the mechanism. In stacking rosette nanotubes, UV-Visible shifts were studied to monitor the planar stacking of aromatic molecules. In nanotubes made of chiral molecules, circular dichroism was used to study chirality. A brief overview of the nanotube systems discussed is presented with the approximate size range of each type of structure in Figure 14.

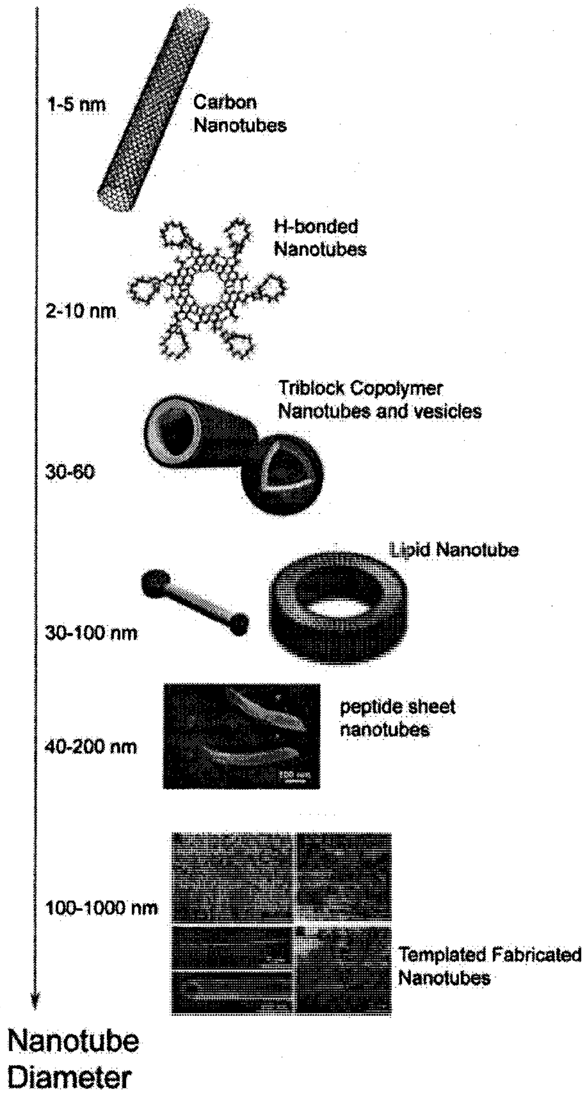

Figure 14: Size distribution of the different types of nanotubes presented. *Images reproduced from* [36,61,80,86,95,101]

Poly(styrene-alt-maleic anhydride) (SMA) has hydrophobic styrene monomers, alternating with hydrophilic maleic anhydride monomers along the polymer backbone. Poly(styrene-alt-N,N-dimethylpropyl amide) (SMI) has hydrophobic styrene monomers, alternating with hydrophobic maleimide monomers, which can be made hydrophobic by amide protonation. It was found that these polymers associate into nanotubes when they are in a linear conformation. Styrene monomers can associate through quadrupole-quadrupole interactions, commonly referred to as $\pi$-stacking, and form association complexes between polymers. The association takes place sideways, along the backbones of the polymers and the minimum energy structure corresponds to closed tubular nanostructures. Because the polymers are not a block copolymer, the self-assembly mechanism is different than the mechanisms described in literature. The association takes place through discrete $\pi$-stacking interactions between styrene monomers, similarly to the Hydrogen bonding responsible for the organization of the cyclic peptides into nanotubes. Theoretical modeling was used[1,109,110] to study the conformation of the polymers and the $\pi$-stacking based association mechanism. TEM and AFM were used to study the nanostructures and support to the proposed theoretical association mechanism. Spectroscopic studies were performed, but were not found to describe the $\pi$-stacking interactions.

## 6. Molecular Modeling and Nanostructure Characterization techniques

There are many useful techniques to probe nano-scale structures. In the research presented, two of the many techniques were extensively used and are discussed.

### 6.1. Theory of Molecular Modeling

The fundamental aim of theoretical calculations[111-113] is to find a structure that corresponds to a global minimum in the potential energy surface (PES). Although this search does not always yield an absolute minimum, there are techniques to get close to the real minimum of the system and give good approximation to the real minimum. The energy obtained by molecular modeling techniques follows the variational theorem, Eq. (8), introduced by Fock,

$$E_{calculated} \geq E_{experimental} \tag{8}$$

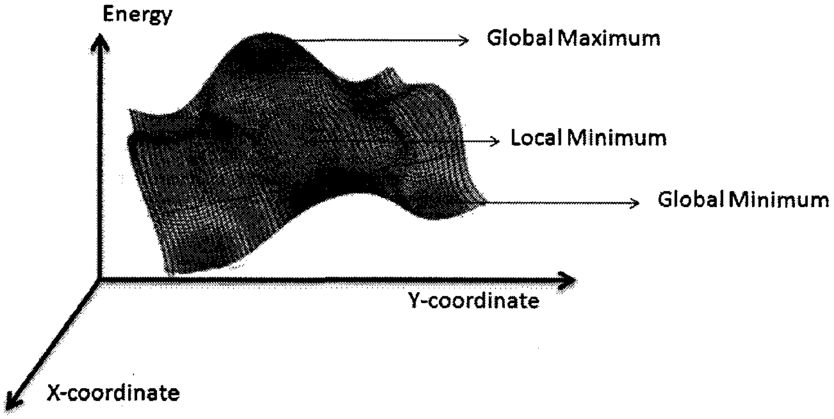

Figure 15: Schematics of a potential energy surface.

### 6.1.1. Hartree-Fock Method

The energy expectation value is always higher than the lowest energy eigenvalue. The expectation value for the energy, for fixed nuclei, only depends on the molecular orbitals and it is refined through iterations of an initial guess of eigenfunctions such that the expectation value no longer changes with small changes in the orbitals. This mathematically corresponds to a minimum search and the molecular orbitals found through these calculations correspond to the electronic ground state. This is commonly known as the *Hartree-Fock method* (HF). However, this method is mostly restricted to small molecules of a few atoms because the calculations are carried out with atomic orbitals expressed in terms of radial functions and spherical harmonics.

Quantum mechanical HF calculations on small molecules are carried out solving the Schrödinger equation, for a multi-particle system, composed of *N* nuclei and *n* electrons, whose wavefunction is defined as:

$$|\psi\rangle = |\psi_{electrons}\rangle|\psi_{protons}\rangle \tag{9}$$

$$|\psi\rangle = |1,2,\dots,N\rangle|1,2,\dots,n\rangle \tag{10}$$

The total Hamiltonian for the system is defined as $\widehat{\mathrm{H}}_{total}(1,2,\dots,N;1,2,\dots,n)$ and the Schrodinger equation to solve to obtain the desired energy is,

$$\widehat{\mathrm{H}}_{total}|\psi\rangle = E|\psi\rangle \tag{11}$$

This is an eigenvalue equation with 3*N*+3*n* Cartesian coordinates. Solving for this many variables is not practical and even impossible. Therefore approximations are useful in reducing the computational effort while providing reliable energies and conformations. The first approximation that can be performed is eliminating the contribution of the nuclei following the Born-Oppenheimer approximation[114] since the latter are assumed to be stationary with respect to electron motion because the proton is 1846 times heavier than the electron. Therefore the nuclear kinetic energy and the nuclear-nuclear repulsion potential may be removed from the total Hamiltonian with no significant loss in generality. The Hamiltonian is consequently a function only of the electrons relative to the position of the nuclei:

$$\hat{H}_{electronic} = -\frac{h}{16\pi^2(m')^2}\sum_{i=1}^{n}\nabla_{\mathrm{i}}^2 - \sum_{\alpha}^{N}\sum_{i}^{n}\frac{e^2\,Z_\alpha}{r_{\alpha i}} + \sum_{i<j}^{n}\frac{e^2}{r_{ij}} \tag{12}$$

$Z_\alpha$ corresponds to the nuclear charge. The first term on the RHS is the kinetic energy of the electron summed over all electrons, the second term is the nucleus-electron attraction for all electrons and nuclei and the third term corresponds to the electron-electron repulsion for all electron pairs *i-j*. This new defined Hamiltonian simplifies to,

$$\hat{H}_{electronic}\left|\psi_{electrons}\right\rangle = \xi\left|\psi_{electrons}\right\rangle \tag{13}$$

where $\xi$ is the total electronic energy. Molecular Orbital theory treats the wavefunction of a system as a product of one electron wavefunctions,

$$\left|\psi_{electrons}\right\rangle = \left|\psi_1\right\rangle\left|\psi_2\right\rangle\cdots\left|\psi_n\right\rangle \tag{14}$$

Hartree developed an approximation technique known as the self consistent field (SCF). If all molecular orbitals are known, the interactions of a single electron with all others can be calculated as an average value from their potential field and added to the one-electron operators to construct *effective* 1-electron Hamiltonians.

$$\hat{H}_{eff}(i) = -\frac{1}{2}\nabla_i^2 - \sum_{k=1}^{N}\frac{Z_k}{r_{ik}} + \frac{1}{2}\sum_{j\neq i=1}^{n}\frac{Z_k}{r_{ik}}\int \psi_j^{*}\left(\frac{1}{r_{ij}}\right)\psi_j\ dV_j \tag{15}$$

The electronic Hamiltonian operator acts on this type of wavefunction. The many-electron operator can be described by many effective Hamiltonian operators for one electron, F(*i*), known as Fock operators.

$$\hat{H}_{electronic} = \sum_{i=1}^{n}\hat{H}_{eff}(i) + \sum_{k<l}^{N}\sum_{l=1}^{N}\frac{Z_k Z_l}{r_{kl}} \tag{16}$$

From the one electron Hamiltonian operator, the wave equation of a one electron system is defined as,

$$\hat{H}_{eff}(1)|i\rangle_1 = \xi_i|i\rangle_1 \tag{17}$$

The Hamiltonian becomes a sum of terms that depend on the coordinates of one electron. The wave function is therefore a product of molecular orbitals. The simplification come at the cost of a mutual dependency of the molecular orbitals and the effective Hamiltonians, i.e. the orbitals can be determined from the effective Hamiltonians, but to formulate the latter the molecular orbitals have to be known. To resolve this conflict requires an iterative solution. Starting from a set of orbitals, $\gamma^0_{electrons}$ and effective Hamiltonian is formed $\hat{H}^0_{eff}(i)$. The eigenfunctions are then improved molecular orbitals $\gamma^1_{electrons}$ and a new effective Hamiltonian is formed $\hat{H}^1_{eff}(i)$, and so on. The process is repeated until the potential field and the molecular orbitals becomes self-consitent. This gives a good approximation of the electronic wave function, Eq. (18).

$$|\gamma_{electronic}\rangle \approx |\psi_{electronic}\rangle = \Pi_{i=1}^{n} \psi_i \tag{18}$$

An example of the self-consistent field method is given in Figure 16, which shows the evolution of the electron density during a HF SCF calculation of HCN from an initial choice of molecular orbitals to the final self-consistent result.

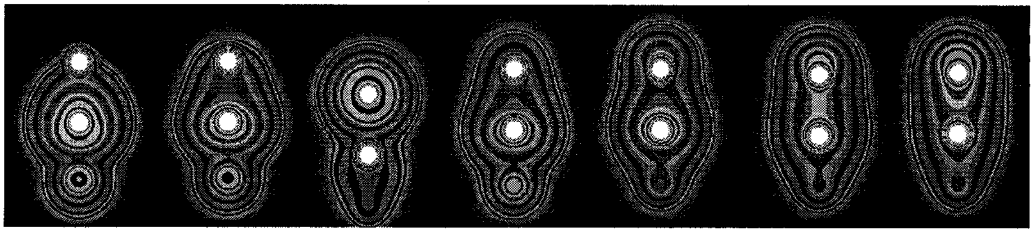

Figure 16: Evolution of the electron density during a SCF calculation of HCN using Hartree-Fock [113].

However, a simple product of wave functions does not fulfill the Pauli principle. The sign of the wave function must change when permutating two electron coordinates. If the wave function is expressed as a slater determinant, Eq. (19), both the Pauli principle and the product of wave functions are satisfied.

$$|\psi_{electrons}\rangle = \frac{1}{\sqrt{n!}}\, det \begin{bmatrix} \psi_1(1) & \psi_2(1) & \cdots & \psi_{n-1}(1) & \psi_n(1) \\ \psi_1(2) & \psi_2(2) & & \psi_{n-1}(2) & \psi_n(2) \\ & \vdots & \ddots & \vdots & \\ \psi_1(n) & \psi_2(n) & \cdots & \psi_{n-1}(n) & \psi_n(n) \end{bmatrix} \tag{19}$$

Molecular orbitals can be separated in a spin function and in a space function and the space functions can always be orthonormalized such that:

$$\int \psi_i^* \psi_j \, dV = 1 \quad \text{for} = j\text{, and 0 for } i \neq j \tag{20}$$

The expectation value of the electronic energy is then given by Eq. (21). The factor of 2 accounts for the fact that each orbital accommodates two electrons.

$$E_{electronic} = \int \psi_i^* \hat{H}_{electronic} \psi_j \; dV = 2\sum_{j=1}^{n/2} H_i + \sum_{i=1}^{n/2}\sum_{j=1}^{n/2}(2J_{ij} - K_{ij}) + \sum_{l=1}^{N}\sum_{k<l}^{N}\frac{Z_k Z_l}{r_{kl}} \quad (21)$$

*where, $H_i$,* defined as a kinetic and potential energy term:

$$H_i = \int \psi_i^* \left(-\nabla^2 - \sum_{k=1}^{N}\frac{Z_k}{r_k}\right) \psi_i \; dV \quad (22)$$

$J_{ij}$ is the Coulomb interaction that corresponds to the potential energy of interaction between a smeared cloud of electronic density and an electron,

$$J_{ij} = \int\int \psi_i^*(1)\; \psi_j^*(2) \left(\frac{1}{r_{12}}\right) \psi_i\;(1)\; \psi_j\;(2)\; dV_1 dV_2 \quad (23)$$

$K_{ij}$ is the exchange energy interaction and is particular to quantum mechanics since no classical analogue can be attributed to it; it ensures that a wave function is anti-symmetric with respect to electron interchange.

$$K_{ij} = \int\int \psi_i^*(1)\; \psi_j^*(2) \left(\frac{1}{r_{12}}\right) \psi_j\;(1)\; \psi_i\;(2)\; dV_1 dV_2 \quad (24)$$

Hartree-Fock theory can be used for both a closed shell and an open shell systems. For a closed shell case, it is assumed that paired electrons are degenerate. This simplifies the restricted Hartree-Fock calculation to a product of molecular orbitals, Eq. (14), and only closed shell systems were studied.

$$|\psi_{electrons}\rangle = |\psi_1\rangle|\psi_2\rangle \ldots |\psi_n\rangle \quad (25)$$

### 6.1.2. HF Methods in Computational Studies

Reformulation of the Hartree-Fock method was developed by Roothaan, in which molecular orbitals are defined as a linear combination of atomic orbitals. This permitted the study of larger molecules more rapidly.

$$\psi_i = \sum_{j=1}^{m} C_{ji}\, \rho_j \quad (26)$$

The atomic orbitals (ρ) are an $m$-dimensional basis of functions. These are specified at the beginning of the calculations and are not modified. The input variables are the molecular orbital coefficients, which are grouped in a matrix **C**. The advantage of the Roothaan method is the use of vectors and matrices, which makes use of matrix algebra and digital computer calculations can easily make use of these vectors and matrices. Inserting the linear combination of atomic orbitals into the Hartree energy formula, which is:

$$E_{electronic}^{HF} = \sum_{\mu<v}^{N}\sum_{v=1}^{N}\frac{Z_\mu Z_v}{r_{\mu v}} + 2\sum_{j=1}^{\frac{n}{2}} H_i + \sum_{i=1}^{\frac{n}{2}}\sum_{j=1}^{\frac{n}{2}}(2J_{ij} - K_{ij}) \quad (27)$$

where, $J_{ij}$ is the Coulomb operator and $K_{ij}$ the Exchange operator, gives the Roothan electronic energy:

$$E_{electronic}^{Roothaan} = \sum_{\mu<v}^{N}\sum_{v=1}^{N}\frac{Z_\mu Z_v}{r_{\mu v}} + 2\sum_{j=1}^{\frac{n}{2}}\sum_{t=1}^{m}\sum_{s=1}^{m}\mathrm{C}_{tj}^{*}\mathrm{C}_{ts}\mathrm{H}_{ts} + 2\sum_{i=1}^{\frac{n}{2}}\sum_{j=1}^{\frac{n}{2}}\sum_{t=1}^{m}\sum_{s=1}^{m}\sum_{a=1}^{m}\sum_{b=1}^{m}\mathrm{C}_{tj}^{*}\mathrm{C}_{vj}^{*}\mathrm{C}_{si}\mathrm{C}_{bj}\left[(ts,ab)-1/2(tb,as)\right] \tag{28}$$

**H**$_{ts}$ and (*tu,vw*) are the following integrals:

$$\mathrm{H}_{ts} = \int \chi_t \left[-\frac{1}{2\nabla^2} - \sum_{\mu=1}^{N}\frac{Z_\mu}{r_\mu}\right]\chi_t \, dV \tag{29}$$

$$(ts,ab) = \iint \rho_t(1)\,\rho_s(1)\left(\frac{1}{r_{12}}\right)\rho_a(2)\rho_b(2)\,dV_1\,dV_2 \tag{30}$$

The minimum condition for determining the electronic energy $E_{el}$ is obtained by differentiating with respect to the MO coefficients of the **C** matrix.

$$\frac{\partial E_{electronic}}{\partial \mathrm{C}_{ti}} = \frac{\partial E_{electronic}}{\partial \mathrm{C}_{ti}^{*}} = 0 \qquad 1 \le i \le \frac{n}{2}\ ,\ 1 \le t \le m \tag{31}$$

Orthonormality of the molecular orbitals add additional constraints,

$$\int \psi_j^{*}\psi_j \; dV \;=\; \sum_{t=1}^{m}\sum_{s=1}^{m}\mathrm{C}_{ti}^{*}\mathrm{C}_{uj}\int \rho_t^{*}\,\rho_s\,dV \;=\; \sum_{t=1}^{m}\sum_{s=1}^{m}\mathrm{C}_{ti}^{*}\mathrm{C}_{uj}\,\mathrm{S}_{ts} \;=\; \delta_{ij} \tag{32}$$

where **S** is the overlap matrix, with matrix elements,

$$\mathrm{S}_{ts} = \int \rho_t^{*}\,\rho_s\,dV \tag{33}$$

Differentiation to reach the conditions determining the electronic ground state gives,

$$\frac{\partial E_{electronic}}{\partial \mathrm{C}_{ti}} = 4\sum_{s=1}^{m}\mathrm{C}_{si}\,\mathrm{F}_{ts} = 0 \tag{34}$$

Differentiation with respect to $\mathrm{C}_{ti}^{*}$ (with $\mathrm{S}_{ts} = \mathrm{S}_{st}^{*}$) gives,

$$\frac{\partial E_{electronic}}{\partial C_{ti}^{*}} = \sum_{s=1}^{m}\mathrm{C}_{sj}\,\mathrm{S}_{ts} + \sum_{s=1}^{m}\mathrm{C}_{sj}\,S_{\mathrm{st}}^{*} \;=\; 2\sum_{s=1}^{m}\mathrm{C}_{sj}\,S_{\mathrm{st}} \;=\; 0 \qquad 1 \le \mathrm{j} \le \frac{\mathrm{n}}{2}\ ,\ 1 \le \mathrm{t} \le \mathrm{m} \tag{35}$$

and introducing Lagrange multipliers, -2**L**$_{ji}$, gives,

$$\sum_{s=1}^{m}\mathrm{C}_{si}\,\mathrm{F}_{ts} - \sum_{j=1}^{n/2}\sum_{s=1}^{m}\mathrm{L}_{ji}\mathrm{C}_{sj}\,\mathrm{S}_{ts} \;=\; 0 \qquad 1 \le \mathrm{j} \le \frac{\mathrm{n}}{2}\ ,\ 1 \le \mathrm{t} \le \mathrm{m} \tag{36}$$

which is the matrix equation:

$$\mathbf{F\,C = S\,C\,L} \tag{37}$$

The matrices **F** and **S** are known, but the matrices **C** and **L** are set as parameters to optimize in the SCF method. **L** is assumed to be diagonal and represents the matrix **E**, the energy eigenvalues. Determination of the molecular orbital coefficient matrix **C** is reduced to a general matrix eigenvalue problem. The reduced equation below is often called the Roothaan-Hall equation.

$$\mathbf{F\,C = S\,C\,E} \tag{38}$$

Many of the calculations performed were based on semi-empirical PM3 calculations which use Slater Type Orbitals (STO) as a basis set. The normalized form of an STO is shown in Eq. (39). Atomic orbitals have nodes and cusp. STO orbitals have no radial nodes but have cusps. Gaussian Type Orbitals (GTO) have radial nodes and the cusp is approximated by using multiple GTOs, Eq. (40).

$$STO(r) = \frac{[2\zeta/a_0]^{n+0.5}}{\sqrt{(2n)!}}\ r^{n-1}\ e^{-\zeta r/a_0}\ Y_l^m(\theta,\varphi) \tag{39}$$

The orbital exponent is defined to be $\zeta = (Z-s)/n$, $s$ being the screening constant. $Y_l^m(\theta,\varphi)$ are the spherical harmonics, $a_0$ is the Bohr radius and $r$ the distance of the electron to the nucleus.

$$GTO(r) = A\, r^l\, e^{-\alpha r^2} \tag{40}$$

In Eq. (40), $A$ is the normalization constant, $l$ is the orbital number and $\alpha$ is the orbital exponent. GTO are preferred as basis functions to represent atomic orbitals because the product of two GTOs centered on two different atoms is a finite sum of Gaussians centered along the axis that connects them. Hence, four-centre integrals reduce to two-centre ones and then to a finite sum of one-centre intergrals. The use of GTO decreases computational time, compared to previously described methods.

The SCF technique requires the MO coefficients to generate the Fock matrix **F**, with matrix elements $\mathbf{F}_{ts}$, Eq. (41). The Fock matrix determines **C**. Therefore, solutions are iterative in the SCF technique.

$$\mathbf{F}_{ts} = \mathbf{H}_{ts} + \sum_{a=1}^{m}\sum_{b=1}^{m} 2\sum_{j=1}^{n/2} \mathrm{C}_{aj}\mathrm{C}_{bj}^{*}\,[(ts,ab) - 1/2(tb,as)] \tag{41}$$

The list of steps provides a general description of a Hartree-Fock calculation for a closed shell system.

1. Define molecular geometry (atom types, distances, bond order), charge and multiplicity
2. Define basis functions with optimizable parameters
3. Calculate **S** and **H**
4. Compute two electron integrals
5. Generate **F**
6. Solve eigenvalue equation (Roothan-Hall): **F C = S C E**
7. Calculate expectation values
8. Modify nuclear geometry or optimizable parameters in steps 1 & 2, and return to step 3. *Repeat until SCF convergence is satisfied*

### 6.1.3. Semi-empirical method

The most useful method in this research was the semi-empirical PM3 method. It is based on the HF method but reduces the *n*-fold integrals to simpler two-electron integrals. This reduction is made possible by parameterization of the integrals by various physical quantities such as the ionization potential. Thus, the computing time is reduced. HF gives the closest energies to $E_{experimental}$ with configuration interaction and relativistic effects. PM3 gives good energy values which parallel experiment and HF results. Therefore, PM3 can be used reliably for structural, and energetic calculations if the exact energy is not required. The decrease in computational time from using PM3 rather than ab-inito methods allows the study of larger systems, as required to study the relation between polymer structure and the polymer association behaviour.

In *Ab-initio* methods, all elements of the Fock matrix **F** need to be calculated, independently of the basis functions chosen. The Roothan-Hall equation needs to be solved. Simplifications are made with semiempirical calculations: there are three groups of Fock matrix elements:

$\mathbf{F}_{\mu\mu}$(diagonal elements),
$\mathbf{F}_{\mu v}$ ($\varphi_\mu$ and $\varphi_v$ have same origin),
$\mathbf{F}_{vv}$ ($\varphi_\mu$ and $\varphi_v$ have different origin).

Elimination and approximations of some of the integrals reduces the computation time. In addition, only the valence electrons are considered in semi-empirical methods, the inner core electrons do not influence chemical bonding and are considered as *nuclear core.* The methods still makes used of basis functions since it is rooted in the HF formulation and uses Slater type functions (*s*, *p* and *d* types) described previously.

Semi-empirical methods were introduced from the first semi-empirical model developed by Popel[115,116]: Zero Differential Overlap (ZDO). The main approximation defines as zero the overlap between different basis functions. The overlap matrix **S** becomes a unitary matrix and the Roothaan-Hall matrix equation becomes:

$$\mathbf{F\,C = C\,E} \tag{42}$$

Various models based on ZDO exist and vary in their approximations of the one and two electron integrals. Models are listed with their references below.

Semi-empirical methods in chronological order of their development:

**ZDO**: zero differential overlap [115,116]
**NDO**: complete neglect of differential overlap [117,118]
**INDO**: intermediate neglect of differential overlap model [119]
**NDDO**: neglect of diatomic differential overlap model [118]
**MINDO/3**: modified INDO [120]
**MNDO**: modified neglect of diatomic overlap [121]
**AM1**: Austin Model 1, analogue of MNDO [122]
**PM3**: third parametrization of MNDO and AM1 [123,124]

MNDO is the method from which PM3 was developed, which is the main computational method used to study polymer systems in this thesis. MNDO is a modified method of ZDO, where a few approximations are used. 3 and 4 centre integrals are neglected if the associated basis functions have different origins. This simplifies the Fock matrix. The 1 and 2 centre integrals are calculated from known spectroscopic data: *<ss|ss>, <pp|pp>, <sp|pp>, <sp|sp>, and <pp|p'p'>* transitions. The 1-electron integrals $\mathbf{H}_{\mu\nu}$ are computed from the overlap $\mathbf{S'}_{\mu\nu}$. The 1-electron integrals are:

$$\mathbf{H}_{\mu\mu} = \mathrm{U}^{A}_{\mu\nu} + \textstyle\sum_{A\neq B} \mathrm{V}^{\mathrm{B}}_{\mu\mu} \tag{43}$$

$$\mathbf{H}_{\mu\nu} = \mathbf{S}'_{\mu\nu} + \textstyle\sum_{A\neq B} \frac{\left(\beta^{\mathrm{A}}_{\mu}+\beta^{\mathrm{B}}_{\mu}\right)}{2} \tag{44}$$

where $\mathrm{U}_{\mu\nu}$ and $\beta_{\mu}$ are treated as parameters to optimize.

MNDO has some disadvantages. It does not provide a description of transition metals since the Slater Type Orbitals are of *s* and *p* type (but some versions now include *d* type orbitals). Intermolecular Hydrogen bonding is not correct because it overestimates the repulsion energy for atomic distances that are close to the sum of Van der Waals radii. Sterically hindered molecules show energies that are too large and results for aromatic systems are poor.

Further modifications to the MNDO method corrected the repulsion energy overestimation were introduced in the Austin Model, commonly known as the semi-empirical AM1 method. The core-core terms are described by Gaussian functions with width parameter *W* and distance parameter *D* and *E*:

$$E_{AB}^{AM1} = E_{AB}^{MNDO} + \frac{(Z_A Z_B)}{R_{AB}}\left[\sum_i D_{Ai} e^{-W_{Ai}(R_{AB}-E_{Ai})^2} + \sum_j D_{Bi} e^{-W_{Bi}(R_{AB}-E_{Bi})^2}\right] \qquad (45)$$

In the AM1 method, four of these terms are present for Carbon, three for Hydrogen and two for Oxygen. These extra parameters correct most errors in the repulsion energies. AM1 is adequate for large organic systems. However, Heats of formation deviate by about 20 kJ/mol, dipole moments and ionization energies are not accurate and rotational barriers are too large.

The PM3 semi-empirical method uses the same Hamiltonian as AM1. However, an automatic parameterization procedure developed by Stewart [123,124] is included. This corrects most of the problems encountered with thermodynamic data. The advantage of the PM3 method is the calculations of accurate molecular geometries and energies which parallel experiment. The major disadvantage with the semi-empirical PM3 method is the low energy barrier encountered in amide molecules and the non planarity of amides.

When performing structural optimizations or energy calculations, one must be aware of the limitations of each method and use the information for which each method is optimal. The self-consistent field calculations presented [125] in this thesis were performed using the program Gaussian 03W [126] along with a visual interface, GaussView, for building molecules and specifying calculation parameters.

### 6.2. Transmission Electron Microscopy

Transmission Electron Microscopy (TEM) can be used to visualize material with nanometre resolution. The TEM used was at the FEMR (Facilities for Electron Microscopy Research) at McGill University. The TEM was a JEOL 2000 FX, which has a theoretical resolution of 0.2 nm. Because the wavelength of electrons is orders of magnitude smaller than visible light, such high resolution is possible. The operation of a TEM is similar to a microscope but instead of using visible light to observe samples, it uses electrons, which require magnetic lenses to deflect and condense the electrons.

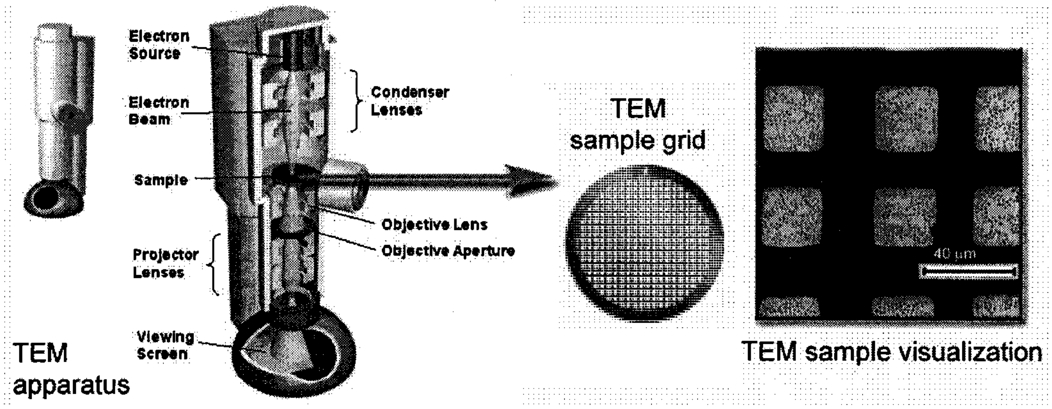

Figure 17: Schematics of a typical TEM apparatus. *Apparatus reproduced from* [127] and scan from [128].

TEM samples can be prepared by different methods, when the sample observed is thinner than 200 nm. The most common method however is to use copper grids, which may vary in mesh size. The smaller the mesh, the more area is available for scanning (Figure 17). The vacant areas on the grids are usually covered with a thin film of material to support the sample. Carbon can be directly evaporated onto the grid to form a thin carbon film, or a polymer, such as poly(vinyl formal), can be deposited onto the grid and then carbon evaporated onto the polymer. Silicon oxide can also be used to form films onto grids. The purpose of carbon and $SiO_2$ is to act as a contrast agent that helps to visualize the samples. Other sample preparation methods involve embedding the sample in a polymer matrix and slicing it into thin films, or producing a replica of the surface topology, by metal evaporation, which is then observed.

Monochromatic electrons are generated at 200 kV by a Tungsten filament source. The electrons are accelerated into a narrow beam by an electron gun under high vacuum. The electrons are then collimated into a stream, which is focused to a small, thin, coherent beam by the use of two condenser lenses. The magnification is proportional to the voltage of the produced electrons. The first lens determines the size range of the final spot which illuminates the sample and refers to the "spot size" control on the apparatus. The second lens typically controls the intensity and is used to change the spot size from a wide dispersion to a focused beam and refers to the “brightness knob”. The beam is passed through the specimen, which is kept under vacuum, and part of the beam is transmitted. The transmitted electrons are focused by an objective lens into an image, which is recorded with a CCD camera. The image obtained is a 2D grayscale image, where the darkness of the area observed is proportional to the density of the material. Dense material appear more black because fewer electrons were transmitted while lighter areas represent thinner or less dense material and therefore illuminate the photographic plate more (Figure 17).

The technique is very sensitive to sample preparation and prone to interpretation errors. Care must be taken to produce a clear sample and avoid over-interpreting the results by taking multiple measurements in different grid areas and with different samples and making statistics from the measurements.

### 6.3. Atomic Force Microscopy

Atomic Force Microscopy (AFM) is used to scan the topography of a surface at the nanometer scale. AFM is part of wider microscopy techniques referred to as scanning probe microscopy (SPM) and essentially scan the surface of samples using different types of probes: magnetic and conducting probes for example. AFM, and other SPM techniques, have a small probe called a cantilever to which is attached a pyramidal shaped tip (Figure 18). For AFM , the cantilever is usually made of silicon nitride and has a tip radius of curvature of of 30-50 nm (Figure 18).

To image the surface, the tip on the cantilever is brought into proximity of a sample surface and scans the surface while the cantilever responds to the interactions of the tip with the surface. Between the tip and the surface, features create a deflection of the cantilever. The deflection is caused by forces such as Van der Waals or capillary forces. A laser beam, which reflects off the top cantilever into an array of photodiodes measures the height of the surface features. There is a feedback mechanism to adjust the tip-to-sample distance and maintain a constant force between tip and surface to avoid tip collision with the sample. Typically the sample is mounted on a piezoelectric tube that moves the sample in the *z* direction to maintain a constant force, and also moves in the *x,y* directions to scan the entire 2D surface. The result is a 3D topographic image of the surface *z=f(x,y)*.

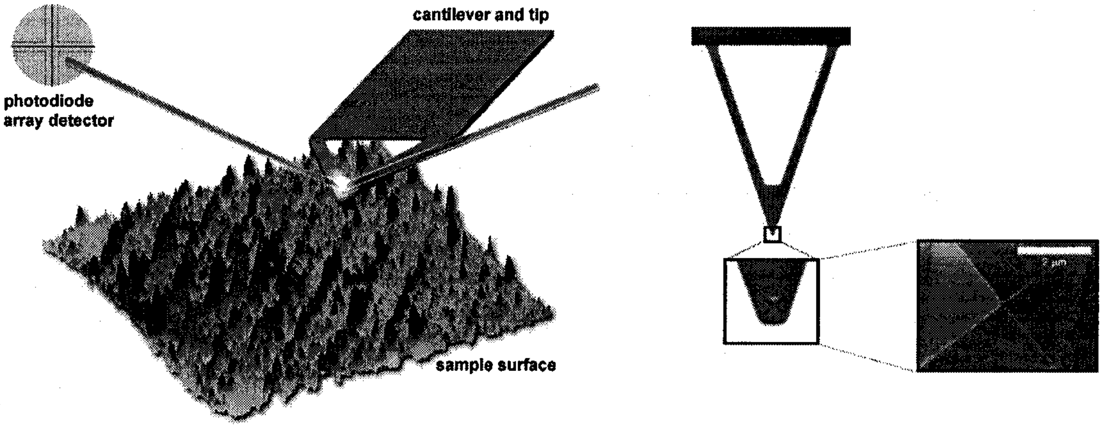

Figure 18: Schematic diagram of the operation principles of AFM. On the left is a static mode cantilever and tip probing a surface and on the right is a Scanning Electron Microscopy image of the tip at the end of the cantilever.

AFM measurements can be obtained by operation in different modes. The two most common modes are the static mode (*contact mode*) and the dynamic mode (*tapping mode*). In static AFM, the tip is kept at a constant distance from the sample, and follows the surface closely where the overall force is repulsive. The deflection is used as a feedback signal; the measurement is prone to noise and drift, therefore cantilevers with low stiffness are used to improve the signal. In dynamic AFM, the tip oscillates close to its resonance frequency and comes near the surface periodically. The oscillation amplitude, and resonance frequency, are modified by the tip-sample interactions and referenced to the external reference oscillation taken before measurement. The cantilevers used in dynamic mode are stiff and provide greater stability when brought close to the surface. Static mode is better suited for *rigid* samples and crystalline material, while the dynamic mode operation is better suited for *soft* samples such as polymers.

AFM has the advantage of providing a 3D surface profile. TEM on the other hand provides only a 2D projection of the sample. Samples observed by AFM also do not require additional preparation, such as staining the sample with heavy metals, or metal/carbon coatings, to view the sample, as is needed with electron microscopy techniques. It can also be performed at room temperature and ambient atmospheric pressure and often offers a better resolution than TEM. AFM also offers the possibility of carrying out experiments in a liquid environment. There are some disadvantages. Image sizes are restricted to small areas of about 10 μm and switching between smaller areas and larger areas requires minutes. Surface scanning is also lengthy and a good scan can take well over 10 min. Electron microscopes allow rapid viewing of large areas, on the order of hundreds to sub of μm sizes, and rapid image capture. When working at high resolution, the quality of the image is limited by the radius of curvature of the tip and an incorrect choice may lead to image artefacts. In this thesis, dynamic mode AFM was used to image the polymer samples.

### 6.4. Dynamic Light Scattering

In Dynamic Light Scattering[129,130] (DLS), a coherent and monochromatic light source, from a laser is passed though a colloidal dispersion. When the diameter of the particles is much smaller than the wavelength of the incident radiation (<250 nm), the particles in solution uniformly scatter light in all directions, Rayleigh scattering. For larger particles, the intensity is angle dependent and is referred to as Mie scattering. The particles studied in this research follow Rayleigh scattering.

The use of a laser light source allows the observation of time dependent fluctuations in the scattering intensity. The scattered intensity is recorded using a photomultiplier, which operates in the photon counting mode (Figure 19).

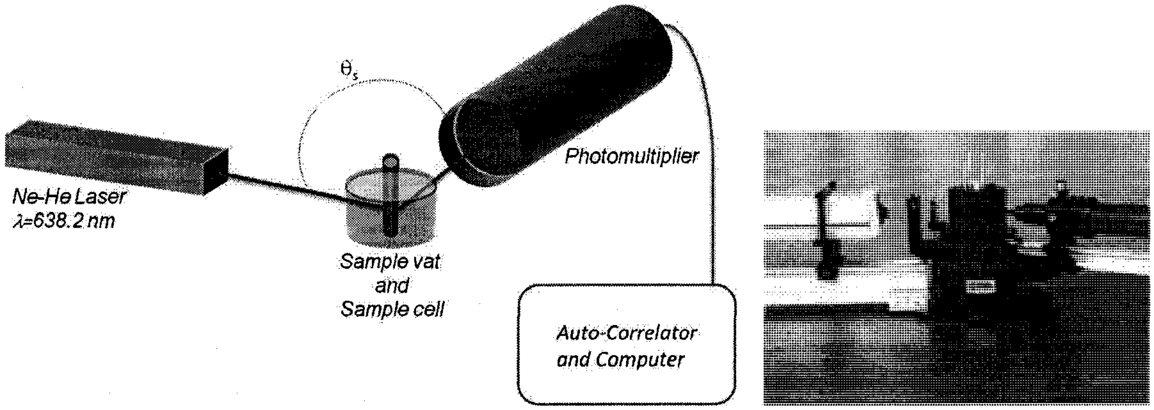

Figure 19: Schematic representation of the set-up used in Dynamic Light Scattering experiments and a photograph of the apparatus used.

In Rayleigh scattering, the particles are small enough that their motion in solution is regulated by random thermal motion, Brownian motion. The particle motion generates intensity fluctuations within the illuminated zone, and the time dependent analysis of these fluctuations, yields the translational diffusion coefficient ($D_T$). The intensity fluctuations are analysed using a digital correlator. The device provides the intensity auto-correlation function, which is an ensemble average of the product of the signal ($I(t)$) with the delayed version of this signal ($I(t+\tau)$) as a function of the time delay ($\tau$), Eq. (46). The signal is obtained from the number of photons detected in one sample interval. For short delays, the correlation is high and decreases to zero for longer sampling time, because random thermal particle motion becomes uncorrelated quite rapidly. The decay is exponential, and is a characteristic of the translational diffusion coefficient of the particles. The delay times are adjusted, depending on the particle sizes, and solution viscosity, so that the auto-correlation function decays to zero with a flat baseline. Using the Siegert relation, Eq. (46), the second order auto-correlation curve can be related to the first order auto-correlation curve. The first order auto-correlation curve relates the exponential decay to the force fitted decay frequency of each different particle size ($\Gamma_i$). The decay frequency is directly related to the translational diffusion coefficient through Eq. (49), where q is the scattering vector.

$$g^2(q,\tau) = \frac{\langle I(t)*I(t+\tau)\rangle}{\langle I(t)^2\rangle} \tag{46}$$

$$g^2(q,\tau) = 1 + [g^1(q,\tau)]^2 \tag{47}$$

$$g^1(q,\tau) = \sum_{i=1}^{\infty} B_i(\Gamma_i)e^{-\Gamma_i\tau} \tag{48}$$

$$\Gamma_i = (D_T)_i\, q^2 \tag{49}$$

From the Stokes-Einstein diffusion equation[130], Eq. (50), the hydrodynamic radius (particle diameter) can be obtained from the translational diffusion coefficient.

$$D_T = \frac{kT}{6\pi\,\eta\,R_H} \tag{50}$$

The auto-correlation function is fitted numerically to a mono or multi-exponential decay model. Monodisperse samples give rise to single exponential decays, but this is rarely the case as most sample are unfortunately polydisperse. Models such as cumulant analysis[131], CONTIN[132,133], multi-exponential[134] or the non-negative constrained least squares[134] are often used to extract the multi-exponential terms and also provide a particle size distribution. Care must be taken with these models as they often give rise to inconsistent results and should always be corroborated by a second type of measurement.

DLS measurements were performed on a Brookhaven Instrument system equipped with the BI 2030 digital correlator and a 25 mW He-Ne laser with a wavelength of 632.8 nm and the temperature of the solutions were maintained at 21°C.

# Theoretical modeling of the π–stacking association between SMA polymers leading to self-assembled polymer nanotubes

# Chapter II

## Abstract

Poly(styrene-alt-maleic anhydride) (SMA) adopts different chain conformations, with different degrees of protonation. Theoretical modeling showed that at neutral pH, which corresponds to 50% degree of protonation, intra-molecular Hydrogen bonds increase the persistence length of the polymer. While linear at neutral pH, the polymers modeled at low and high pH are not linear, and have step-like kinks along their backbones. The structures show a chirality dependence at low and high pH, but different chiralities all lead to linear structures at neutral pH. Association can occur between styrene monomers through π-stacking at neutral pH and this is thermodynamically favourable. SMA polymers can form rigid dimer associations. Association between many rigid dimers leads to flexible associations. The lowest energy structures for large aggregates of SMA polymers are sheets of polymers linked though rigid and flexible associations and hollow tubular SMA polymer structures, which are more stable than sheets. Similarly to proteins, SMA nanotube aggregates have a primary, secondary and tertiary structure. The primary structure can be viewed as the individual polymer conformation. The secondary structure is the nanotube formation from many SMA polymers associating into a nanotube. The tertiary can be described by the association of SMA nanotubes into sheets of tubes and the further stacking between these sheets.

## Introduction

Poly(styrene-alt-maleic anhydride) (SMA) is an alternating copolymer: a hydrophobic monomer, styrene, and a hydrophilic monomer, maleic anhydride. This composition imparts unusual properties to the polymer, which have generated interest in a wide range of scientific fields in the later 20th century. SMA has many applications in the fields of nanotechnology[1,104,135-141], drug delivery[142,143] and the pulp and paper industry as a surface sizing agent for paper products[144-148]. However, studies involving molecular modeling of the structure of strictly alternating copolymers are rare. These studies are useful because they provide details at the molecular level, which cannot be readily determined by experiment. Studies involving modeling of the isotactic alternating copolymer of styrene and carbon monoxide provided a molecular understanding of the crystal packing geometry[149]. Solvation simulations on SMA[150] provided explanations of the variations in viscosity measurements in different solvents. On the other hand, irregularly alternating copolymers like DNA and RNA have been studied[151-153] using theoretical modeling to explain experimental results and to establish accurate methods to allow simulation of these polymers.

The structure and conformation of SMA polymer in solution was studied by Malardier[1,109,110,154,155]. SMA was shown to adopt a different structure depending its degree of protonation and the sequence of chiral sites. SMA has three different protonation states, with two pKa values[156] at pH 4.9 and pH 10.2 (Figure 1).

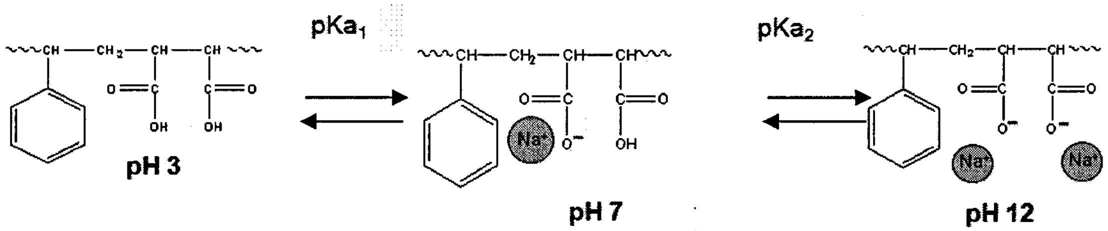

Figure 1: Protonation states of SMA polymer. $pKa_1$=4.4, $pKa_2$=10.2. At low pH, the polymer is in its dicarboxylic state, at neutral pH it is in its monosalt state and at high pH it is in its disalt state.

Three Chiral sites are present in the hydrolysed SMA polymer which self-associates (Figure 2). The first chiral site, located at the carbon linked to the phenyl group, can be of R or S chirality. The second and third chiral sites can each be either R or S and originate from the initial conformation of the maleic anhydride before hydrolysis, which was either E (RR or SS) or Z (RS or SR) before hydrolysis.

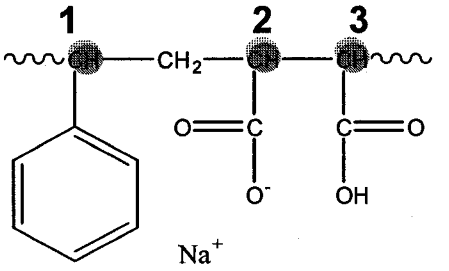

Figure 2: Monosalt form of SMA with its three chiral sites identified. Each site can be either R or S.

Previous experimental work on SMA had shown a strong dependence of the size of the polymer in solution as a function of pH[157]. At low and high pH, the polymer shows low aggregation sizes of around 20 nm, while at neutral pH, the sizes of the aggregates are an order of magnitude larger. The original explanation for the aggregation was an association through a zipper-like mechanism between styrene monomers. A molecular modeling approach taken by Malardier[1], provided a molecular explanation to the size dependence of SMA in aqueous solution.

Using Hartree-Fock calculations with 6-31G** basis set, the structure of the monomer was studied. It was determined that the structure at neutral pH, corresponding to the monosalt form of SMA, had a Hydrogen bond between the $COO^-$ and the COOH groups. This Hydrogen bond is not present at low or high pH due to protonation or deprotonation of the functional groups involved in the Hydrogen bonding[110]. Figure 3 shows the modeled monomer at different pH values and the Delocalized Molecular Orbital (DLMO) corresponding to the Hydrogen bond are shown in Figure 4. The binding sites for another monomer to be bound to the first monomer in order to form a dimer at pH 3 and 12 are identical. So pH 3 and 12 conformations are equivalent. pH 3 was used for simplicity.

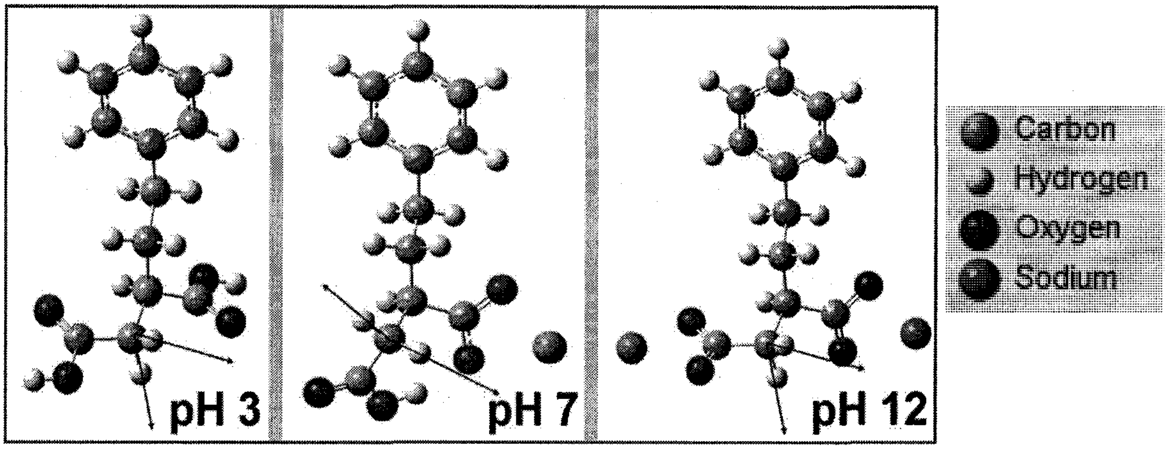

Figure 3: Conformation at pH 3, 7 and 12 of the SMA monomer studied using Hartree-Fock 6-31G**. The binding sites for additional monomers to be bound to SMA monomer shown, in order to form a dimer at pH 3 and 12, are identical[1].

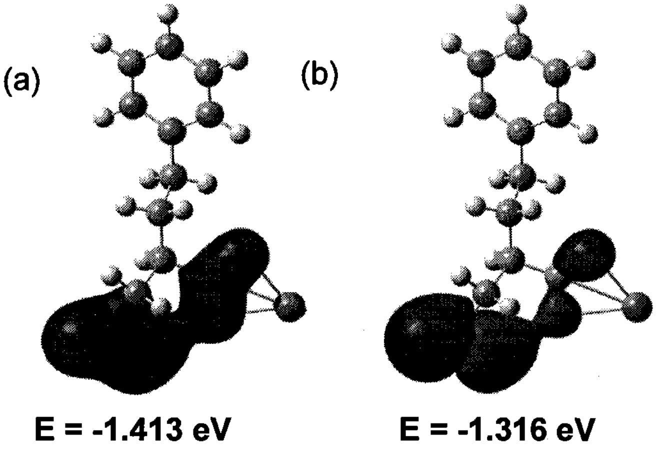

Figure 4: Delocalised molecular orbitals (a) and (b) covering the internal Hydrogen bond of the monomer of SMA at pH 7. The bond length is 1.68 Å [1].

From the monomer, the polymer was built and optimized using semi-empirical PM3 calculations because of the large size of the system [1]. The result showed a similar structure at low and high pH, where the polymer was modeled in its dicarboxylic form and its disalt form. The conformation of the polymer was highly dependent on chiral sites along the polymer chain.

Different chiral sequences gave different polymer backbone structure, none that were linear. However, when the polymers were modeled in their monosalt form, the polymers were linear, irrespective of the chirality chosen. This was attributed to the Hydrogen bonds that form close to neutral pH, at a 50% degree of protonation. The calculations were performed by ignoring the chiral site 1[110] and only assuming that the sites 2 and 3 affect the structure. Figure 5 shows the results of the conformations of SMA quadrimers when there is Hydrogen bonding at neutral pH, and when there is none. This thesis research takes into account the three chiral sites.

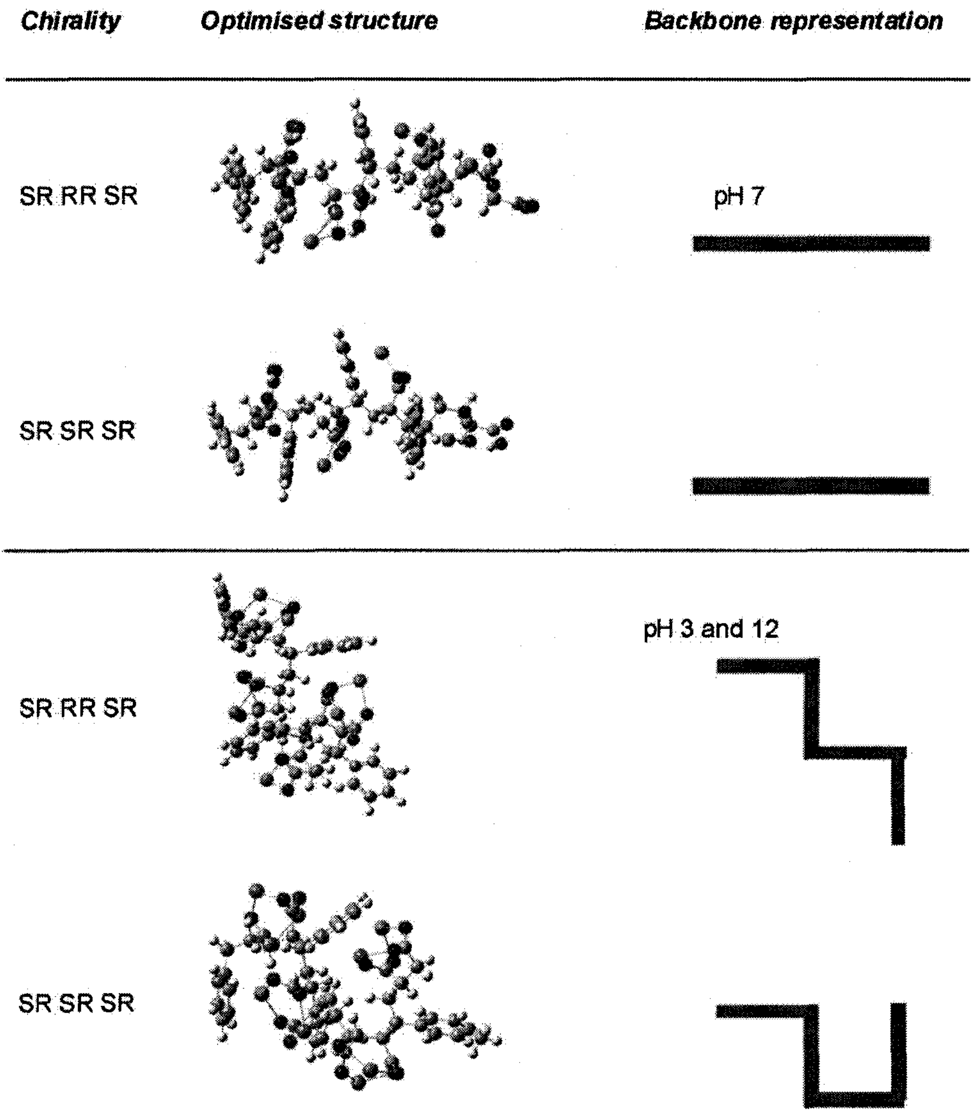

Figure 5: Two different conformations of the quadrimers of SMA at pH 3, 7 and 12 corresponding to two chiralities (SR RR SR and SR SR SR). The structures are very linear and the orientations of the styrene monomers are similar at neutral pH, but at low and high pH the structure has a step-like conformation and the second a well-like conformation [1].

## 1. Primary structure: Polymer structure and conformation

Theoretical modeling of the hydrolyzed SMA polymer, at low, neutral and high pH, showed a strong structure dependence on pH. At low and high pH, the structure of the polymer backbone was random and an ordered association between polymers to give nanotubes was not possible; only weak associations between styrene monomers were possible[110]. However, at neutral pH, an internal Hydrogen bond could form between the $COO^-$ and COOH groups of the maleic anhydride monomers and this stiffened the structure of the polymer. Polymers modeled at neutral pH conditions were linear and all the phenyl groups were available to associate. It is the linearity of the polymers that allowed the formation of linear nanotubes.

Although the conformation of the polymer was extensively studied, its association properties were not studied in great detail. Using the optimized conformations from previous work on hydrolyzed SMA, the association was studied in more detail to both confirm and gain a deeper understanding of the mechanisms leading to SMA polymer nanotube formation. The first set of calculations performed were to confirm that different chirality sequences of the SMA polymer did give linear structures, and that the structures had similar distribution of functional groups in space. The association between the polymers was subsequently investigated to establish the stability of the association caused by π-stacking of the styrene monomers.

The association between hydrolyzed SMA polymers was originally studied by Malardier [1,109,110,154]. It was found that the polymers could associate through π-stacking, of the styrene monomers, along their backbone. The structure of the polymer in its monosalt state was re-investigated by semi-empirical PM3 calculations with a Li atom instead of the Na atom because Li has been parameterized in the PM3 method[158]. The optimizations were also performed without metal ions using negative charges. Both methods gave comparable results and showed no change in the polymer conformation. The results obtained for the overall structure were different from the structure found by Malardier [1] and also offer a clearer understanding of the association mechanism. The previous results tend to suggest that all chiralities are identical. However, it is shown here that different chiralities are similar, but not identical.

The SMA polymer structures[1] for a nonamer were re-optimized using semi-empirical PM3 geometry optimizations. The terminal monomers were removed because they do not behave like the centre monomers; the heptamer structures were analyzed. The isotactic polymer was first optimized, as a reference structure, to study the effect of changes in chirality on the polymer structure. Subsequently, the syndiotactic polymer was modeled. The chiral centres were then randomly modified. Finally, the structures were compared.

The optimized SMA polymers are all linear and adopt different conformations, depending on the choice of chirality sequence; the different chiralities are not super-imposable. By not superposable, it is meant that two different chiralities, while being similar in their cross section view, may have styrene monomer in different spatial locations along the polymer chain: the styrene monomers do not follow the same distribution along the polymer chain. Hence, superposing them may give identical cross-sections views, but different lateral views: a visual description is shown in Figure 6.

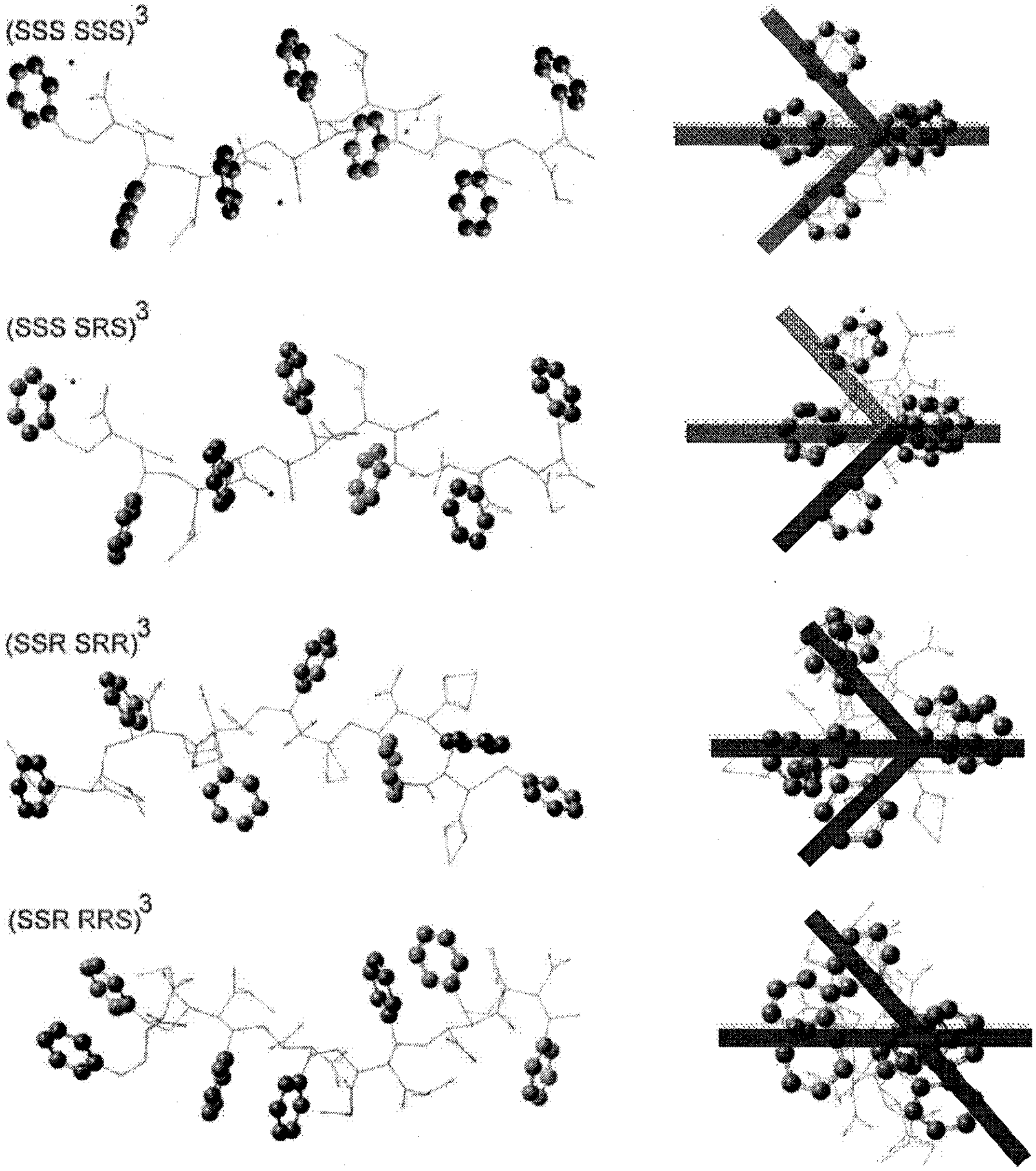

Figure 6: Lateral and cross-section views of different chirality heptamers, obtained from optimized SMA nonamers with the terminal monomers removed. The polymers are not superposable, except for chirality changes in the chiral site 2 (Figure 2). The cross-section view is similar for different chirality sequences. The styrene monomers are in different shades of grey, darker ones are closer and more faded ones are further away.

The most linear and ordered polymer conformation is for an isotactic polymer. The styrene monomers are most prevalent at opposite ends with styrene monomers that deviate by about 45° concentrated on one end. Figure 7 shows both a cross-section and a lateral view of the polymer with the distribution of styrene monomers highlighted. Chirality changes of chiral site 2 of the isotactic SMA polymer does not influence the spatial arrangement of the styrene monomers such that (SSS SSS)$^3$ and (SSS SRS)$^3$ are superposable. Chirality changes in the chiral site 3 gives a similar cross-section view to the isotactic polymer and a different, but similar, styrene monomer distribution along the polymer chain. However, chirality inversions in all three chiral sites (SSR RSS)$^3$ leads to a different cross-section view and a different lateral view. These preliminary results do not give a complete picture of the relationship between chirality and structure but serve as an insight for further theoretical investigations.

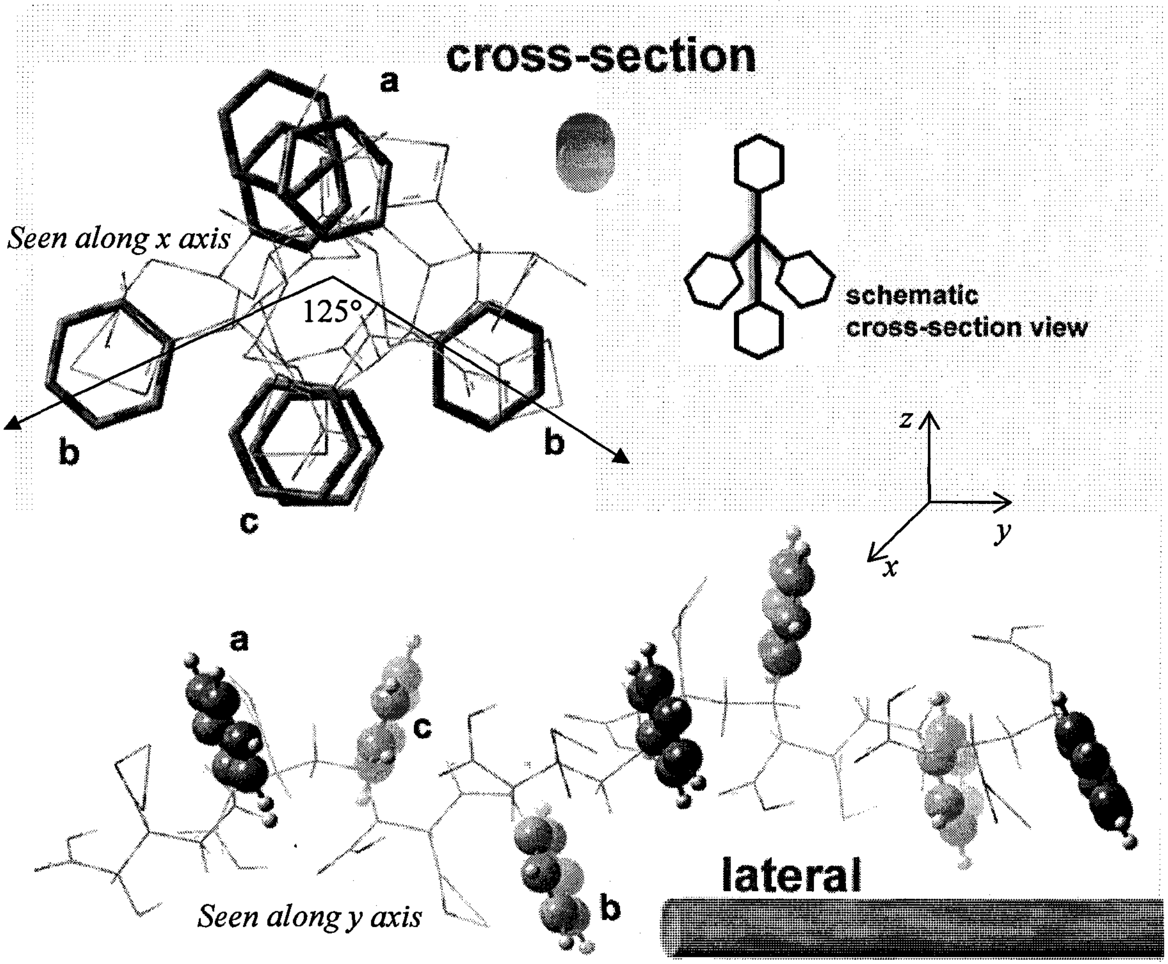

Figure 7: Cross-section and lateral view of the general structure of an isotactic SMA polymer capable of forming ordered associations, modeled with LiOH in the monosalt form. The overall structure does not change much with variations in chirality (see previous Figure), but the styrene monomers distribution is different, therefore different chiralities are not superposable. The lower structure shows three darkness values (lighter atoms are further away) and similar shades are located at the same height. Cylinders indicate the orientation of the polymer shown.

## 2. Secondary structure: association between SMA polymers

The fact the different chirality polymers are linear when modeled at neutral pH explains the increase in persistence length of the polymer as neutral pH is attained. In addition, association can still take place between non-identical chirality polymers, but this is not likely to produce any ordered structure, and can explain amorphous SMA polymer aggregation.

As in any structure in nature, if order is to be achieved on a large scale from small building block, these need to exhibit a certain degree of periodicity. Rarely are ordered structures built from random structure constituents. Therefore, the association calculations for SMA nanotube formation were carried out with isotactic SMA polymers.

Two types of association are possible between isotactic SMA polymers, (SSS) monomer chirality sequence: a rigid association and a flexible association (Figure 8). It is important to note that the association takes place sideways and the figure represents the cross-sectional view of the polymers. This is the only possible favourable association that can produce stabilized complexes, because the polymers are alternating in nature, and phase segregation between similar block segments cannot take place, unlike block copolymers and surfactants. The SMA association can be viewed as short phase segregations between the hydrophobic styrene monomers. The succinic acid moieties that undergo Hydrogen bonding are shorter than the styrene monomers and therefore cannot form regular stabilizing inter-polymer Hydrogen bonds, only intra-polymer Hydrogen bonds; in Figure 8, where the oxygen (red) atoms are located towards the interior of the polymer backbone, the sideways association between linear isotactic SMA polymers is shown.

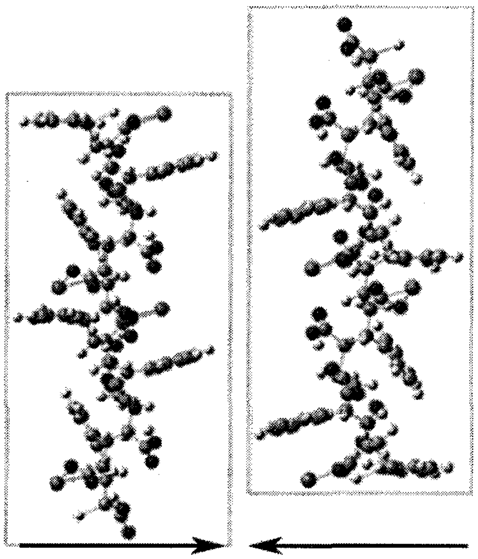

Figure 8: Association between linear isotactic SMA polymers is possible at neutral pH. Due to the alternation of hydrophobic and hydrophilic monomers along the polymer, association can only take place when polymers π-stack sideways.

In a flexible association, 2 sequences styrene monomers (rows), from each SMA polymer, π-stack (Figure 9): the sequences are located along the x axis in Figure 9. In the case of a rigid associations, four sequences of styrene monomers, π-stack, one on the main axis and one at 45° tilt to the main axis. Rigid dimers have less rotational freedom. Additionally, the styrene monomers sequence at a 45° angle to the main axis, is less populated with styrene monomers than the main axis sequence. Rigid associations between SMA polymers are supported experimentally from fluorescent studies of SMA polymer aggregates in water, where measurements of the fluorescence quenching of pyrene dissolved in SMA solutions was measured. The slow quenching observed indicated a rigid, micelle-like, hydrophobic interior [159].

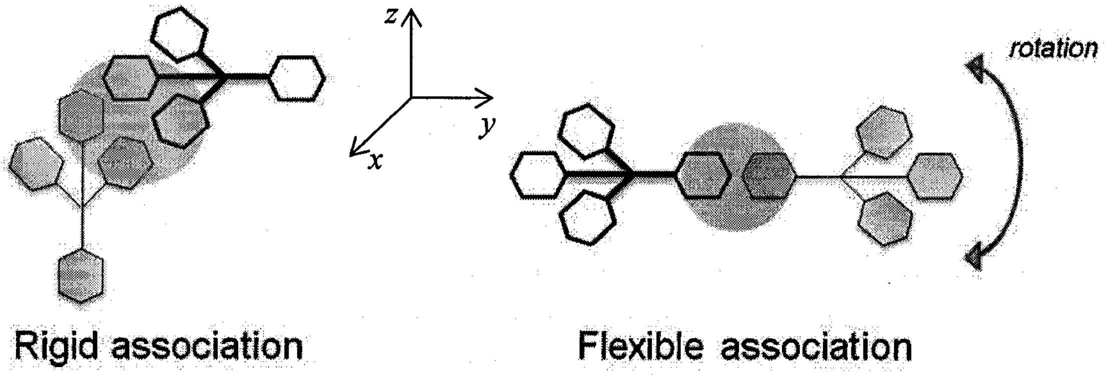

Figure 9: Association geometries between SMA polymers viewed from a cross-section view. The π-stacking association takes place along the polymers. Left: Rigid association with no possibility of rotation. Right: Flexible association which can rotate about the π-stacks.

The size of dimer associations are too small to account for the large sizes seen in DLS studies of aqueous solutions of SMA[157]. Therefore larger polymer aggregates, based on this type of association, were studied. Rigid dimer associations form preferentially because they generate more stabilizing energy than flexible associations from a larger number of π-stacking styrene monomer pairs. Rigid associations can only associate with other polymers through flexible associations. Both rigid and flexible associations occur because of association between the main rows of highly populated styrene monomers, but the rigid association has a few of those off centre, at 45°, styrene monomers which also π-stack and make the association rigid and bent at 90°. Quadrupole-quadrupole interactions, presented in Chapter I, are at the origin of this association.

## 2.1. Thermodynamics of the association between linear isotactic SMA polymers

The exact distance between SMA polymers was determined using a method developed to handle the large system. The association was studied using isotactic SMA pentamers, $(SSS)^5$, because they are sufficiently large to model the behaviour of larger polymers. Full geometry optimization, performed on the polymer structure [110], could not be performed on the association complex because of the many degrees of freedom of the molecules, being free in space. Terminal monomers exhibit edge effects in gas phase calculations, which distort their spatial arrangement with respect to the inner monomers, and their arrangement is not representative of the overall polymer structure. Therefore the pentamer polymer fragment was obtained from the optimization of an isotactic heptamer,$(SSS)^7$, and the terminal monomers were removed. The choice of a pentamer also reduces the degrees of freedom since it limits the π-stacking interactions to a linear polymer association. Hence, a computational scheme was developed to guide the optimization towards its optimal geometry using the initial optimized geometries of the polymers as starting points, and known experimental data on the π-stacking from similar systems involving π-stacking of benzene or styrene monomers; x-ray crystallographic data of styrene based alternating copolymer [149,160] and benzene dimers in phenylalanine [15,16,161].

Semi-empirical PM3 calculations were used to study the association because of its reliability in predicting the geometry of SMA polymers. Also, to determine the relative energies of π-stacking, PM3 had to be used because of the large system studied. Although high level Hartree-Fock calculations and Moller-Plesset[162] (MP2) methods with diffuse-polarized basis sets are most commonly used to study π-stacking energies and conformations of π-stacked complexes [23,151,163], semi-empirical methods closely reproduce the trends, although not providing exact energies. The PM3 results consistently overestimate the electrostatic contribution, but predict the changes in stabilization energies from changes in conformations between the aromatic moieties of $\pi$-stacked complexes[151]. Hobza *et al.*[151] studied different computational methods for determining the stabilization energies of DNA base pairing and found that MP2 and AMBER4.1 methods offer the best predictions for the true energy of association but that PM3 closely follows the energies. Because the interest is not in determining the true interaction energy of association, but relative energies and best association geometries, PM3 was chosen to search for the optimal association conformation and the relative changes in energy, with the knowledge that they do not represent accurate values. However, to confirm that the PM3 result is reasonable, MP2 single point energy calculations were carried out on a small section of the minimum energy PM3 conformation. Experimental values for the $\pi$-stacking energy of benzene groups are 7.5–25 kJ/mol while the optimal distance between the centres of the aromatic groups is between 4.5–6 Å.

The optimized isotactic SMA pentamers were placed in an association geometry, which maximizes $\pi$-stacking between styrene monomers (Figure 10). All atomic cartesian coordinates were frozen and the polymer backbones were separated by a certain distance, the inter-polymer distance (*r*). Constrained optimizations were performed by releasing only the coordinates of the styrene monomers that could interact and the geometry of system was left to optimize to a minimum energy. The inter-polymer distance was varied from 9.5 to 14 Å by increments of 0.5 Å: from overlapping styrene monomers to beyond the range of strong interactions. Constrained optimizations were carried out at each step.

The stability of the complex was evaluated by calculating the stabilization energy, Eq. 1. The Energy of the association geometry at a specified distance is given by $E(r)$, while the energy of the unassociated complex is given by $E(r \to \infty)$, where $r$ = 20 Å, beyond the range for any interactions between polymers. Subtracting both of these values provides a value for the stability of the association: negative values indicate a stabilized association, while positive values indicate a destabilizing association. Figure 10, is a summary of the method used.

$$E_{stabilization}(r) = E(r \to \infty) - E(r) \qquad r \to \infty,\ r = 20\text{Å} \qquad (1)$$

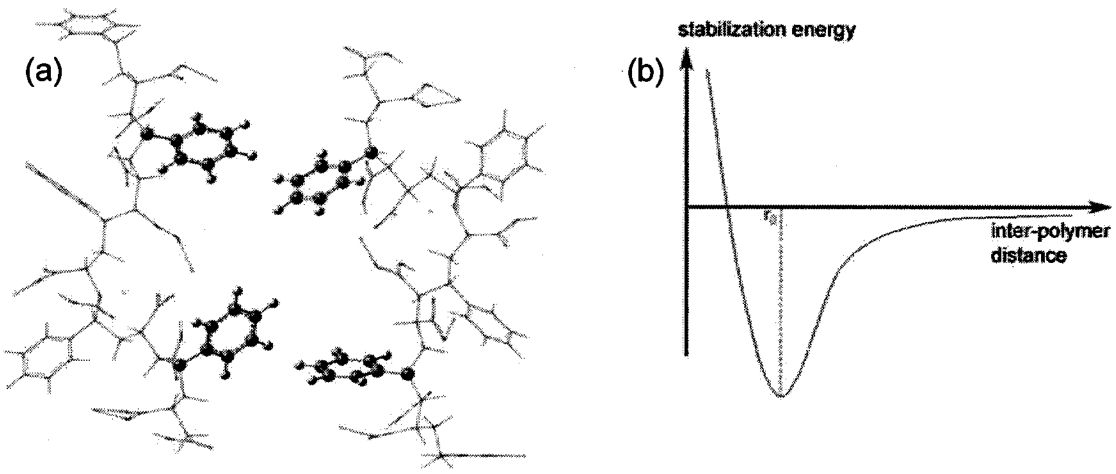

Figure 10: Visual representation of the method used to determine the distance between the polymers which corresponds to the minimum energy. (a) The cartesian coordinates of the geometry studied are frozen, only the styrene monomers that can π-stack are released (highlighted by the "balls and bonds" model). The inter-polymer distance is varied and the geometry is optimized at each step while maintaining the constraints. (b) Typical result, similar to a Lennard-Jones potential energy curve, obtained for the stabilization energy Eq. (1) as a function of polymer separation. Where styrene monomers π-stack, there is a maximum stabilization energy (minimum). At close distances there is steric repulsion and no stabilization energy is present, while at large separations there is no interaction between styrene monomers and the stabilization energy returns to its limiting case where $r=\infty$. The constraints on the $r_0$ association, with the lowest energy, are then removed and re-optimized using PM3.

To compare the minimum inter-polymer distances between the different optimizations with literature, the distance between the centres of the aligned styrene monomers in Figure 10 was measured, the inter-phenyl distance ($r'$). Figure 11, shows the relation between the stabilization energy as a function of $r'$. Results show an inter-phenyl distance of approximately 5.3 Å. The styrene monomers take on a configuration similar to a herringbone and T-shape association, expected for closely packed phenyl rings[17-19,164].

**Table 1**: Tabulated results of the stabilization energies, Eq. (1), and inter-phenyl distances for the modeled flexible association between two isotactic SMA pentamers.

| Inter-phenyl distance (Å) | Total PM3 energy (kJ/mol) | Stabilization Energy per styrene pair (kJ/mol) |
|---|---|---|
| 3.4 | -12176.1 | 26.6 |
| 4.0 | -12206.5 | 11.5 |
| 4.4 | -12225.1 | 2.13 |
| 4.8 | -12235.1 | -2.85 |
| 5.1 | -12242.9 | -6.75 |
| 5.6 | -12240.0 | -5.31 |
| 20.0 | -12229.4 | 0.00 |

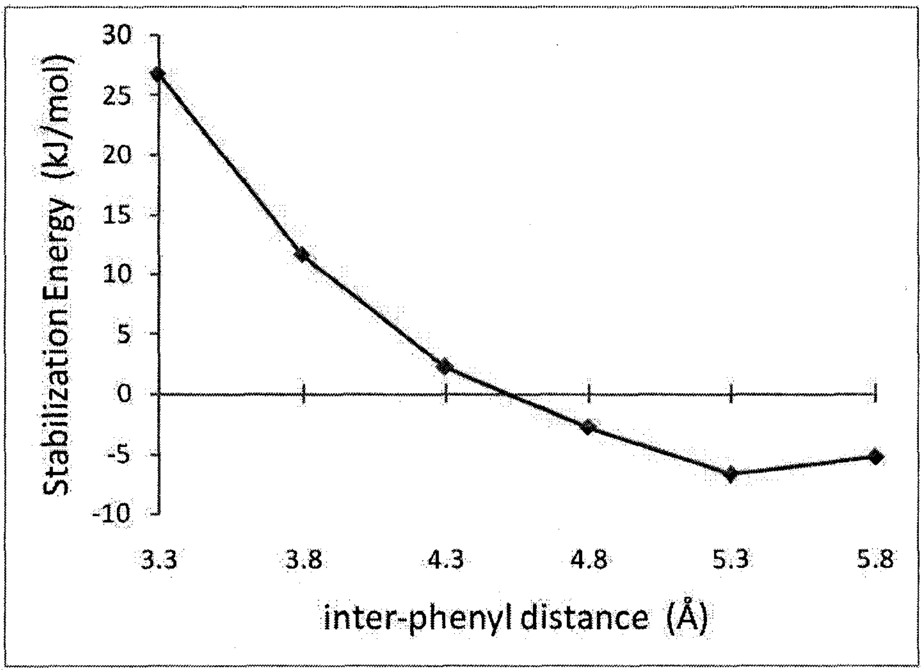

Figure 11: The stabilization energy for the association between two isotactic SMA polymers in a flexible association is shown as a function of inter-phenyl distance (*r*′ ).

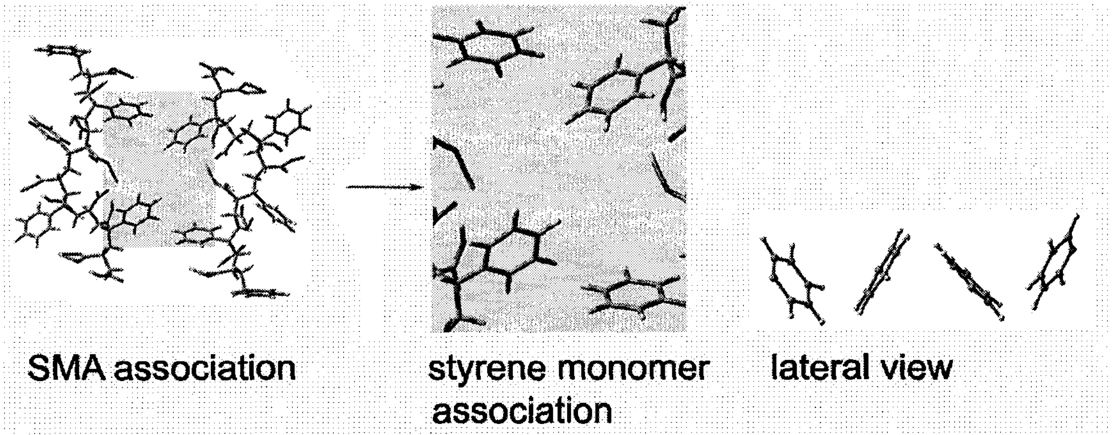

Figure 12: Optimized geometry of a two SMA polymers in a flexible association. From left to right: two pentamers in their minimum energy association, close-up view of the association and finally the lateral arrangement of the aromatic groups with the polymer chains removed.

To confirm that the PM3 conformation for the association is stable, MP2 single point energy calculations were carried out on a small section of the minimum energy PM3 conformation (Table 2). The MP2 energy was computed at the optimized distance and at 20 Å separation and then both were subtracted. The stabilization energy found was 13 kJ/mol. This value is similar to results obtained from experimental and theoretical values of π-stacking between benzene dimers[15,16,164]. The PM3 method therefore seems reliable in finding the minimum energy conformation, although the actual energy is not accurate and MP2 calculations are required.

The Delocalized Molecular Orbitals (DLMO) obtained using Hartree-Fock 6-31G* basis set for the SMA complex, show that the electronic density is shared between styrene monomers for σ–σ, σ–π and π–π bonding (Figure 13). The range of bonding type is better observed in the molecular orbitals obtained from the MP2 energy calculation of the π-stacking styrene pair taken from the PM3 optimized association between SMA polymers (Figure 13).

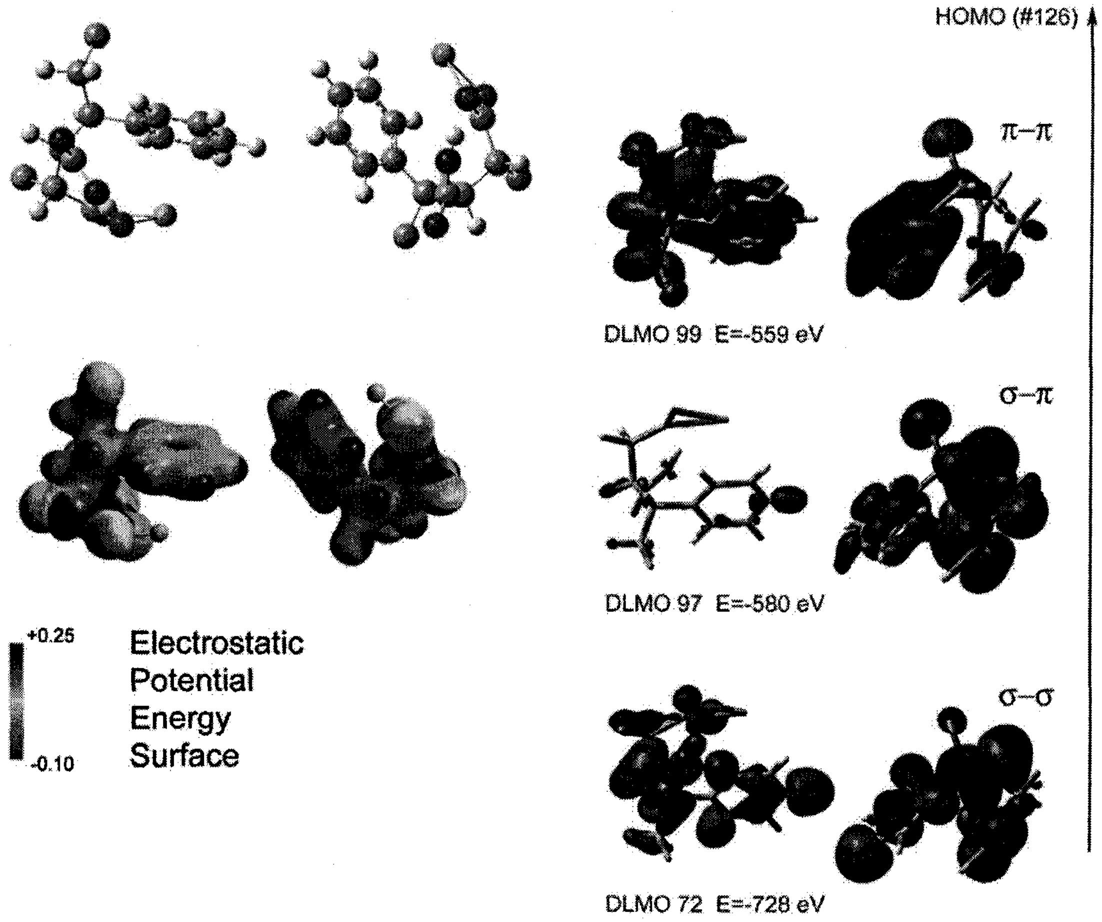

Figure 13: Fragment of the SMA association used to perform single point MP2 energy calculations. The fragment corresponds to two SMA monomers taken in the same association position as the PM3 optimized result. Shown, are the different character delocalized molecular orbitals that show shared electron density between the monomers through the aromatic styrene monomers. Also shown is the electrostatic potential energy surface, which illustrates the electrostatic attraction between styrene monomers.

Polymer association is enthalpically ($\Delta H$) favorable because each π-stack of styrene monomers, between SMA polymers, provides a stabilization of energy of about 13 kJ/mol. However, the loss of rotational, vibrational and translational degrees of freedom from the association creates a loss in entropy ($\Delta S$). The Gibbs free energy, which includes both enthalpy and entropy, Eq. 2, must be negative for the association to be favourable. If the negative enthalpy term is large enough and if the loss in entropy, which translates into a negative $\Delta S$ value, small, then the association complex preferentially forms.

$$\Delta G = \Delta H - T\Delta S \tag{2}$$

The change in enthalpy, which corresponds to the stabilization energy of SMA polymer association, was never calculated by theoretical methods. However, the loss in entropy factor ($T\Delta S$) was previously calculated by Malardier [1] and was found to be -2.9 kJ/mol for two SMA heptamers associating in a rigid association geometry, but for a flexible association, the loss of entropy is expected to be less. The entropy was calculated using Eq. (3), where the subscript *assoc* refers to the associated SMA complex and the *opt* subscript refers to the single optimized polymer. The values of enthalpy and Gibbs free energy were obtained from a semi-empirical PM3 Frequency calculation at 298.15°K, which provides thermo-chemistry data.

$$T\Delta S = \left(H_{assoc} - 2H_{opt}\right) - \left(G_{assoc} - 2G_{opt}\right) \tag{3}$$

Using the values from these calculations, The Gibbs Free Energy for two SMA pentamers in a flexible association with two π-stacking pairs, Figure 13, is $\Delta G = -21.9$ kJ/mol (Table 2). The association is therefore favourable because of the large gain in enthalpy from the ordered stacking of styrene monomers and the low loss of entropy caused by the stiffening of the chain from the multiple Hydrogen bonds along the chain. The polymers used in this research are typically composed of over 50 monomers and therefore the gain in stabilization energy, corresponding to $\Delta H$, from the association of two styrene monomers is additive. The polymer gains in stability by associating.

**Table 2**: Thermodynamic data showing the stability of a flexible association between isotactic SMA pentamers.

| Thermodynamic parameter | Energy, (kJ/mol) |
|---|---|
| Stabilization energy **PM3**<br>$r'$=5.3Å *(per styrene monomers pair)* | -3.4 |
| Stabilization energy **MP2**<br>$r'$=5.3Å *(per styrene monomers pair)* | -13 |
| | |
| $\Delta H$ , Enthalpy of association | -26 |
| $\Delta S$, Entropy of association | -2.9 |
| $\Delta G$, Gibbs Free Energy of association at 298°K | -21.9 |

## 2.2. Association between more than two SMA polymers

The most stable association between two SMA polymers is the rigid association because of the greater number of π-stacking pairs. Further association of these rigid complexes with other SMA polymers can occur through the weaker, flexible association. The π-stacking described is in

Figure 14. The flexible associations can bend without any loss in enthalpy and no steric hinderence, such that different types of sheet structures are possible (Figure 14 on the right).

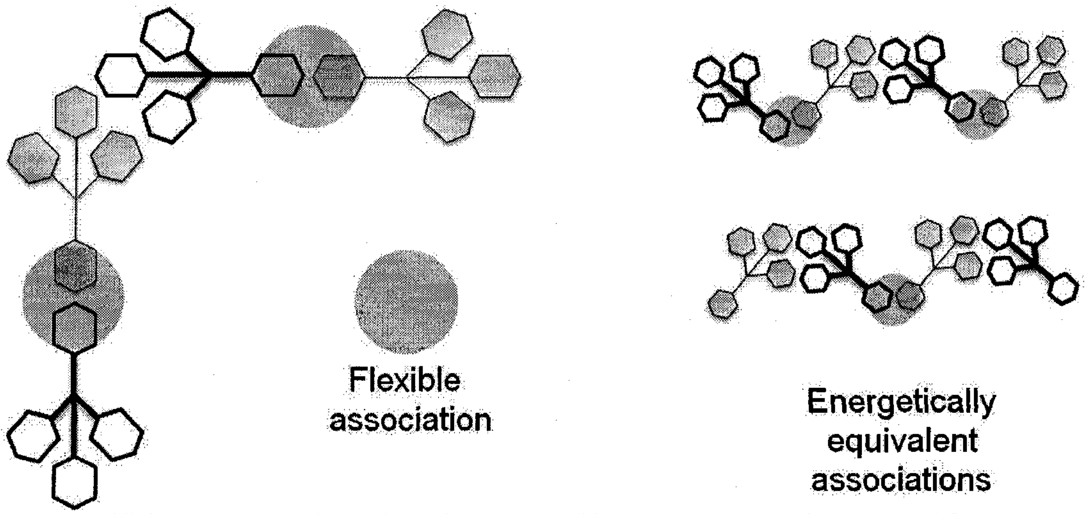

Figure 14: Higher order complexes from rigid and flexible associations. Left: Additional SMA polymers can add to the rigid association through flexible associations. Right: SMA polymers in flexible associations can rotate and form different sheet structures that are energetically equivalent to the left pictures.

## 2.3 SMA Nanotubes: from polymer sheets to closed tubular structures

Using the model above, the theoretical dimensions of the nanotube can be determined more accurately and an improved understanding of the association of SMA polymers into nanotubes and the association between nanotubes can be achieved. It is thought that rigid associations form first and then flexible associations can form between the rigid ones.

A mixture of flexible and rigid associations leads to flexible polymer sheets, because the rotation about the flexible association of styrene monomers occurs without any loss in stabilization energy because the polymers have no steric strain (Figure 9). Each polymer-polymer association is stabilizing. Sheets can grow from a series of flexible associations between rigid associations until the size of the sheet becomes a destabilizing factor to the addition of further polymers because entropy is lost as the system grows. The gain in stabilization energy from two polymers associating is not negligible and the system lowers its Gibbs Free Energy by associating more polymers. As sheets grow there are free styrene ends on each side of the sheet. The system can reach a more stable configuration and avoid the free styrene ends by forming a closed loop, therefore maximizing styrene-styrene interactions and minimizing unfavourable styrene-solvent interactions. This forms a closed square structure of 8 SMA polymers, which is a short segment of a polymer nanotube. Figure 15 shows how sheet structures from 8 SMA polymers can associate by π-stacking of the terminal aromatic groups of the sheet; optimized inter-phenyl distances and association angles were taken from the PM3 optimized flexible association of isotactic SMA polymers. Measurements of the inner diameter and outer diameter using different reference points, gave an outer diameter of (4.1 ± 0.2) nm, and an inner diameter of (2.5 ± 0.2) nm. These measurements are similar to the diameters found in cryo-TEM and neutron diffraction studies[1].

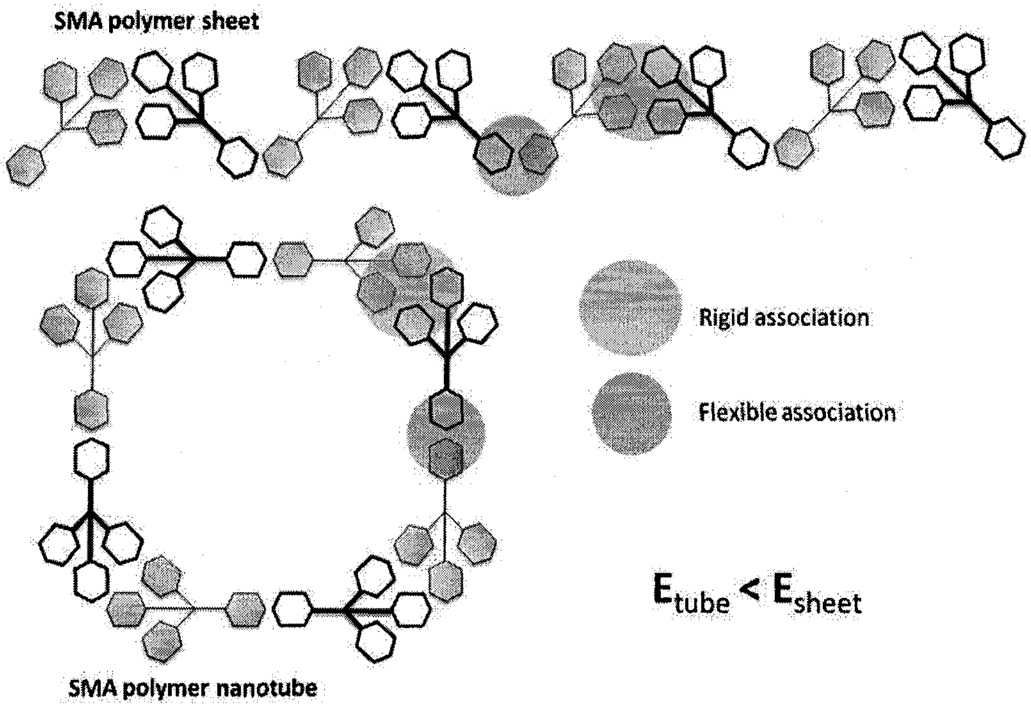

Figure 15: Association of SMA polymer sheets of rigid and flexible associations into nanotubes from the association of free styrene monomers at the ends of the sheet. The nanotube structure is more stable than the sheet structure because it gains further stabilization energy with minimal loss of entropy.

The short nanotube segment can grow linearly, particularly if the polymer is polydisperse. Polymer chains which extend beyond the short segment can behave as nucleation points for the continued growth of the nanotube (Figure 16). This allows the nanotube to grow longer than the contour length of an SMA polymer.

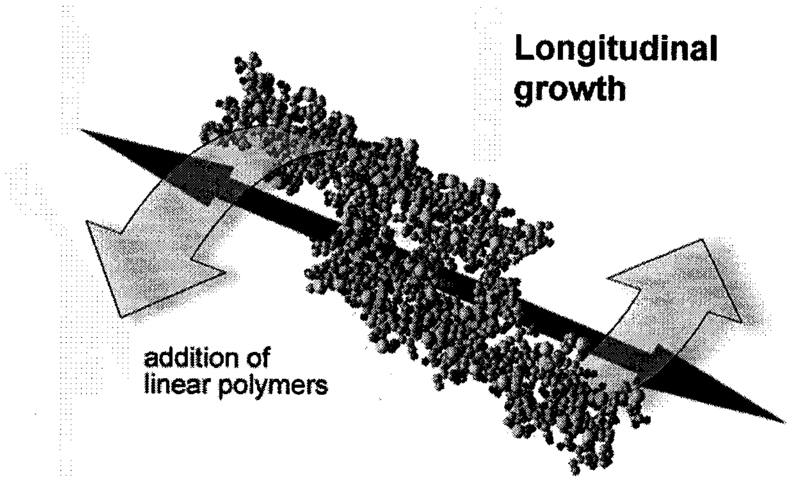

Figure 16: Mechanisms by which SMA associates into long hollow nanotubes (**left**) that can stack side by side (**right**) because of further $\pi$-stacking from the unassociated styrene monomers at the edges of the nanotube. Shown are SMA pentamers associated into a nanotube as described in Figure 15.

## 3. Tertiary association structure: association between SMA nanotubes

Free styrene monomers remain at the outer edges of the nanotubes, therefore these structures can interact by this common row of styrene monomers and form stacks of the nanotubes (Figure 17). This represents the tertiary structure of associating SMA polymers. The association is expected to be similar to the studied case of flexible SMA association.

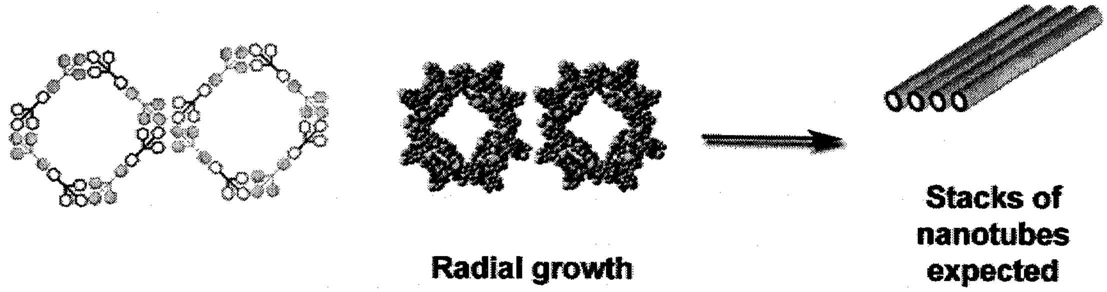

Figure 17: Schematic of the aggregation between SMA nanotubes corresponding to the tertiary structure.

## Concluding remarks

The relationship between SMA polymer structure and its association behaviour in solution was investigated using molecular modeling. It was shown that when modeled at neutral pH, the SMA polymer becomes linear because of an internal Hydrogen bond between the carboxylate groups of the succinic acid monomer. It was shown that the structure of SMA remains similar for different chirality sequences, the spatial arrangement of the monomers is similar, but not identical, such that two different chiralities are of similar structure but cannot be superimposed. Furthermore, changes in the chiral site 2 do not appear to change the structure of the polymer. Polymers with superposable structures, such as two isotactic polymers, can associate through rigid and flexible associations and the rigid association is more stable since it forms more π-stacking interactions. Once polymers associate into the more stable rigid associations, they can only further associate through flexible associations. The π-stacking of a model system composed of two isotactic pentamers was modeled and the stabilization energy obtained, and the minimum energy geometry of the styrene monomers, both agreed well with literature values of enthalpy and geometry. The lateral association between SMA polymers produces polymer sheets, which can form nanotubes from 8 SMA polymer chains by bending at the flexible rotation points, in the flexible associations. The polymer nanotubes grow in length by π-stacking of additional polymers to the free styrene monomers at the tube extemities. The nanotubes also have free styrene monomers ouside the tube and can aggregate into stacks of nanotubes. Therefore, experimentally, it is expected that the length of the tubes is greater than the contour length of the SMA polymer used, their diameter is of the order of 4 nm and the nanotubes can stack toghether.

The theoretical calculations were performed using isotactic isomers because it is in theory possible to produce such polymers with the proper stereo-selective catalyst, but this has however not been possible to achieve experimentally. The general structure of different chiralities is similar (similar cross-section styrene monomer distributions). The distribution of styrene monomers is however different between different chirality sequences, and are therefore not superposable. No general conclusion can be reached at the moment, since these calculations are only preliminary and it is difficult to cover the range of all different chiralities. It is therefore possible that only superposable structures can self-assemble into nanotubes. The chirality of the SMA polymer samples available are however random. It would be of great value to obtain an isotactic polymer. This would simplify both the theoretical studies and the experimental optimization of the nanotube fabrication.

The experimental preparation and characterization of these structures and the evidence of the proposed mechanism for the association of SMA into sheets, tubes and stacks of tubes was investigated and the experimental results obtained are presented in the Chapter II.

# Experimental investigation of the self-assembly poly(styrene-alt-maleic anhydride) nanotubes

## Chapter III

## Abstract

The experimental conditions to obtain linear poly(styrene-alt-maleic anhydride) (SMA) nanotubes were investigated. Theoretical modeling of the association between SMA alternating copolymers at neutral pH, when the polymer is close to its monosalt form, provided detailed requirements for obtaining linear SMA nanotubes. The chemical composition of the polymer, and its degree of protonation, seem to be the two most important factors governing nanotube formation. A highly alternating SMA polymer was synthesized. Additionally, an improved method to achieve the monosalt condition was found, and proved to be a reliable method to prepare SMA nanotubes. Different molecular weight SMA polymers were studied and the synthesized 12,000 Da polymer seemed to provide the best SMA nanotubes. TEM and AFM size measurements agreed, within experimental error, with the theoretical conclusions from Chapter II.

## Introduction

It was theoretically shown how SMA polymers can self-associate into linear nanotubes with an outer diameter of 4.1 nm, and an inner diameter of 2.5 nm (Chapter II). It was also shown that these nanotubes can grow in length by associating additional polymers and that should have a tendency to stack parallel to each other, caused by additional $\pi$-stacking along the side walls of the nanotubes. The self-association mechanism was supported thermodynamically (Chapter II) and the theoretical SMA conformational results (Chapter II) agree with previous theoretical work[110] and with experimental studies of the viscosity changes[165] and of the changes in polymer aggregate sizes in aqueous solution[157] as a function of pH. The experimental preparation of the SMA nanotubes was based on the conclusions from theoretical modeling. Linear polymer nanotubes should form at a 50% degree of protonation, where intra-molecular Hydrogen-bonding stiffens the polymer and allows linear conformations. In addition, the polymer should be strictly alternating to allow $\pi$-stacking. The hollow interior of the nanotube is more hydrophobic than the exterior and allows the SMA nanotube to be loaded with monomers; this was studied using pyrrole monomers.

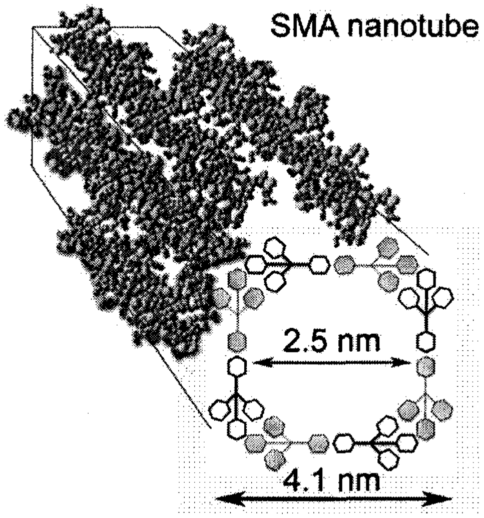

Figure 1: Cross-section view of 8 SMA polymers associating into a nanotube and theoretical dimensions.

Initially, the composition of the SMA polymer was controlled by a radical addition fragment transfer (RAFT) type polymerization that ensures that the alternation of styrene (St) and maleic anhydride (MAh) is present in high yield (~95%). The effect of changing the molecular weight of the polymer was investigated, because the length of the polymers in self-assembled structures usually influences the type of structures formed, and also their stability[166-173]. Three different $M_w$ samples were available, two commercial ones and one which was synthesized. The best results were obtained using the synthesized polymer of intermediate $M_w$. Secondly, the preparation method initially used did not produce a detectable amount of nanotubes, and therefore the preparation conditions were re-investigated to establish a reliable method to prepare SMA nanotubes in quantity and reproducibly. The main challenge was to control the degree of protonation of the polymer and restrict it to the area of 50% protonation of the succinic acid. Titration experiments were conducted with the synthesized polymer and compared to literature. The stability of the nanotubes formed at different pH was also investigated with the synthesized SMA sample. The base used to prepare the nanotubes was modified and showed different aggregation behaviour. The pH was also controlled using a buffer solution.

## 1. Control of the Alternation in SMA using RAFT Polymerization

To characterize the SMA nanotube samples, Transmission Electron Microscopy (TEM) and Atomic Force Microscopy (AFM) were used. These methods allow the direct observation of the nanostructures. Spectroscopic methods were used investigated to probe the formation of $\pi$-stacking complexes, but proved unsuccessful. Further details on these studies are given in Chapter VII.

For SMA polymers to self-assemble as theoretically predicted, the polymer composition must match the structure modeled. The polymer must be strictly alternating, with the absence of polymerization errors, between St and MAh monomers. Typically, SMA is polymerized using free radical polymerization methods. These methods rely on the reactivity ratios being sufficiently different that the resulting polymer is generally alternating, but unfortunately not throughout its structure. The selectivity of the free radical polymerization, and the high temperatures used (~80°C), produce non-alternating sequences along the polymer, which are short polystyrene blocks involving two or more St monomers between MAh monomers. The alternation is good, but not excellent, and this can prevent the ordered association between SMA polymers to occur as modeled theoretically. This was in fact observed when using commercial SMA products for which lower yields were observed than for the synthesized sample. To remedy this problem, SMA was synthesized using a UV-controlled RAFT polymerization method developed by Wu *et al.*[174] The method produced a polymer with a 50.1% styrene content and a 49.9% maleic anhydride content. It was also important to verify the alternating sequence of the polymer; this was done by $^{13}$C NMR DEPT and comparing the chemical shifts for different triad distributions with literature[174-176]. The SMA polymer synthesized had >95% alternating St-MAh-St sequences. The synthesis is described below.

The SMA polymer used in the experiments was synthesized by a RAFT type method using a UV sensitive initiator, 1-(ethoxycarbonyl)prop-1-yl dithiobenzoate (EPDTB) [174]. The proposed reaction mechanism is shown in Figure 2.

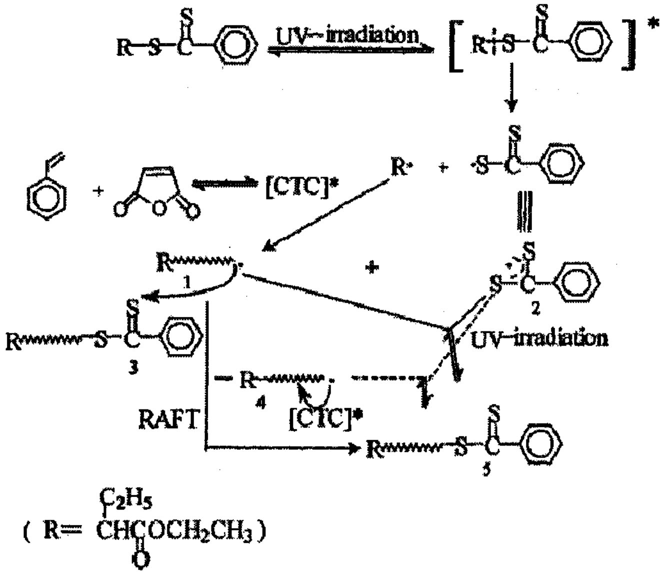

Figure 2: Proposed reaction mechanism for the synthesis of highly alternating poly(styrene-alt-maleic anhydride) by a UV-controlled radical copolymerization by Wu *et al.* [174].

### 1.1. Synthesis of EPDTB Initiator

Using the procedure of Wu *et al.*[174], phenyl magnesium bromide was prepared from bromobenzene (6.25g, 0.04mol) and magnesium turnings (1.05g, 0.04mol), both purchased from Aldrich. The reaction was carried out in dry THF. THF was distilled from a constant deep purple solution of sodium benzophenone under nitrogen. The THF solution was kept at 40°C and carbon disulfide (3.00g 0.04mol) was added dropwise over 10 min. Ethyl $\alpha$-bromobutyrate (7.05g, 0.036mol) was added to the brown solution. The temperature of the solution was increased to 80°C and kept constant for 48 hours. Ice water was added (50mL), the organic layer separated and the aqueous phase extracted with diethyl ether (3x 100mL). The organic phase and the extracts were combined and washed with water, brine and dried with anhydrous magnesium sulphate. The solvent was removed by rotovap. The residue was purified by column chromatography (mesh type) using n-hexane/diethyl ether (9:1) as an eluent. The product, EPDTB, was a red oil (2.85g, % yield). The $^1$H NMR (300 MHz, $CDCl_3$) of the product confirmed the identity and agreed with the work of Wu *et al.*: ppm (d, TMS, H) 1.26 (m, 6H, $2CH_2CH_3$), 2.06 (m, 2H, $CHCH_2CH_3$), 4.22 (q, 2H, $OCH_2CH_3$), 4.69 (t, 1H, SCHCOO), 7.49 (dd, 2H, meta-ArH), 7.65 (dd, 1H, para-ArH) and 8.02 (d, 2H, ortho-ArH).

### 1.2. Synthesis of Polymer

St (Aldrich) was distilled under reduced pressure after the polymerization inhibitor was removed by filtering the commercial St through neutral alumina, and leaving the filtered St over calcium hydrate overnight. MAh was purchased in form of briquettes (Aldrich) and was recrystallized from benzene. The polymerization was performed in THF under nitrogen. EPDTB, St, MAh and THF were added successively into the flask in the following molar ratio: EPDTB:St:MAh = 1:150:150. The volume of THF used was 0.75mL per g of monomers. The solution was stirred and degassed by 3 freeze-thaw-vacuum cycles and the flask was sealed under nitrogen. The flask was left in a UV chamber (4 lamps, 150 watts, 20 cm from lamps) at room temperature under constant nitrogen pressure. The polymerization was carried out for 48 hours.

After polymerization, the polymer was recovered by precipitation in a 30 fold volume of methanol. The polymer was dried in a vacuum oven at 50°C. The composition of the polymer was verified by $^1$H NMR and the peak integration indicated a St content of 50.1% and a MAh content of 49.9%; an aromatic region at 6 – 8 ppm and maleic anhydride at 1.5 – 4 ppm. The Alternating sequence and the ratio of E to Z configurations [174,176,177] was evaluated by performing $^{13}$C NMR DEPT, and revealed a E:Z ratio close to 1:1.

## 2. Degree of protonation of SMA in deionized water at different pH

The degree of protonation is important to find the pH at which the monosalt form of SMA occurs. In Chapter II, it was shown that for the monosalt condition, internal Hydrogen bonding occurs, stiffening the polymer and allowing ordered polymer associations.

SMA has three different protonation states, with two pKa values at pH 4.4 and pH 10.2[156], which were confirmed experimentally by titrating a 0.1% solution of the synthesized SMA polymer, $M_w$ 12,000 Da, in its monosalt form with NaOH and back-titration with HCl. Back-titration gave the most reliable results because the rate of protonation of succinic acid is much faster than the rate of hydrolysis of maleic anhydride.

The SMA polymer in solution has a characteristic spectrum (inset Figure 3), with a high absorbance in the UV region from the aromatic styrene monomers and a particular set of 3 peaks around 250-260 nm, which are independent of the pH and which can be used to follow the concentration. Using the peak at 258 nm, a linear calibration curve for the wt. % concentration of SMA polymer in water, 12,000 $M_w$, was plotted (Figure 3). The initial solution was prepared in a 1 L volumetric flask, to which 0.0996 g of polymer was added, and dissolved using excess NaOH. The solution was diluted to the concentration in the calibration plot. There was no change in the UV-Visible spectrum of SMA at different pH.

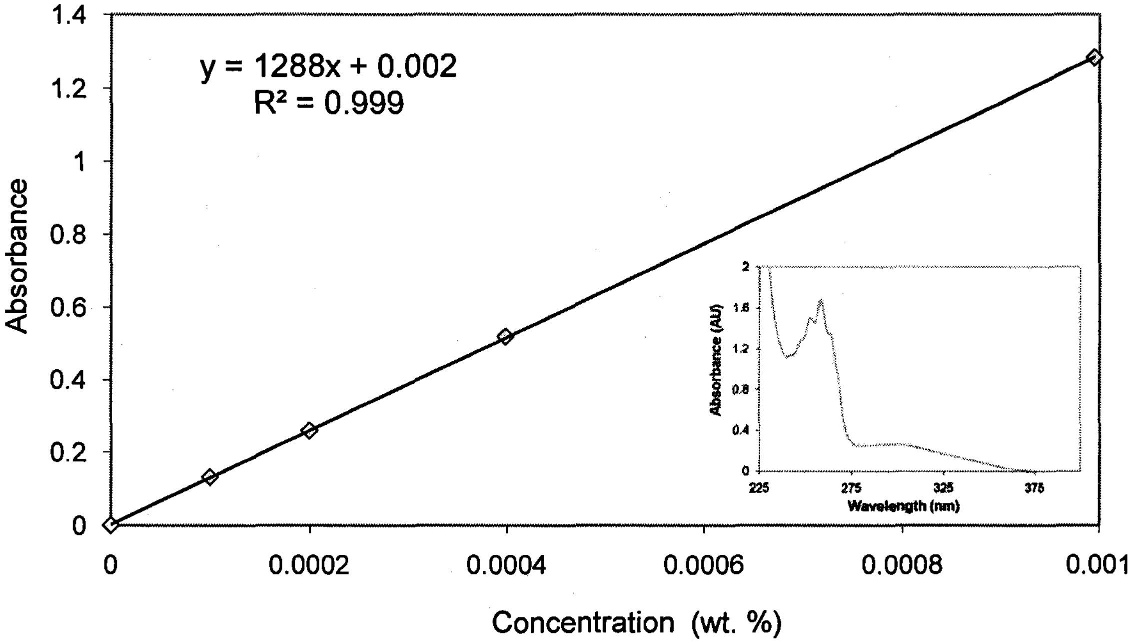

Figure 3: Linear calibration curve for the concentration of SMA in water. Synthesized SMA (Mw 12,000) was used. NaOH was initially used to dissolve the polymer. Inset: UV-Visible spectrum of SMA dissolved in water, the sharp peak at 258 nm was used as a reference.

SMA was dissolved in deionized water (0.1 g in 100 mL) and the solution sonicated to give a homogeneous suspension. The initial pH was 3. The solution was titrated with a 0.01 N NaOH solution to give pH 12. pH measurements were recorded for every 2 drops added, and waiting ½ min for the pH to stabilize. The solution was then back-titrated with a 0.01 N HCl solution requirering approximately 10 s for the pH to stabilize. The titrating solutions were prepared from standard 1 N solution (Riedel-de Haën). The polymer concentration was calculated from a calibration curve by measuring the absorbance of the final solution at 258 nm. The front and back titration curves are shown in Figure 4.

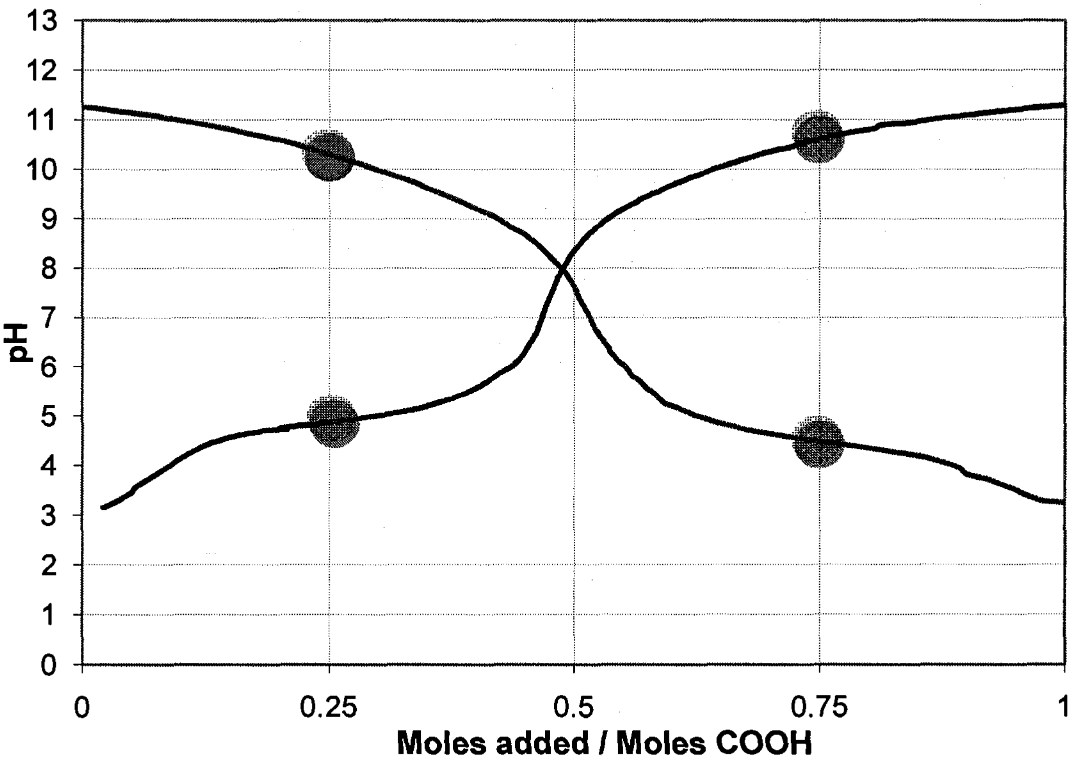

Figure 4: Front (Blue) titration with NaOH and back (red) titration with HCl of 0.1% wt. solution of 12,000 Da $M_w$ SMA dissolved in deionized water. pKa values were identified as being at 0.25 and 0.75 molar equivalent of acid or based added to moles of COOH groups in succinic acid.

The degree of protonation, or deprotonation, was calculated from the pKa values at 0.25 and 0.75 equivalent of acid, or base, added to the polymer, taken from the titration curves: experimental values for $pKa_1$=4.5 and $pKa_2$=10.3. Eq.1 was used to calculate the degree of protonation. At 50% protonation pH=pKa. To plot the curve, the two $pK_a$ values were treated as separate curves with two half protonation states (0.25 and 0.75). The degree of protonation $\alpha$ is given by Eqs.[178] 3 and 4 for the both the front and back titrations. The results are plotted in Figure 5.

$$\text{pH}=\text{pKa}+log\left(\frac{[A^-]}{[HA]}\right) \quad (1)$$

$$\gamma = \frac{[A^-]}{[HA]} \quad (2)$$

$$\alpha = \frac{\gamma}{1+\gamma} \; pH < 7 \quad (3)$$

$$\alpha = \frac{\gamma}{1+\gamma} + 1 \; pH > 7 \quad (4)$$

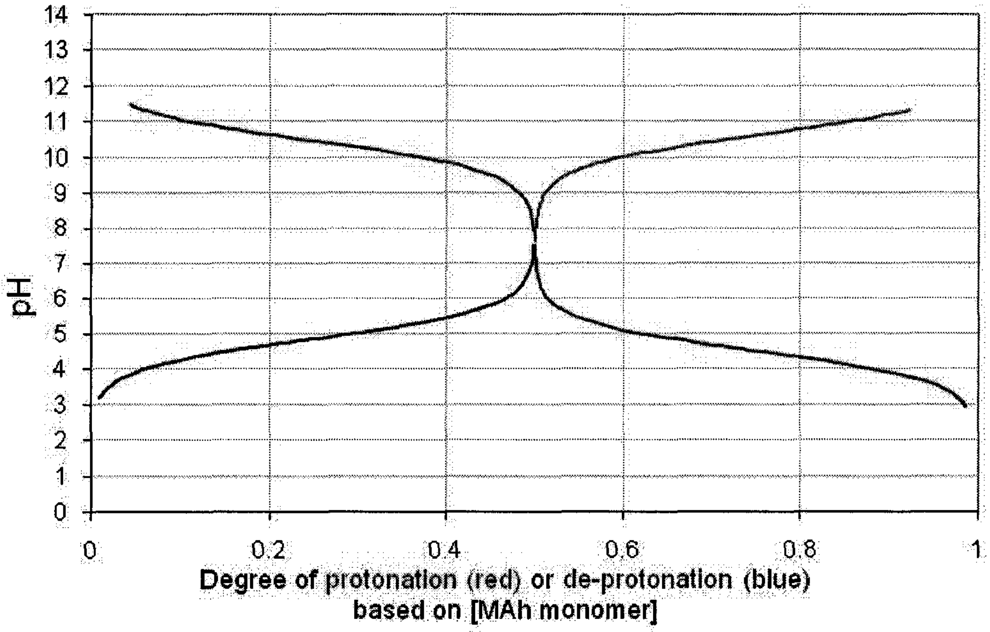

Figure 5: Degree of protonation at different pH values for SMA obtained from the front and back titrations of a 0.1% wt. 12,000 Da $M_w$ SMA dissolved in deionized water.

## 3. Experimental preparation of SMA nanotubes

Having established the importance of reaching a monosalt form for SMA to give linear nanotubes, a method to arrive at the required pH was investigated. Three main variables are at play to give the SMA monosalt: the type of base used to form the monosalt, the method of addition of the base, and the properties of the solvent, the ionic strength and aqueous/organic ratio.

### 3.1. Nanotube preparation by addition of base: *initial preparation*

Following Malardier's work[1], SMA nanotubes were prepared from three molecular weight SMA polymers: commercial SMA, $M_w$ 1,600 Da, purchased from SP$^2$, SMA synthesized following the method described above, $M_w$ 12,000 Da and SMA from Aldrich having a $M_w$ of 50,000 Da. Malardier's method is referred to, as the *initial* method.

SMA of $M_w$ 12,000 Da, was added to deionized water to form a 0.1% wt. solution. The mixture was stirred and sonicated until the polymer was dispersed, forming a milky opaque solution. Using standard 1 N NaOH solution, an equivalent molar amount of NaOH was added, to moles of MAh monomers. The solution was stirred and sonicated until the dispersion formed a homogenous transparent solution. The final pH of the solution was approximately 6.2. AFM and TEM studies of the polymer morphologies obtained using this initial method of preparing SMA nanotubes did not produce any linear nanostructures, neither with the low nor high molecular weight SMA polymer, but gave amorphous aggregates and large compound micelles. AFM and TEM results are shown in Figure 6 for $M_w$ 12,000 Da SMA.

One main problem observed was the difficulty in hydrolyzing the maleic anhydride monomers. When only adding the equivalent amount of base, nothing guarantees that all the maleic anhydride monomers will reach monosalt equilibrium in an experimental acceptable time period. Referring to Figure 5, at pH 6.2, the degree of protonation has not reached 50% and this method cannot itself guarantee against variable amounts of dissolved $CO_2$ or variations in the ratios of moles of base to moles of MAh. For example, water taken directly from the deionized water distributor has a pH of 6.5-7, but leaving the water exposed to air for a few hours decreases the pH up to 2 pH units. In addition, the association between SMA polymers is enthalpically favourable as shown in Chapter II (Table 2) and consequently, disordered polymer associations can form, and remain locked in that association. Once locked, the energy required to break up the aggregate and form an ordered flexible or rigid association exceeds the gain in energy from the disordered associations. Disordered associations cannot form nanotubes.

### 3.2. Improved nanotube preparation method by slow equilibrium to monosalt using dialysis: *Improved preparation*

Theoretical modeling of the polymer structure showed that the SMA polymer must be in its monosalt form to be linear and capable of self-assembling. Therefore the *initial* approach to fabricate these SMA nanotubes cannot provide a reasonable yield of nanotubes to be experimentally detected and produces amorphous polymer aggregates. A slow transition from disordered polymer chains (random coils) to linear polymers would also improve the ordered association.

A different approach to reach monosalt equilibrium was developed and tested to ensure that it was reliable and robust for fabricating SMA nanotubes, the *improved* method. The procedure involved completely hydrolyzing the MAh monomers in the SMA polymer using an excess of base, to reach a pH beyond the second pKa. This ensures that all MAh monomers are hydrolyzed and no anhydride remains on the polymers. The next step involves reaching the monosalt state. Here two options were available: i) acidify the basic solution with an acid or ii) dialyze the basic SMA solution against deionized water to lower the pH back to its monosalt state. While both may work, the second one was chosen because it allows a slow equilibrium from a disordered conformation to a linear conformation, which is caused by the internal Hydrogen bonds that form along the linear polymer. This is though to occur though a slow formation of Hydrogen bonds as the pH is lowered and could decrease the number of disordered associations formed. This method did produce a greater yield of SMA nanotubes; the method was applied to both the commercial low $M_w$ SMA and to the synthesized higher $M_w$ SMA.

Solutions of 0.01 to 0.1% wt. were prepared; the SMA polymer was dissolved in deionized water, with a resistivity of 18 MΩ·cm, from a NanoPure system. An excess of base was added (NaOH), 2 to 2.5 Eq. moles to MAh monomers. This allows all the maleic anhydride rings to be fully hydrolyzed. The pH of this solution was around 13. The solution was dialyzed against deionized water using a 1000 $M_w$ cut-off membrane from SpectraPore. The water was changed every 6 hours for 2 to 3 days, until the pH inside the dialysis bag was in the proper pH range, between pH 6.5-8, where the degree of protonation is approximately 50%, corresponding to the monosalt form of SMA.

### 3.3. Characterization of nanotubes using pyrrole as a marking agent

The association interactions are sensitive to drying, which causes the nanotubes to decompose rapidly. Air exposure for more than a few hours destroys most nanostructures. Also, TEM observation of the hollow tubes does not allow for a clear measurement of the structure because they decompose in less than a few seconds, too short a time to collect data under the electron beam.

To avoid this problem, a method developed by Malardier[1] was used to make the structures more resistant to drying. Pyrrole was used to fill the hollow interior of the tubes and stiffen the structure. The pyrrole was used as a marking agent, to improve the contrast. Pyrrole can polymerize after diffusing into the hydrophobic interior of the nanotube or depositing onto the polymer through Hydrogen bonding, therefore increasing the density and the stability of the tube, and improving its detection with TEM. It is not yet understood where the pyrrole is located.

1 drop of pyrrole per mL was added to a 0.1% wt. SMA-NaOH nanotube solution. The mixture was kept under dark and stirred for 12 hours; the solution was light brown in colour. The solution was poured into a quartz vial and exposed to a UV source for 24 hours, consisting of 4 lamps of 150 W. The solution turned dark brown and after leaving it under ambient light for 3-4

days, turned green without precipitates. The solution remains homogeneous independent of time but does turn black with time because of the polymerization of free pyrrole. However, the green colour is recovered after diluting the poly(pyrrole) filled solution in deionized water. Poly(pyrrole) is insoluble in water, but becomes soluble when in the SMA nanotubes.

### 3.4. Experimental results for the *initial* and *improved* preparation methods

The *initial* and the *improved* method of preparing SMA nanotubes were both done with the synthesized SMA polymer of $M_w$ 12,000 Da. SMA nanotubes were prepared using the *initial* method (section 3.1). To the solution, pyrrole was added and polymerized (section 3.3). Nanotubes were not observed, only amorphous aggregates and unassociated polymer were present. AFM and TEM samples were prepared by depositing a drop of the solution, letting it stand for 5 min. and absorbing the excess on a filter paper (Wattman 100) (Figure 6). The pH of the solution was pH 6.2. The pH was then increased using a 0.1 N standard NaOH solution to the pH 7.5, close to a 50% degree of protonation. The same results were observed as for pH 6.2. The slow hydrolysis rate of maleic anhydride in deionized water, non-uniform hydrolysis of maleic anhydride monomers because of an unequal molar ratio of base to MAh monomers and the formation of non-reversible disordered associations from the rapid pH change may explain the absence of nanostructures.

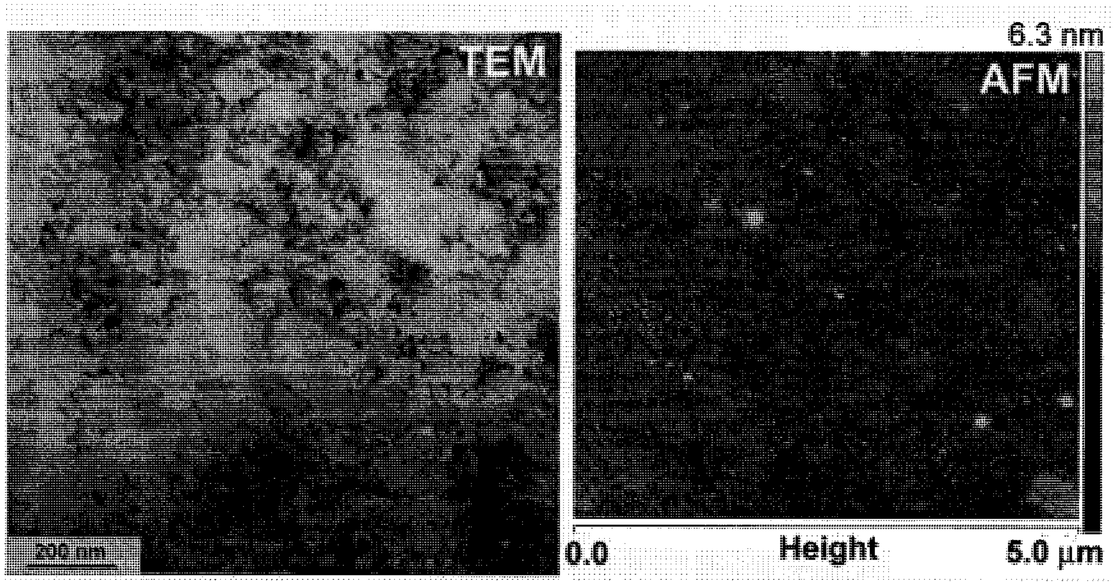

Figure 6: SMA polymer aggregates prepared using the method described by Malardier [1] where an equivalent molar amount of NaOH was added to a 0.1% wt. solution of SMA and pyrrole was used as a marking agent. Nanotubes were not observed, only amorphous aggregates and free polymer. Left: TEM scan. Right: AFM scan with 0–5 µm distance scale bar and 0–6.3 nm colour gradient height bar.

The preparation involving dialysis was also used, with NaOH as the base, to prepare the SMA nanotubes from the SMA, $M_w$ of 12,000 Da. The SMA nanotubes were observed without use of pyrrole as a marking agent. The nanotubes were (4.5 ± 1.6) nm in diameter, and 20–50 nm in length, on the order of the contour length of the SMA polymer used (Figure 7). The nanotubes were difficult to observe because of the organic nature of the sample and the rapid decomposition of the nanostructures under the electron beam. The decomposition rate was reduced by the poly(pyrrole), allowing improved sample imaging. The pyrrole core in the nanotubes seems to stabilize the polymer nanostructures and allow a more stable longitudinal and radial growth.

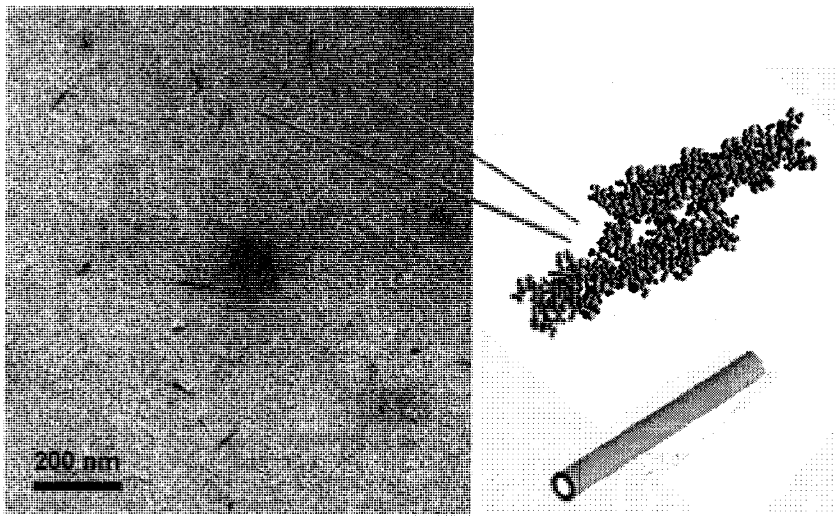

Figure 7: TEM of empty 12k $M_w$ SMA nanotubes, lengths are on the order of the polymer contour length.

Pyrrole was consequently used as a marking agent. The method described in section 3.3 was used. Stacks of linear rods were observed scattered over the surface. The rods observed by TEM formed stacks of 10-50 rods, each having lengths of 100-800 nm (Figure 8).

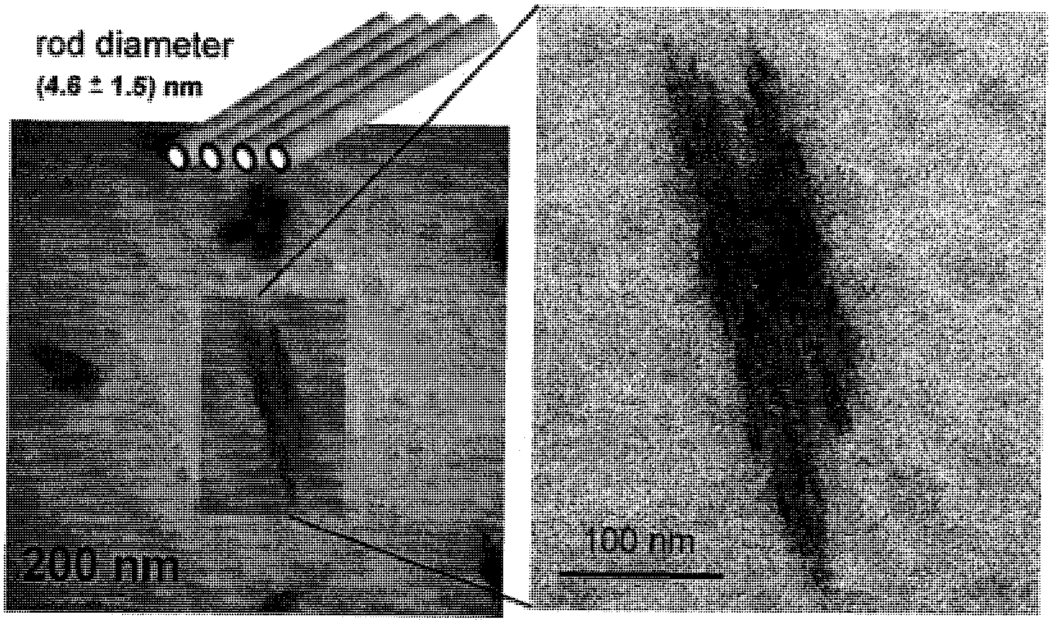

*Figure 8:* TEM results *for* poly(pyrrole) filled SMA nanotubes (0.1% wt. solution). Stacks of nanotubes were observed on the right hand side; the cartoon represents what is observed. The dark lines represents short oligomers of poly(pyrrole) inside the SMA nanotube and the lighter material is the SMA polymer which composes the nanotube walls.

Pyrrole was polymerized under different pH conditions, using NaOH and HCl, to reduce or increase the pH. The samples were imaged by TEM as a control experiment. The shapes observed were dendritic aggregates on the surface. Structures similar to the stacks of nanotubes were not observed. The results are shown in Figure 9.

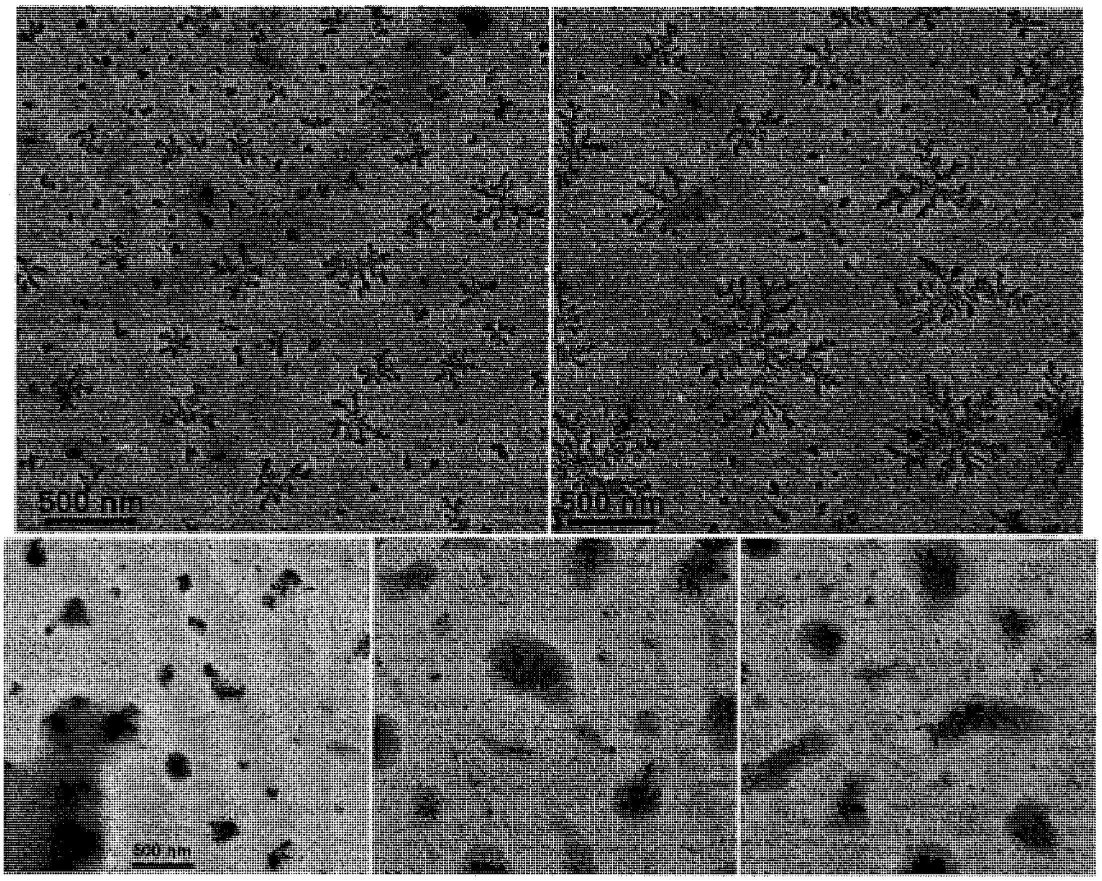

Figure 9: TEM images of control experiments of pyrrole without SMA. Deonized water samples were pH adjusted to **3 (top)** and **7 (bottom)**, pyrrole added in the same concentration and polymerized in the same UV conditions as the samples which included SMA nanotubes. No linear rod-like structures were observed.

## 4. Effect of varying molecular weight on the size of SMA nanotubes

The three different molecular weight SMA polymers were used to prepare nanotubes using NaOH as a base and dialysis; for $M_w$ 1,600, 12,000 and 50,000 Da. The SMA nanotubes were treated with pyrrole to characterize them. For the 1,600 Da sample, no nanotubes were observed, only amorphous aggregates. If there are tubes with this $M_w$ sample, these were too small to be detected because the contour length of the polymer is approximately 4 nm. In addition, low molecular weight can prevent rigid associations from forming because of off centre styrene monomers needed for rigid associations are not present, often enough, along the short polymer backbone, consequently flexible associations might preferentially form instead. When modeling the heptamer conformation (Chapter II), which is a good model for the octamer in SMA 1,600 Da, the amount of off-centre styrene monomers are ¼ of the number of styrene monomers on the main axis. The off-centre monomers are responsible for the rigidity, if there are not enough off-centre $\pi$-stacking pairs, the association becomes flexible and nanotubes do not formed. For the 12,000 Da sample, stacks of 10-50 nanotubes were observed with length varying from 100-

800 nm as in the previous experimental section. With the 50,000 Da sample, stacks of 10-20 nanotubes were observed with lengths of around 100-200 nm. The poly(pyrrole) filled 50k $M_w$ SMA nanotubes are shown in Figure 10.

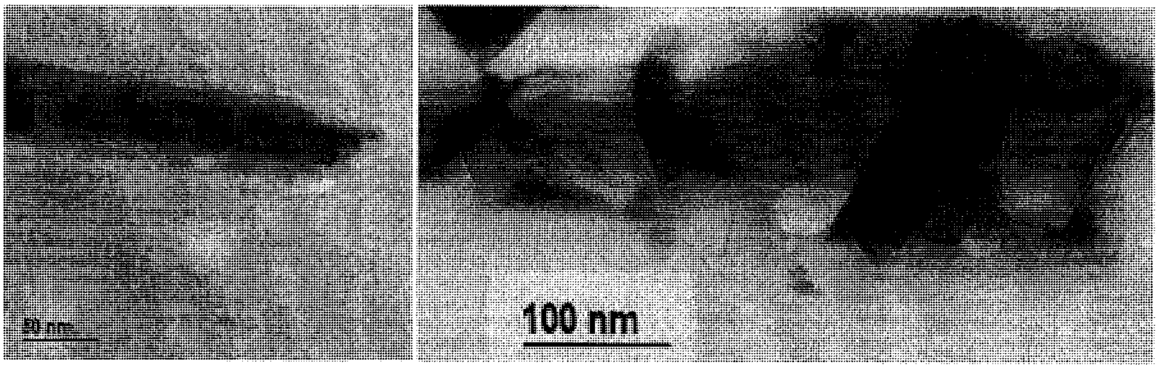

Figure 10: TEM images of SMA $M_w$ 50k filled with pyrrole. **Left**: nanotubes with diameter of 5 nm protruding from an amorphous aggregate similar to the bottom TEM image **Right**: The nanotube stacks are the ordered stripes on the amorphous material. The dark areas are believed to correspond to poly(pyrrole) and are 1.5 ± 0.4 nm diameter.

Both the 12k and 50k $M_w$ samples self-assembled into nanotubes of similar diameter. The yield of nanotubes was larger for the 12k Da sample. If the surface morphology is representative of the solution morphologies, the 12k Da SMA has about 25% of the polymer associated into nanotubes. The 50k Da SMA had a lower percentage of polymer associated into nanotubes, less than 5%. The 50k SMA sample is commercially produced using radical polymerization, which may introduce non-alternating sequences in the polymer and prevent ordered self-assembly. In addition, the 12k SMA polymer has a contour length of approximately 30 nm. The length of the tubes observed varies from 1 to 10x the contour length. Whereas hand, the 50k SMA nanotubes have lengths on the order of the contour length. This indicates that the 50k $M_w$ polymer forms nanotubes of similar length but associates less polymers than the 12k $M_w$ sample. The 50k $M_w$ SMA nanotubes seem more linear and rigid than the lower molecular weight nanotubes of comparable length as seen from the denser poly(pyrrole), which is distributed linearly with equal spacing between nanorods, more so than the 12k Da SMA sample (compared Figures 8 and 10). This may be due to the lower amount of polymer required to form a nanotube that has the same length with high $M_w$ SMA than with the intermediate $M_w$ SMA sample because the high $M_w$ sample polymers are longer. A 12k $M_w$ SMA nanotube behaves more like a chain of rigid segments linked by flexible junctions, when compared to a 50k $M_w$ SMA nanotube.

## 5. Stability of SMA nanotubes at different pH values

The preparation method involving dialysis was used with NaOH as the base to prepare the SMA nanotubes from the 12,000 $M_w$ SMA sample. The pH was varied by adjusting the dialysis time and tracking the pH of the solution during dialysis. Different pH values were studied: 7.9, 7.6, 7.2, 6.5, 6 and pH 5. The poly(pyrrole) filled nanotubes observed with TEM for pH 7.9 to 6 solutions were not significantly different. However as the pH was lowered to 5, the nanotubes observed were shorter and the stacking was disrupted. Nanotubes were not observed in solutions whose pH was greater than 8 or lower than 5: pH 3, 4, 8.5 and 9 were studied.

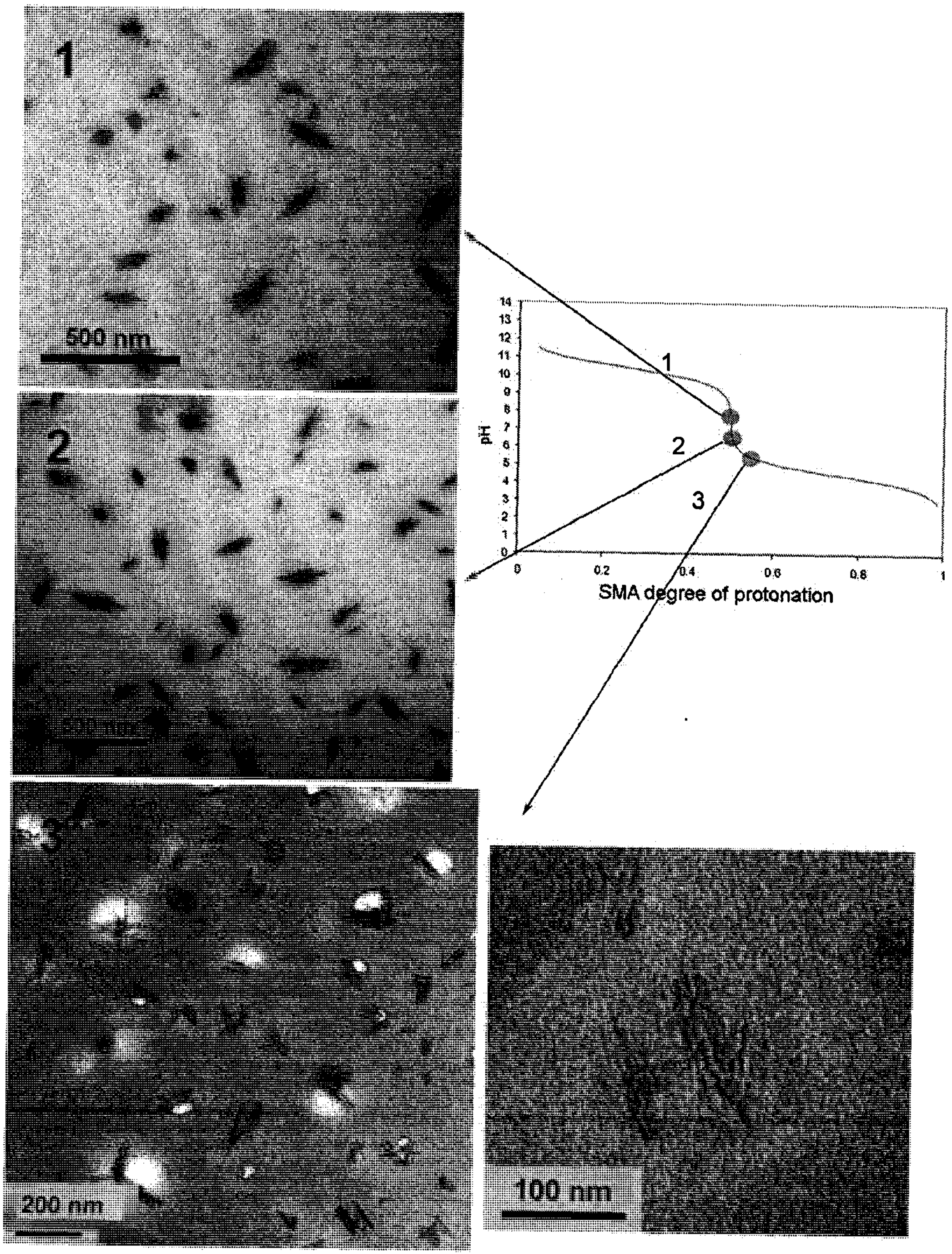

Figure 11: Stability of SMA nanotubes at different pH values. At around 50% protonation of the maleic anhydride groups, the yield is similar and the surface is covered with stacks of rods. However at a pH>8 and pH <5, nanotubes are not observed.

## 6. Effect of alkali metal (X) XOH bases on aggregation of SMA nanotubes

Using different bases, $X^+OH^-$, to prepare the SMA nanotubes showed different aggregation properties for different bases. There appears to be a relation between the counter ion used and the length of the obtained tubes and their stacking properties.

When the different nanotubes were imaged, using the poly(pyrrole) filling technique, different aggregation behaviour were observed. 0.1% wt. SMA solutions were prepared, thereby maintaining the concentration constant for purposes of comparison. For LiOH, the nanotubes were short and small stacks were observed. Using NaOH, the original base, the nanobutes were longer and stacked in similar flat aggregates of nanotubes. When KOH was used, large disordered aggregates were observed, with nanotubes longer than obtained using NaOH. For RbOH longer nanotubes were observed and the nanotube stacks were longer and composed of fewer nanotubes . Nanotubes prepared with CsOH seemed to be much longer than with RbOH, and aggregated into stacks of 2 or 3 nanotubes. The TEM scans of the nanotubes prepared using these different bases are shown in Figure 12 and the average rod sizes are shown in Table 1.

**Table 1**: SMA nanotube aggregation properties and sizes with different bases.

| ***Base used*** | ***Hydrated cation size*** (Å) [179-182] | ***Hydrated cation volume*** (Å$^3$) | ***Aggregation size*** | ***Rod diameter*** (nm) |
|---|---|---|---|---|
| **LiOH** | 3.40 | 165 | Rods < 50 nm<br>Stacks 5-10 tubes | 4.1 ± 1.1 |
| **NaOH** | 2.76 | 88 | Rods ~100-800 nm<br>Stacks ~10-50 tubes | 4.6 ± 1.5 |
| **KOH** | 2.32 | 52 | Rods > 500 nm<br>Stacks > 50 tubes | 4.0 ± 1.2 |
| **RbOH** | 2.28 | 50 | Rods ~ 30-500 nm<br>Stacks < 5 tubes | 4.7 ± 2.0 |
| **CsOH** | 2.28 | 50 | Rods > 1 µm<br>Stacks < 5 tubes | 5.2 ± 1.4 |

The secondary and tertiary structures of the SMA nanotubes can be observed in the TEM images in Figure 12. The primary structure was presented in Chapter II, as the linear SMA polymer chains. The secondary structures are the nanotubes formed from many SMA polymers, which associate into similar diameter nanotubes. The tertiary structure is the stacks of nanotubes, in which nanotube length and in the number of nanotubes that aggregate.

As shown in Table 1 and in Figure 12, the use of different bases to form SMA nanotubes does not affect the secondary structure because all nanotube diameters are similar, within experimental error. However, the tertiary structure seems to be dependent on the nature of the base used because nanotube lengths and aggregation numbers vary with the nature of the cation used. It was also noted that the contrast of the nanotubes increased with the increasing atomic number of the cation. CsOH SMA nanotubes were denser than nanotubes prepared with LiOH. This may indicate that the cations are electrostatically condensed on the SMA polymers, which increases the overall density of the nanotube and its presence may also influence the tertiary structure properties.

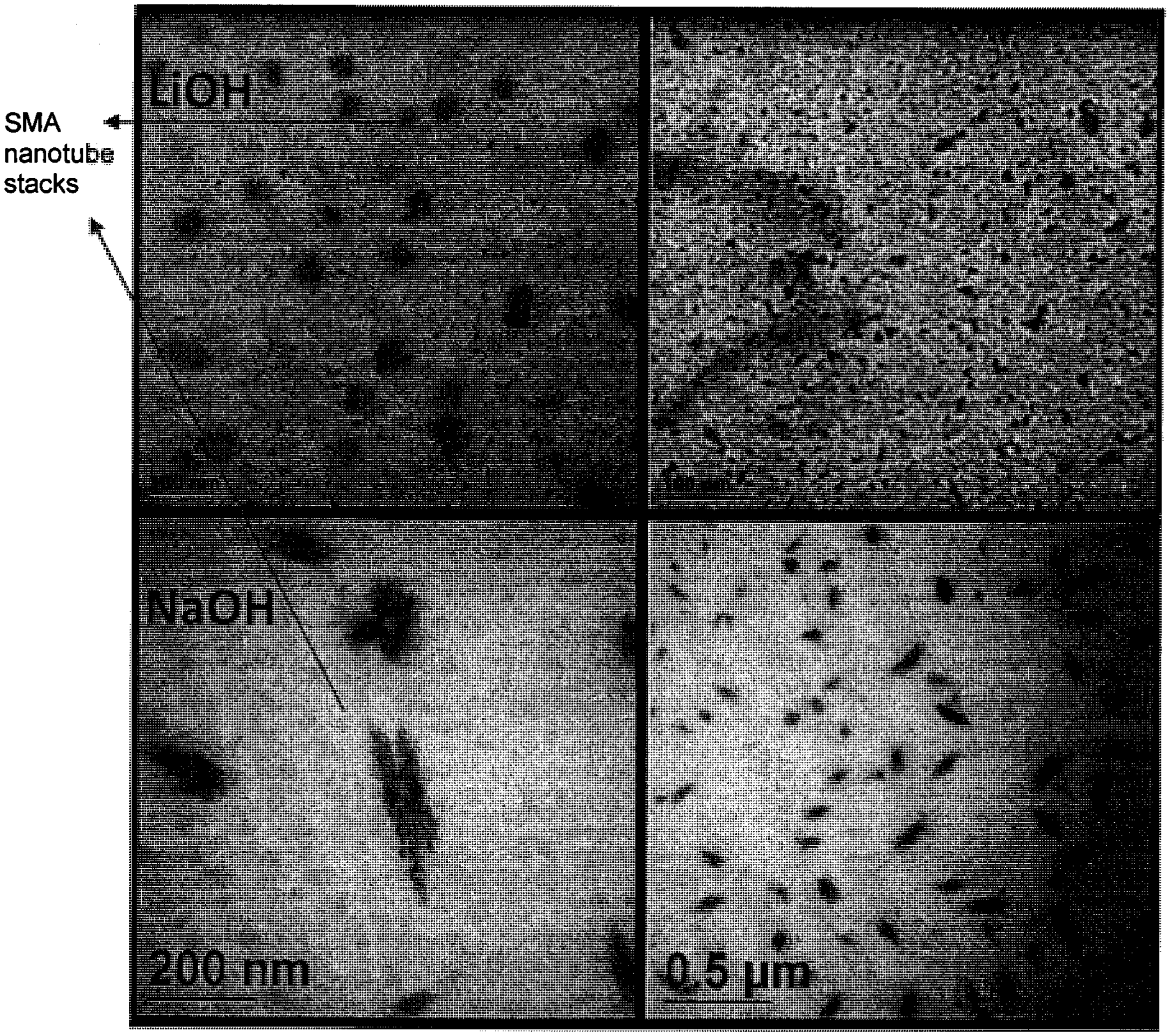

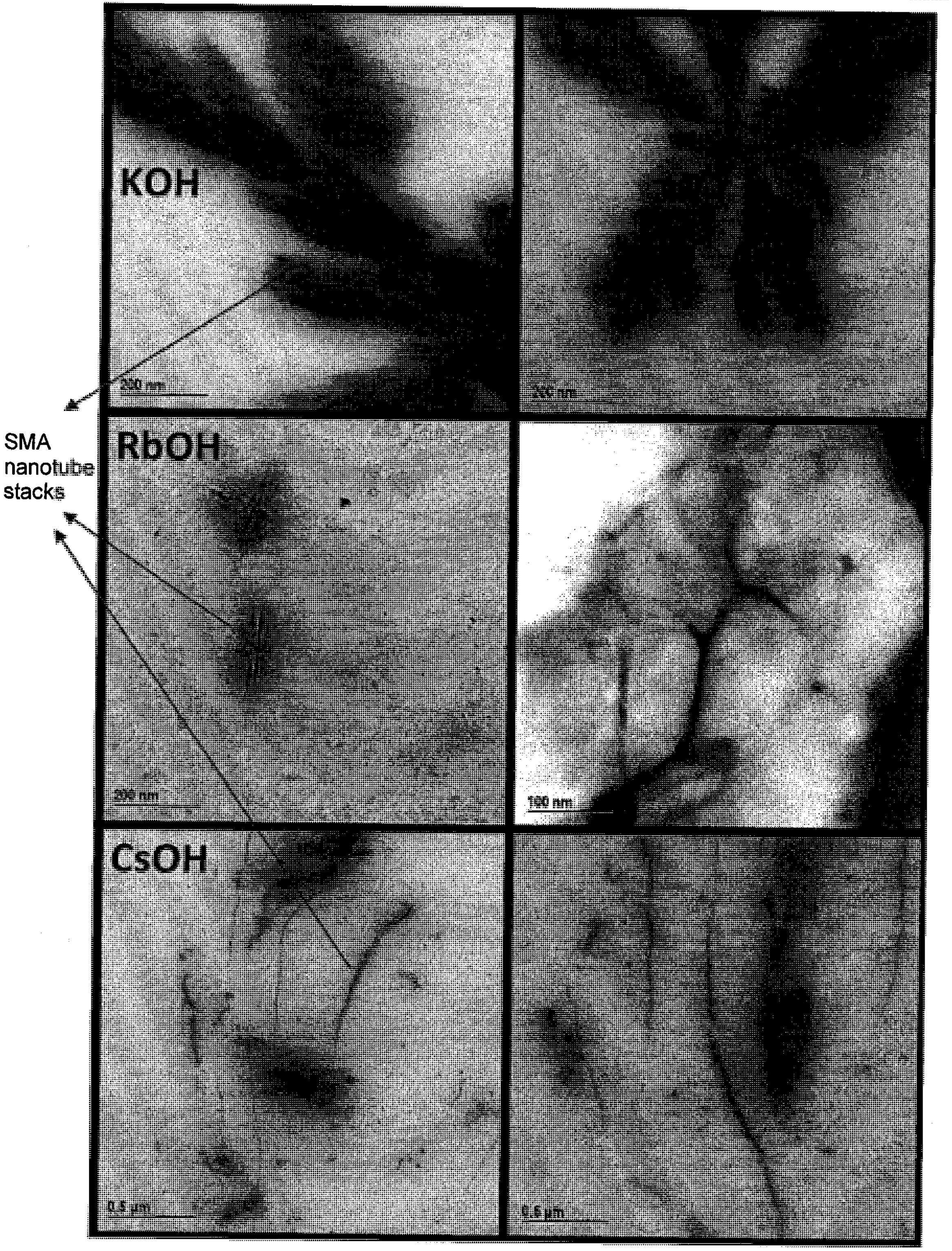

Figure 12: TEM micrographs of the poly(pyrrole) filled SMA nanotubes at pH values ranging between 7 to 8, corresponding to a 50% degree of protonation of the polymer. Different bases were used and the concentrations were kept constant for each preparation as well as the amount of pyrrole added.

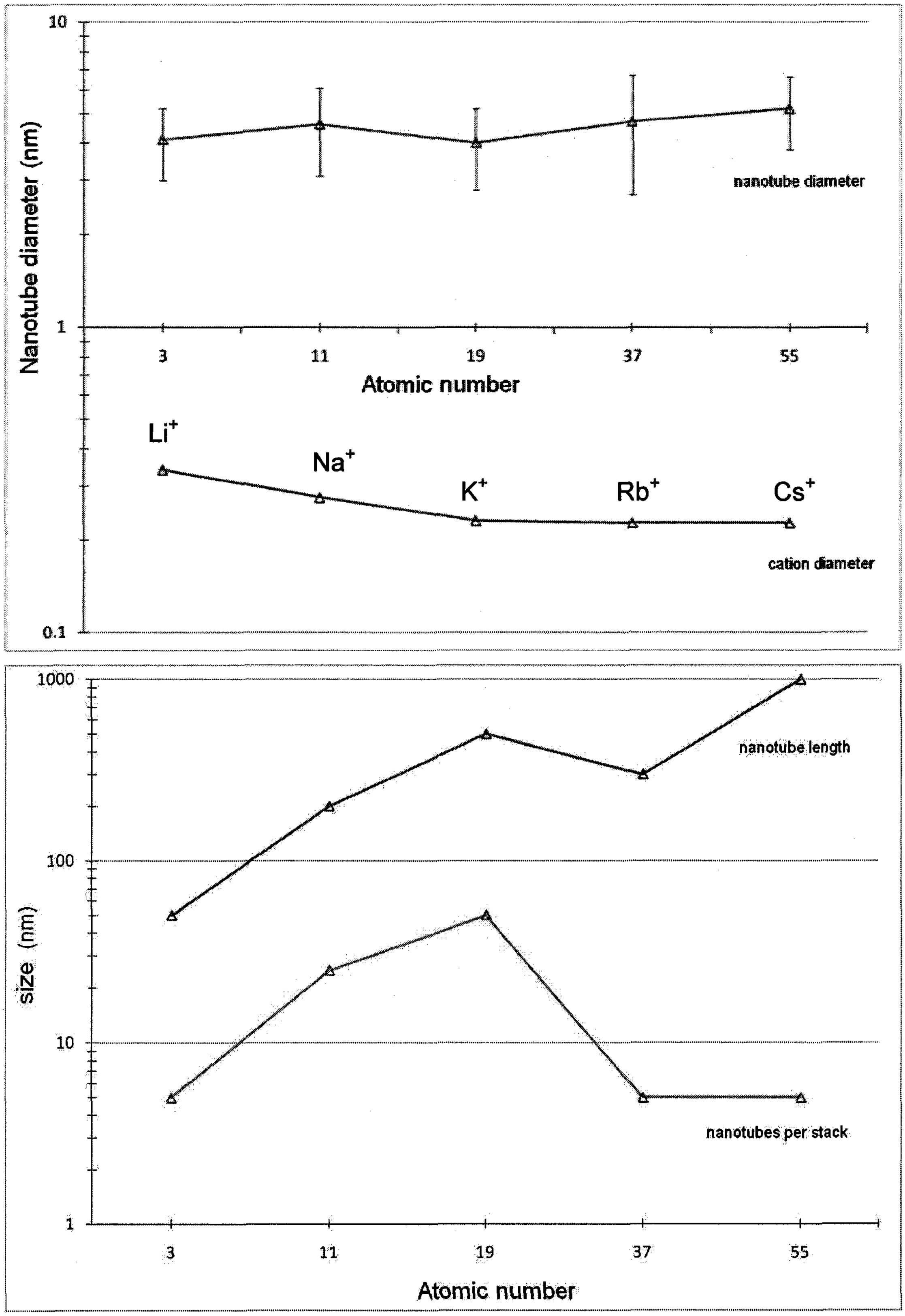

Figure 13: dimensions of the secondary (*top*) and tertiary (*bottom*) structure of SMA nanotubes as a function of the base used to dissolve SMA polymer for nanotube formation.

## 7. pH control, dialysis against a buffer solution: SMA nanotubes and sheets

To control pH, the 0.1% wt., 12k $M_w$ SMA polymer solution was dissolved in excess base dialyzed against a 0.1 N $KH_2PO_4$ and NaOH buffered to pH 6.5. The solution was observed under AFM on freshly cleaved mica after freeze drying a drop of the solution diluted 100 fold.

The results are in Figure 14; the polymer forms layer structures of uniform height, which correspond to the height of the SMA polymer sheets described in Chapter II. The measurements show a height of approximately 1.1 to 1.3 nm. The height of the domains is constant and in some areas increases to double height values, and this may be caused by polymer sheets stacking over each other or the presence of nanotubes, which have the same height as two sheets.

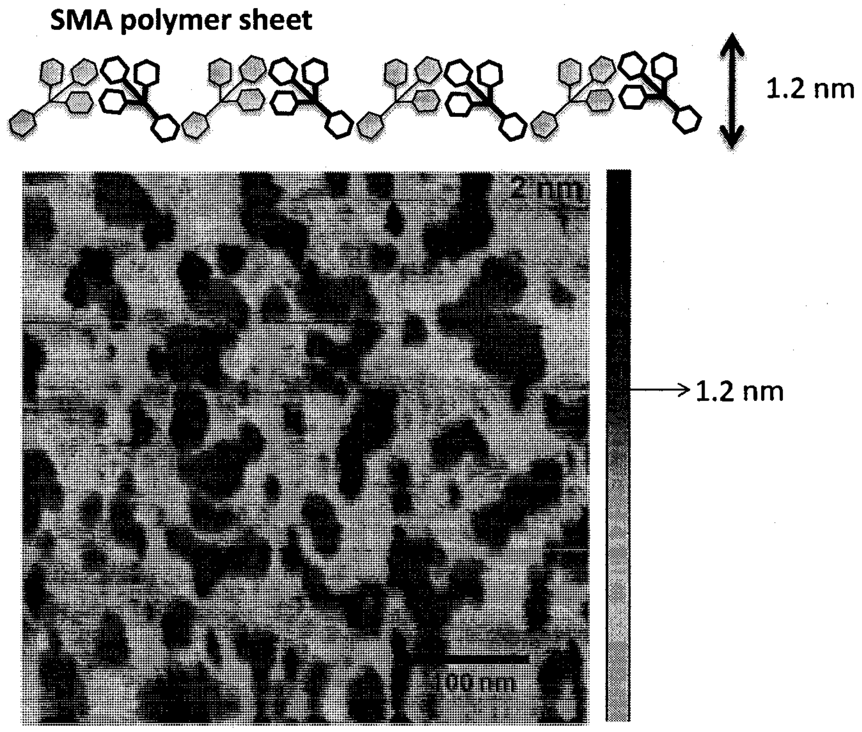

Figure 14: AFM of SMA sheets measuring between 1.2 and 1.4 nm in height. The associated polymer forms aggregates of uniform height and are composed of tens of polymers. One SMA polymer has a contour length of approximately 30 nm and a diameter of 1 nm.

In other regions, linear features of similar height to the theoretically estimated diameter of SMA nanotubes were observed (Figure 15). These structures agree with the theoretically predicted structures of stacked nanotubes also observed experimentally by TEM. The height of the structures varies from 3.5–4.5 nm, which agrees with the theoretical dimensions in Chapter II. However, because of the lack of stability of the nanotubes when dried, the features observed were discontinuous, and may be attributed to Raleigh instabilities, which are also observed in other polymer nanotube systems[183]; as the solvent sublimates, the nanotubes loose their stability and coil into small amorphous aggregates, a phenomenon termed *pearling*. The TEM technique of adding pyrrole was performed, but the artefacts attributable to poly(pyrrole) outside the tubes prevented adequate sample imaging.

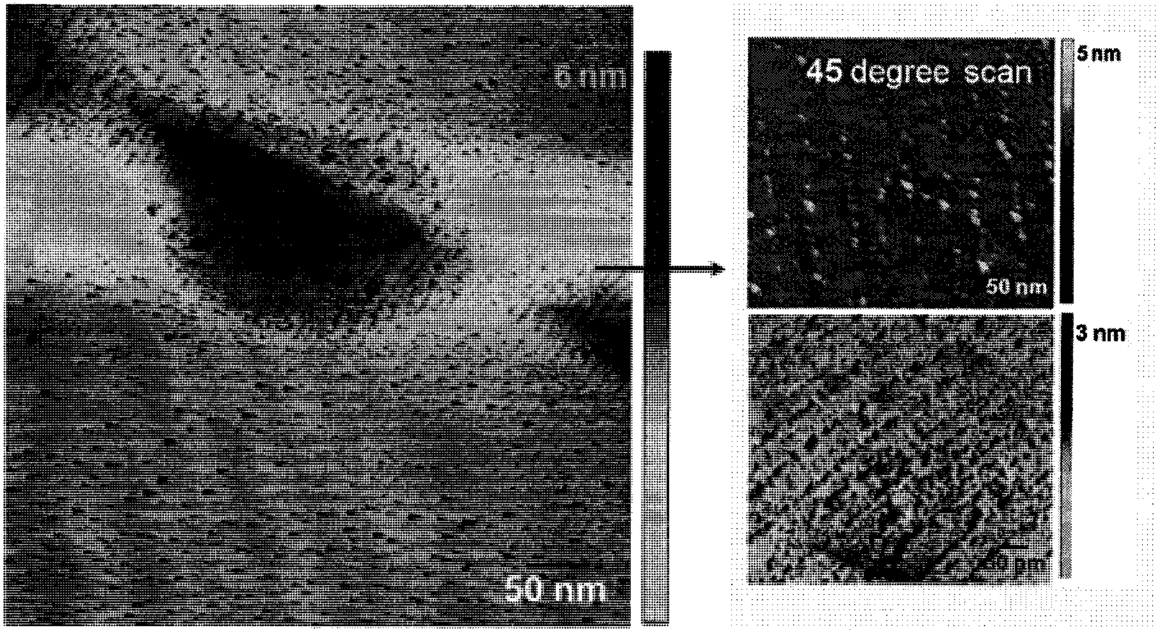

Figure 15: AFM scans of a freeze dried 0.1% SMA solution of empty nanotube diluted 100x on a mica sheet. Linear features are around 4 nm in height. The regular striations are stacked SMA nanotubes. The highlighted region was scanned to obtain more detail and a scan at 45° was performed to ensure that the features were not cause by tip effects.

## Concluding remarks

The theoretical modeling studies in Chapter II helped understand and predict the type of nanostructures expected. However, a number of factors have to be taken into consideration to experimentally reproduce, as well as possible, this theoretical system. The preparation, making use of dialysis, is an improvement to the original preparation method and can be used to reliably fabricate SMA nanotubes. The preparation of nanotubes seems to be best with a polymer of average molecular weight, such as with the 12,000 Da SMA sample. The nanotubes obtained were many polymer contour lengths long and were present in much higher yield than with high $M_w$. Low molecular weight SMA did not associate into nanotubes. The 50,000 Da $M_w$ SMA had the advantage of producing nanotubes with lengths on the order of the contour length of the polymer, which may make them more stable to pH changes or organic solvents.

The SMA nanotubes seem stable to moderate pH variations once they are formed. The optimal range is between pH 6.5-8. Different bases produce different linear and radial nanotube growths. These changes are not yet understood. Nanotube preparation using a buffer gave interesting AFM results which agreed with the TEM observation of stacks of nanotubes and AFM provided a height measurement, which also agreed with the theoretical nanotube dimensions from Chapter II. AFM also showed sheet structures that were predicted theoretically. The height of the uniform domains observed in AFM also agrees with the predicted height of SMA polymer sheets discussed in Chapter II.

The most interesting aspect of these results is that different preparation conditions were used and produced similar results. The secondary structure was consistently observed, while the tertiary structure of SMA nanotubes varied substantially. Rigid rod-like structures were observed with diameters of approximately 4 nm and varying aggregation behaviours. Also, these results were observed with two different techniques: TEM and AFM.

# Nano-composites from the self-assembly of styrene maleic anhydride alternating copolymers and noble metals

# Chapter IV

## Abstract

Poly(styrene-alt-maleic anhydride) (SMA) was synthesized using a controlled UV-initiated polymerization. The initiator remains bound to the polymer as a terminal functional group forming a dithioate. This functional group can be converted to a thiol and reacts with noble metals. Nano-composites of SMA with gold and silver were investigated. Although preliminary, these results establish a basis for future experiments.

## Introduction

Synthetic methods to fabricate colloidal metal particles with controlled diameters on the order of nanometers have been studied since the early 1950's. Self-assembly can be used to produce metal nanoparticles of Pt, Au, Ag and Cu because of the high affinity of these metals towards thiols. The nature of the sulphur-metal bond is not yet fully understood, but it has successfully been used to control the self-assembly of molecules onto surfaces[184-189] and build new molecular architectures[190-195]. In this chapter, the stabilization of metal nanoparticles using SMA was investigated.

The SMA polymer ($M_w$ 12,000), synthesized using the UV-initiated radical copolymerization scheme presented in Chapter III, was used for the self-assembly of noble metal nanoparticles. The polymer synthesized is terminated with a dithioate, which is the initiator. This functional group can be converted to a thiol commonly used in self-assembled structures involving gold and silver surfaces and nanoparticles.

## 1. Experimental preparation of SMA polymer for self-assembly

To convert the terminal dithioate group to a thiol, two methods were used. The experimental results presented were carried out with the second method discussed.

The first method consisted in dissolving the synthesized polymer[196] (0.2g, $1.6*10^{-5}$mol), in deionized water with two molar equivalents of NaOH, with respect to moles of maleic anhydride, which was saturated with Ar for 1 hr. to remove dissolved $O_2$, which catalyses the formation of S-S bonds before polymer addition. The solution was maintained under Ar until all the polymer was dissolved. Each mole of polymer has one mole of initiator. Concentrated HCl was added dropwise until the polymer precipitated: poly(styrene-alt-succinic acid). The polymer was recovered by vacuum filtration using a fine fritz glass filter under an Ar stream. MeOH was degassed with Ar for 30 min. and the filtered polymer dissolved. An excess of 3-(dimethylamino)-1-propylamine (2 ml, 0.016 mol) was added to the solution and left to react for 20 min. The pink colour associated with the presence of the initiator disappeared in the first 5 min. and the solution became colourless. The thiol terminated polymer was recovered by precipitation in degassed ether and was vacuum filtered under an Ar stream. Ellman's test[197,198], which is used to detect the presence of free thiol, was performed and indicated the presence of free thiols in solution. A shoulder peak was observed at 410 nm, where expected.

In the second method, the synthesized SMA polymer was dissolved in water with two molar equivalents of NaOH with respect to moles of maleic anhydride. Once the polymer was dissolved, the solution was dialyzed against deionized water, until the pH was between 6.5 and 8. In this case the disulphide bond formed due to $O_2$ oxidation and the pink colour disappeared with the formation of this bond. The experiments were carried out using this method because the disulphide can be reduced to a thiol when a reducing agent is added during nanoparticle preparation.

## 2. Experimental preparation of silver nanoparticles and nano-composites

A molar ratio of 1:1:20 of the disulphide 12,000 Da SMA:$AgNO_3$:$NaBH_4$ was used to prepare silver nanoparticles in water. Silver nitrate (1 mg, $5.9*10^{-6}$ mol) was dissolved in deionized water (5 ml) and added to the solution of disulfide SMA nanotubes 0.1% wt. (10 ml, $10^{-6}$ mol). The solution was stirred and $NaBH_4$ was dissolved in 10 ml of deionized water. The reducing agent was added dropwise over 5 minutes with the first 10 drops being added at 20 s. intervals. The solution was left stirring overnight. A UV-VIS spectrum was taken to confirm the presence of a Surface Plasmon Resonance (SPR). A peak at 400 nm confirmed the presence of Ag nanoparticles[199-201]. TEM was used to characterize the size distribution of the nanoparticles. The results are shown in Figure 1.

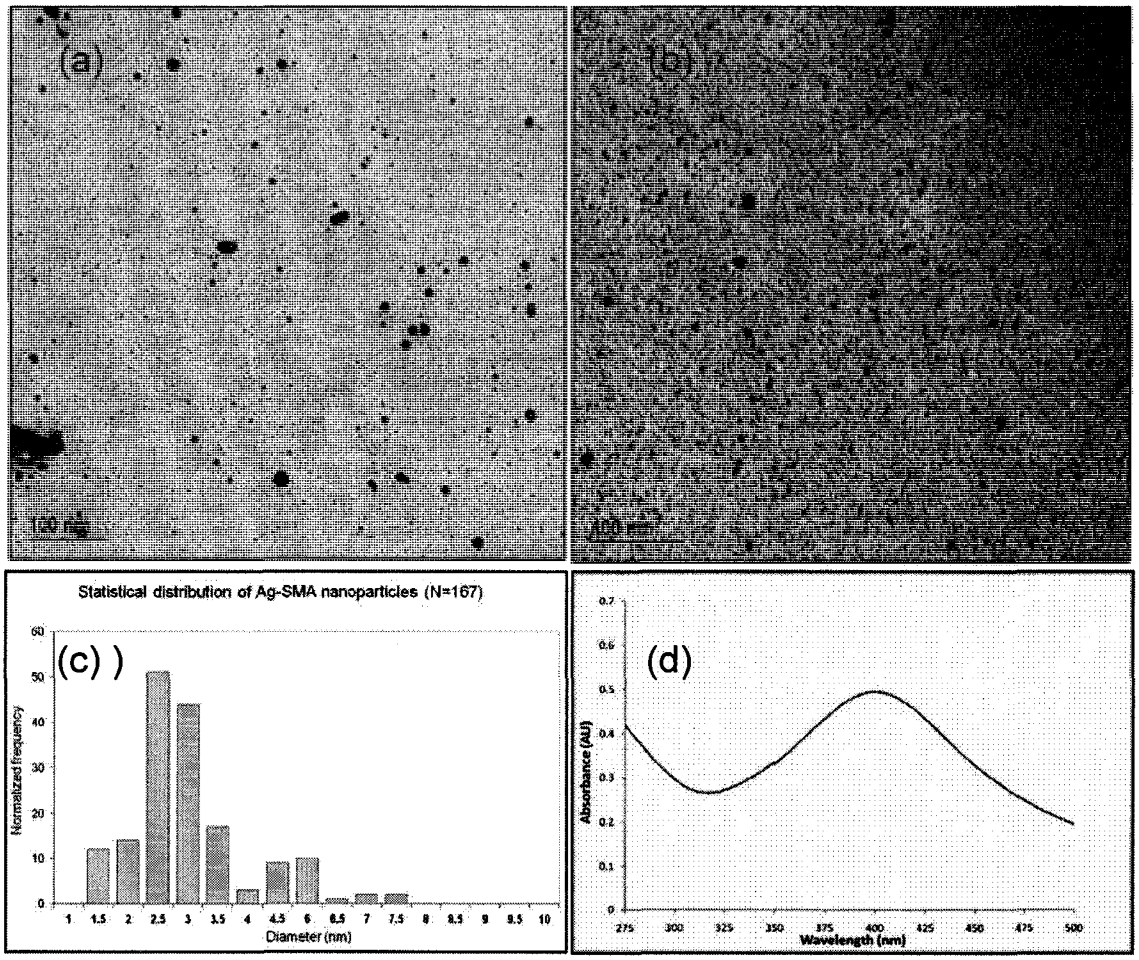

Figure 1: (a) and (b): TEM micrographs of spherical Ag-SMA nanoparticles prepared in water. (c) Size distribution of the Ag.-SMA nanoparticles based on 167 measurements. (d): SPR of the Ag nanoparticles taken in water.

A slow reduction of the $AgNO_3$ (1.4 mg, $8*10^{-6}$ mol) was carried out in a SMA 50,000 Da, nanotube solution (5 ml 0.1% wt., $5*10^{-7}$ mol). A solution of 3 molar equivalents of $NaBH_4$ (1 mg, $2.5*10^{-5}$ mol) dissolved in 5 ml of deionized water was added dropwise over 5 min. The pH of the solution was monitored so that it remained below pH 8, at which pH nanotubes form. The sample showed linear structures, similar to those observed when the nanotubes were filled with pyrrole. Regular dark striations were observed, which suggest that the silver was reduced at either the outer region of the nanotube, or in the interior. The dark stripes are 3 nm in diameter and separated by 1.5 nm. These dimensions are likely to correspond to stacks of nanotubes with outer walls that are less dense and an interior of the tube filled with Ag metal. The tubes measure about 4.5 nm in diameter with this approximation: 3 nm for the interior with 2x(½*1.5 nm) for the walls, giving about 4.5 nm in total.

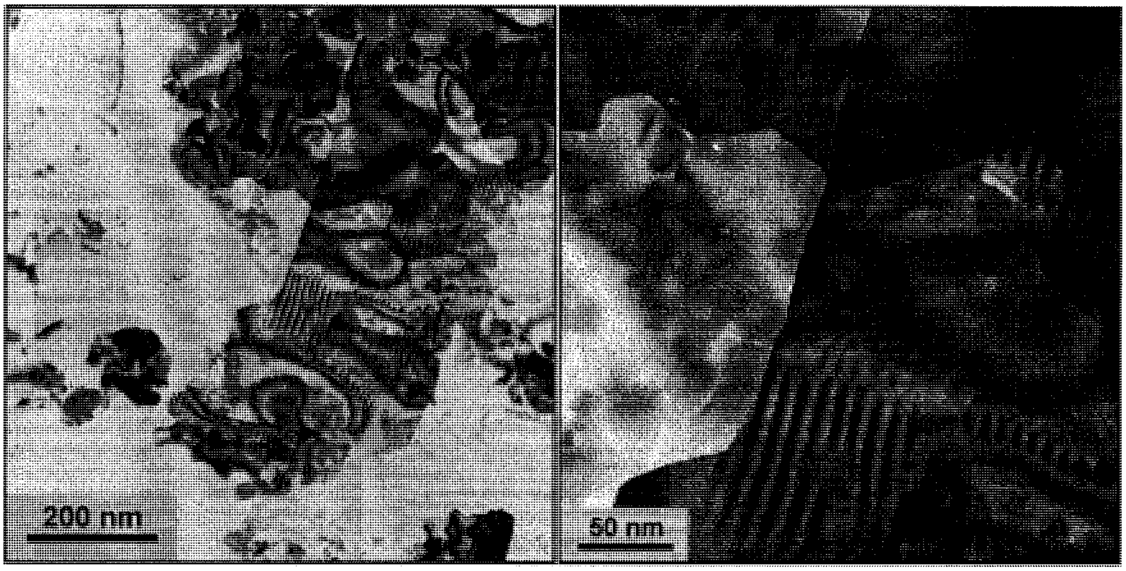

Figure 2: $AgNO_3$ SMA 50,000 Da reduced slowly with a dilute solution of $NaBH_4$ with a pH of 7. Lines are 3 nm in diameter. The darker areas are most likely reduced silver onto the inner or outer nanotube walls. The line diameter and spacing agree with the theoretical values predicted in Chapter II.

## 3. Experimental preparation of gold nanoparticles and capped nanotubes

A molar ratio of 1:20:1 of SH terminated SMA:$NaBH_4$:$HAuCl_4$ was used to prepare gold nanoparticles in water, using a similar technique to Brust *et al.*[202], but without the use of an organic phase and a phase transfer reagent. The gold complex (0.44 mg, $1.3*10^{-6}$ mol) was dissolved in deionized water and added to the solution of SH terminated SMA, obtained from the dialysis process (5 ml of 0.1% wt., $5*10^{-7}$ mol). The solution was stirred and $NaBH_4$ (1.55 mg, $4*10^{-5}$ mol) was dissolved in 10 ml of deionized water. The reducing agent was added dropwise over 5 minutes, with the first 10 drops being added at 20 s. intervals. The solution was left stirring overnight. A UV-VIS spectrum was taken to confirm the presence of a Surface Plasmon Resonance (SPR) peak confirming the presence of gold nanoparticles[200,201,203]. TEM was also carried out to measure the particle size distribution of the nanoparticles and to verify the particles were gold core with polymer coronas. The UV-VIS and the TEM analysis are shown in Figure 3. The Au nanoparticles obtained this way are stable over time but become unstable with large pH changes, solvent change and drying.

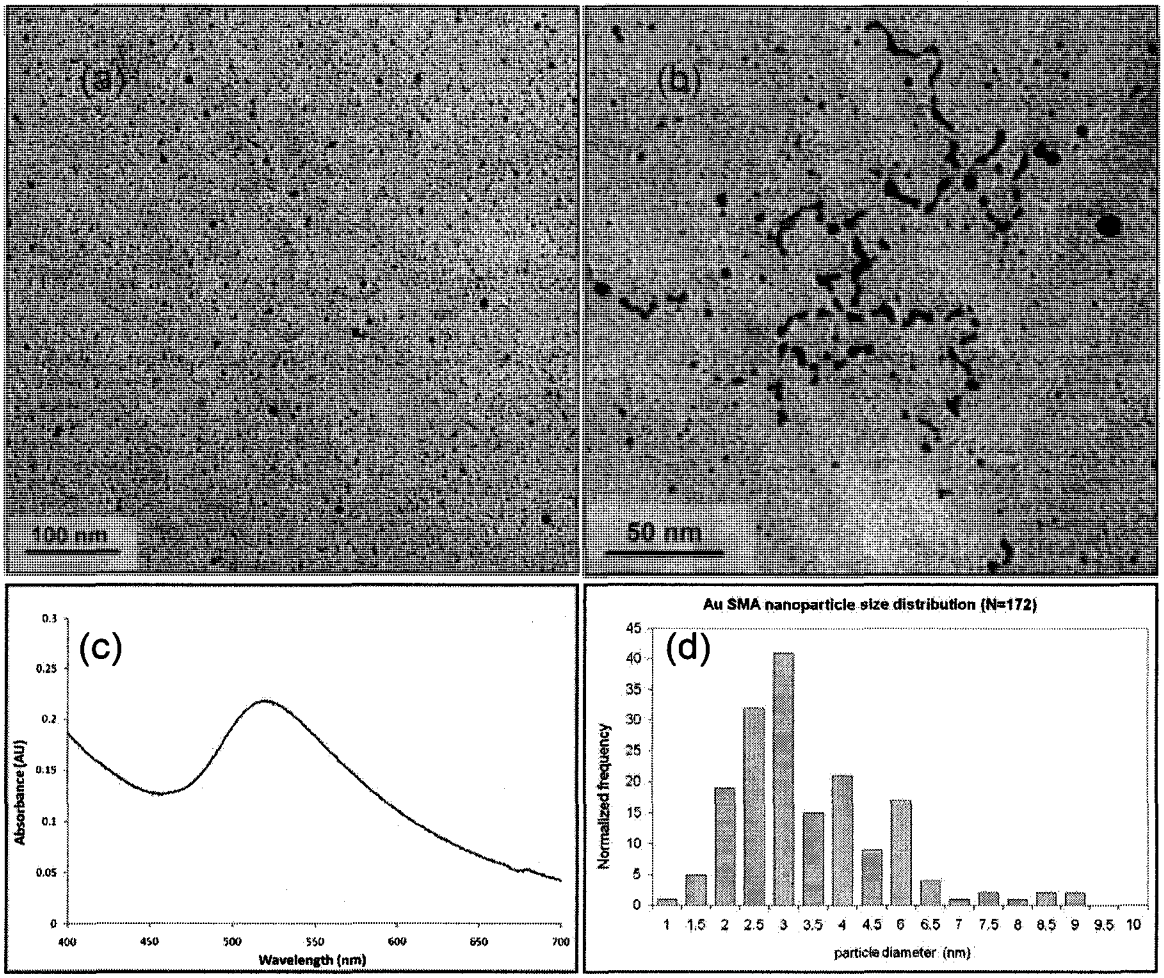

Figure 3: (a) and (b): TEM micrographs of Au-SMA nanoparticles prepared in water. (c) SPR of the Ag nanoparticles (d) size distribution based on 172 measurements.

Besides the uniformly polymer coated Au nanoparticles, there are many other types of nanostructures that have a solid gold nanoparticle core with an extended rod of much lower density, most likely a protruding polymer nanotube. These structures were observed in three different Au-SMA (12,000 Da) nanoparticle preparations. The first preparation is described above. The second preparation was the mixing of Au-SMA nanoparticles with SMA nanotubes and letting the solution rest. The third preparation consisted in adding Au-SMA nanoparticles to the basic solution of SMA, before performing the dialysis, which lowers the pH and allows a slow self-assembly of the nanotubes. Figure 4 shows more detailed pictures of the structures obtained by these three methods and the results are similar. Au-SMA nanoparticles either terminate the polymer rods or link two or more of these together. The polymer rods have a diameter corresponding to SMA nanotubes, ~4 nm. The average length of the polymer rod segments is on the order of the persistence length of the SMA, 12,000 Da, polymer: ~20-25 nm (see Table 1). It is also interesting that the individual nanotubes do not stack, most likely because of their short length. The capping of the SMA rods by Au-SMA nanoparticles seems to be more likely than a linear growth of the nanotube. Most of the SMA nanotubes appear to be capped at both ends and some of the Au-SMA nanoparticles acting as caps for two or more SMA nanotubes.

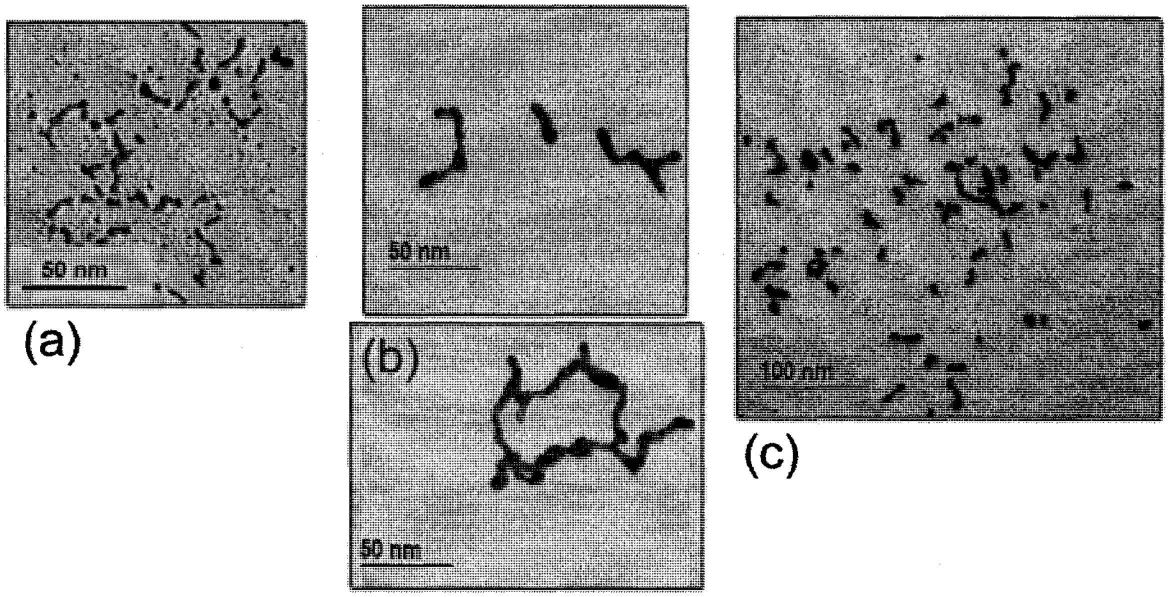

Figure 4: Au-SMA nanoparticles (Au-SMA NP) capped SMA nanotubes (SMA NT). (a) Au-SMA nanoparticles were formed by reduction of $HAuCl_4$ in water using $NaBH_4$. (b) Au-SMA nanoparticles were added to a SMA nanotube solution. (c) Au-SMA nanoparticles were added before dialysis and are present while SMA nanotubes are forming.

Table 1: Dimensions of Au-SMA composite nanostructures.

| *Au-SMA preparation method* | *Rod diameter (nm)* | *Rod length (nm)* |
|---|---|---|
| (a) | 2.7 ± 0.5 | 18 ± 8 |
| (b) | 4.1 ± 0.6 | 16 ± 6 |
| (c) | 4.5 ± 0.6 | 24 ± 8 |

The Au-SMA composite nanostructures are most probably short SMA nanotubes capped with Au-SMA nanoparticles of similar diameter to the nanotube. The 12,000 Da SMA sample is polydisperse and when stabilizing the gold nanoparticles, the longer polymer chains, which extend past the average polymer layer thickness, can act as a nucleation point where an SMA nanotube can start growing by $\pi$-stacking. The fact the Au-SMA NP are only attached at the ends of the SMA nanotubes tends to support the proposed mechanism of longitudinal growth because only the ends of the SMA nanotube have accessible free styrene monomers that can further $\pi$-stack with other polymers. It is also possible that longer tubes are broken up because of the strong thiol-Au interaction at the terminal end of a polymer, and only short nanotube fragments remain intact and attached to a gold nanoparticle when the solution is reduced with $NaBH_4$.

A second method was used to prepare gold nanoparticles, which yielded more stable nanoparticles, resistant to solvent change, pH modification and drying. The nanoparticles were prepared in THF using lithium superhydride, $HAuCl_4$ and disulfide SMA in a ratio of 20:1:1. The disulfide SMA 12,000 Da (5 ml of 0.1% wt., $5*10^{-7}$ mol) was dissolved in THF under an Ar flow. The gold complex (0.45 mg, $1.3*10^{-6}$ mol) was dissolved in 5 ml of THF and added to the SMA solution. An excess of Li superhydride dissolved in deionized water (2 ml) was added dropwise to reduce the gold. The mixture was left stirring overnight.

The difference in stability between the two methods of preparing gold nanoparticles can be explained by the stabilization of the gold nanoparticles by carboxylic acids rather than thiols. For Ag, $Ag^+$ ions are reduced. These can complex with the $COO^-$ groups on the polymer and stabilize the silver ions in solution. When reduced, Ag is stabilized by $COO^-$ groups that are more prevalent than SH groups. However, for Au nanoparticles, $HAuCl_4$ is used and can be stabilized with $COO^-$ groups. Upon reduction the gold is only slightly stabilized by these groups and drying or changing the pH destabilizes the nanoparticles. When prepared in an organic solvent, the polymer is in its succinic acid state with few $COO^-$ groups and can be selectively stabilized with the thiols rather than the carboxylate ions.

## Concluding remarks

The preliminary results presented demonstrate the potential of using SMA to build more complex systems involving metals. Silver tends to be more readily stabilized by the carboxylic acids, to which $Ag^+$ ions have a high affinity. Although the affinity of silver to thiols is greater than to carboxylates, the outnumbering of carboxylate groups to thiol groups on the SMA polymer has to be considered. This also explains the similar morphologies obtained by slowly reducing the silver nitrate to the morphologies obtained by polymerizing pyrrole. The carboxylate groups alternate along the polymer chain and interact with the $Ag^+$ ions.

The gold nanoparticles were mostly spherically shaped and were often capping a SMA nanotube. The stabilization of gold is likely due to thiol stabilization rather than carboxylate due to the lower affinity of $Au^{3+}$ ions to $COO^-$ groups[31]. Capped SMA nanotubes structures by Au-

SMA nanoparticle, were observed as a dense spherical core objects surrounded lower density material that surrounded the dense core and extended into a rod with a diameter of ~4 nm and lengths varying from 15-30 nm.

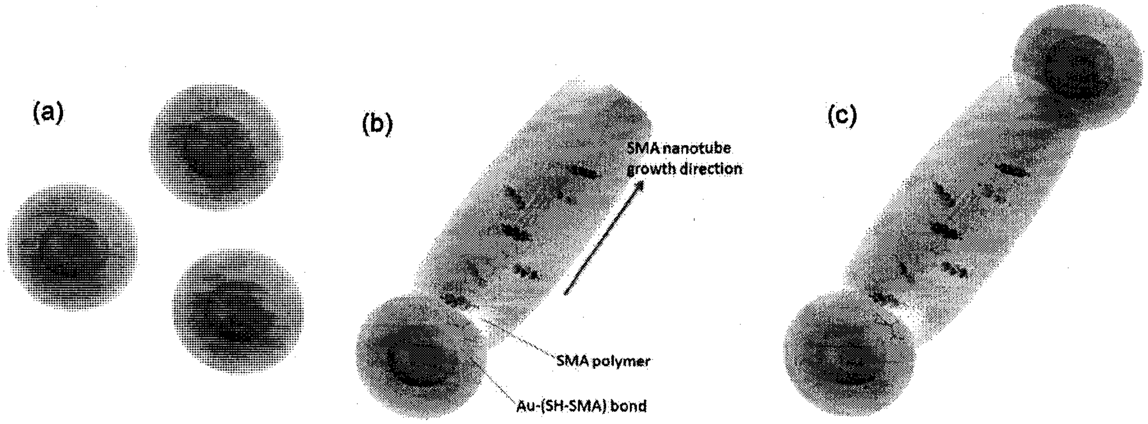

Figure 5: Illustration of the SMA and noble metal nanocomposite studied. (a) Individual spherical nanoparticles (b) SMA nanotube capped by Au-SMA nanoparticles (c) SMA nanotube capped at both ends by Au-SMA nanoparticles; longitudinal growth of the nanotube prevented.

While the synthesis of spherical nanoparticles is interesting, a more challenging and useful goal is to use the chemistry presented in this chapter to try and develop SMA-metal materials. It would be valuable to be capable of anchoring SMA nanotubes onto gold surfaces or gold nanoparticles to pattern surfaces, and for the development of sensors. Deposition of metal around or inside these nanotubes could lead to the development of ultrathin metal wires with diameters comparable to current techniques[204] and at a competitive cost. Many experiments remain to be performed such as varying the experimental metal reduction conditions and studying different molecular weight SMA samples.

# Effect of chirality on π-stacking in styrene and maleimide alternating copolymers

# Chapter V

## Abstract

The effect of different chiral sequences in alternating copolymers of styrene and maleimide was studied. Poly(styrene-alt-dimethyl-N,N-propylamide) (SMI) was studied and it was found that the methods used for SMI could be extended to a general class of alternating copolymer of styrene and maleimides. Only isotactic polymers can associate into complexes because of the symmetrically distributed styrene and maleimide monomers. The chirality of such ordered polymers is restricted to E(SS or RR) chirality in the maleimide moiety, and the complementary S or R chirality in the styrene moiety. Structural deviations from an isotactic polymer induce an asymmetry in the distribution of styrene monomers and introduce bends in the polymer backbone, which prevent association through π-stacking interactions. Semi-empirical PM3 calculations on the SMI polymer have shown that these π-stacking occur when the polymers are separated by a distance close to 10 Å.

## Introduction

In this chapter, the association behaviour of a different styrene based alternating copolymer to was investigated. Poly(styrene-alt-dimethyl-N,N-propylamide) (SMI) was studied in a similar manner as was SMA in Chapter II. Styrene is important for π-stacking interactions, which form the nanotubes in SMA. Therefore, in this alternating copolymer, the maleic anhydride monomer is functionalized to a maleimide with a short carbon chain, while retaining the styrene monomers.

SMI is a commercially available derivative of SMA obtained by reacting SMA with 3-(Dimethylamino)-1-propylamine[205]. The maleimide copolymer (SMI) formed has different structural properties to SMA. It is also used as a coating agent to increase hydrophobicity of surfaces [206] and is typically used in aqueous solution by dissolving it with an acid. The interest in studying this polymer was to determine its geometry, to improve the understanding of its hydrophobic properties and to explore its potential use in nanotechnology as is the case for SMA [207].

The microstructure of a polymer affects its bulk properties. For SMA, it was shown [110] that when hydrolyzed, the chirality is not important to the overall distribution of monomers along the polymer backbone at neutral pH. However, SMI behaves differently in solution, because the maleimide is not affected by variations in the pH. The SMI polymer therefore loses the flexibility, which is gained from hydrolysis of the maleic anhydride in SMA (Figure 1).

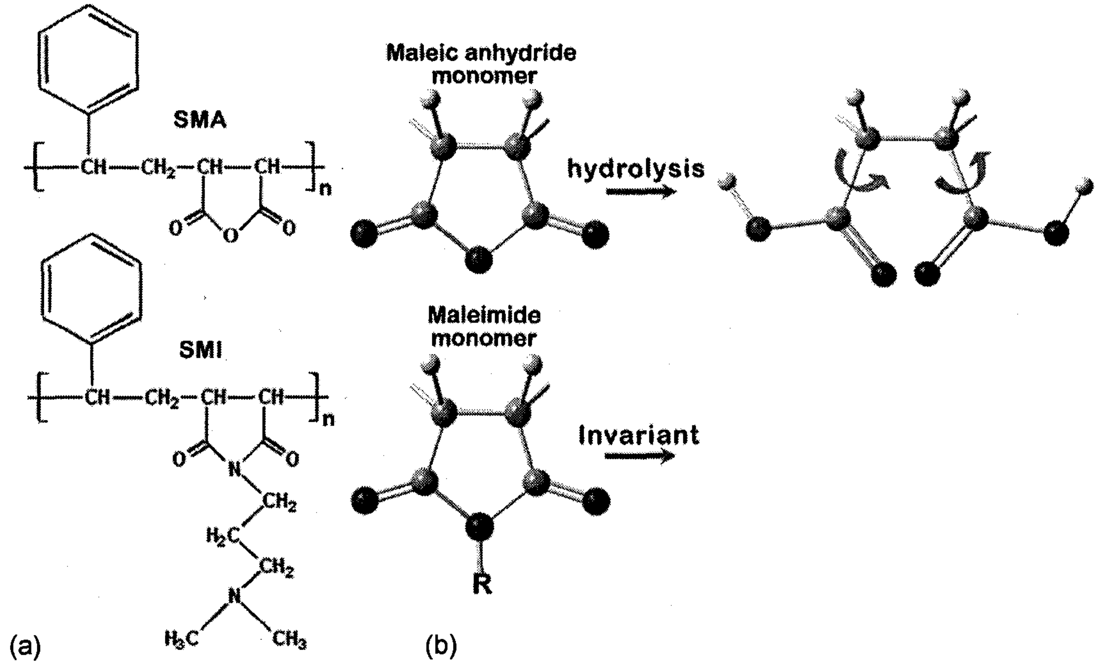

Figure 1: (a) Structure of SMA and SMI alternating copolymers. (b) Structure of the maleic anhydride monomer and the maleimide monomer before and after hydrolysis.

The possibility that SMI polymers self-assemble through π-stacking between the styrene monomers, as does SMA, motivated this research. Therefore, a conformational search was performed to predict which chirality sequences would lead to linear polymers with ordered styrene groups along the backbone. The association properties of maleimide and styrene alternating copolymer were then studied.

## 1. Theoretical methods

SMI is a large monomer, thus only the hexamer, containing six styrene and six maleimide monomers was studied. The hexamer is equivalent to six SMI alternating monomer units. Semi-empirical PM3 calculations were used because PM3 is reliable in predicting accurate geometries and it provides satisfactory electron correlations, which account for intra-molecular interactions [64,65,208]. The PM3 calculations also have the advantage of being less time consuming than Hartree-Fock (HF) or DFT calculations and give conformational results equivalent to higher level calculations. The PM3 geometries were determined to be reliable, because PM3 results on smaller polymer fragments gave geometries similar to those obtained by DFT using the B3LYP method with a 6-31G* basis set. Molecular Mechanic methods were not used, because quadrupole moment interactions between the styrene monomers in the polymer are important, as are as chain-chain and chain-styrene interactions between the maleimide chains. Molecular Mechanics calculations do not reproduce well the DFT or semi-empirical results for polymers larger than a trimer.

### 1.1 Monomer structure and solvation

The building block of the polymer is the alternating monomer of SMI, composed of a styrene and a maleimide monomer. The minimum energy conformational search of the SMI monomer was performed using PM3. The Tree Branch Method [209] was used to build the monomer and to search for the minimum energy conformation (Figure 2). The benzene ring was first built and were the carbon atoms added one at the time. As each atom was added, a z-matrix optimization was performed in the Gaussian program [126] using PM3, giving an optimized geometry at each step.

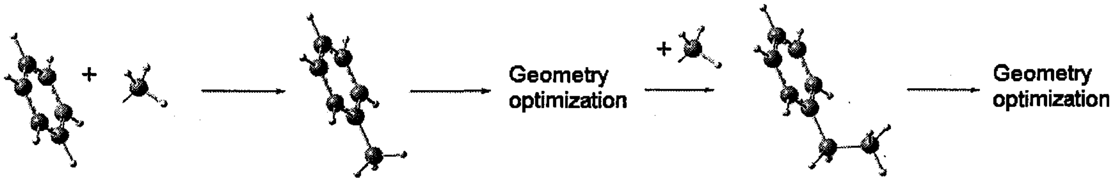

Figure 2: Visual representation of the "Tree Branch Method" used to find the optimal geometry of the SMI monomer.

The PM3 optimized monomer structure obtained was also geometry optimized using DFT B3LYP 6-31G* in the gas-phase, without and with the addition of HCl, needed to experimentally solvate the polymer, where a chlorine atom was placed near the protonated amide. The structures obtained for both the DFT calculations on the monomer and its HCl salt gave comparable bond lengths and bond angles.

To simulate the experimental conditions, water was introduced in a solvation model with HCl, similar to the solvation of SMA [155]. SMI monomer salt and the structures were optimized at the DFT B3LYP 6-31G* level and compared with the PM3 results. It was found that the SMI gas phase PM3 optimized structure of the monomer agreed with the DFT model in an aqueous acidic medium. These two structures are shown in Figure 3, overlaid to show their similarity. As was found for solvation of SMA, the solvent does not appreciably change the geometry of SMI. The equivalence of the DFT method compared to the semi-empirical calculation in predicting the geometry allowed the continued use of PM3, a method which is more convenient for large molecules because of its speed and above all its reliability.

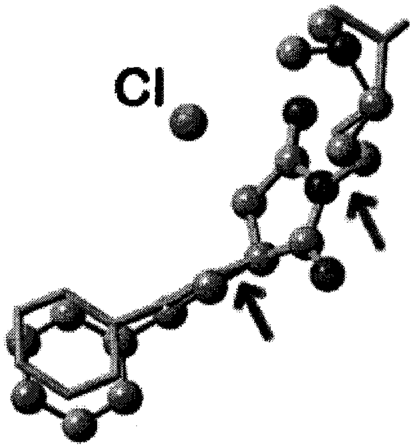

Figure 3: The SMI monomer (Hydrogens removed for clarity): comparison between the gas-phase PM3 (tube model) optimized structure and the DFT B3LYP 6-31G** (balls and bond model) solvated in water with HCl. The maleimide ring shows deviations (arrows) of 8° at the styrene and 20° at the maleimide.

### 1.2. Modeling the polymer structure

The SMI polymer structures were determined by building the polymers using a substitution method, which had also been used to model the behaviour of SMA in solution [210]. The monomers were joined together to form a dimer and optimized through a series of scans about the new bond, followed by a PM3 z-matrix geometry optimization to give the lowest energy conformation. The trimer was optimized the same way. The trimer is effectively the smallest repeat unit with two end monomers and a centre one, all having different constraining environments, the exterior monomer (styrene-maleimide) with styrene as an end group, the exterior monomer with maleimide as an end group and an interior monomer. The middle monomer of the trimer is constrained by its neighbouring monomers and therefore has the same constraints as monomers in the centre of a larger polymer.

The quadrimer was built from two trimers: opposite end-monomers were removed and the two centre monomers were linked. Because the constraints of the trimer centre monomer are similar to the centre ones for a quadrimer, the obtained structure is closer to the optimum geometry. The same procedure was used to build the hexamer from two quadrimers. These structures were optimized using PM3. Figure 4 shows the progression of the structure for an isotactic configuration of the polymer.

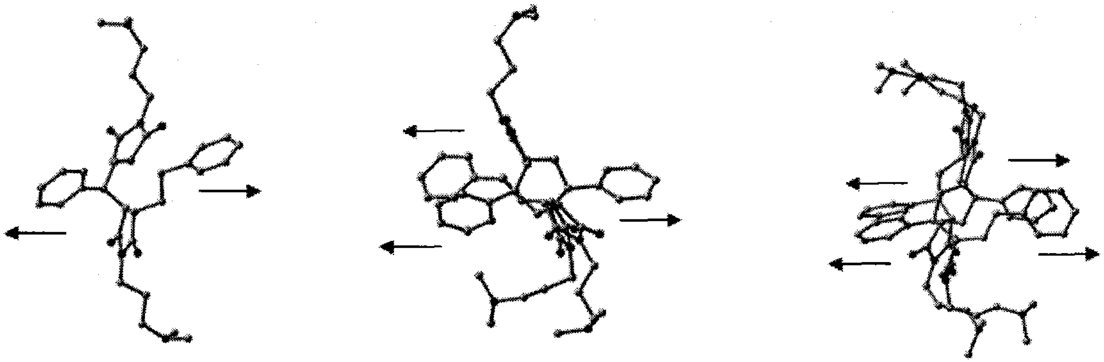

Figure 4: Progression of the PM3 optimized polymer, from dimer to quadrimer. Arrows represent the orientation of the styrene monomers along the polymer backbone, which is perpendicular to the view plane shown.

## 1.3. Chiral sites in styrene and maleimides alternating copolymers

For maleic anhydride, the hydrolysis provides additional chain flexibility, and allows the polymer to reorganize into a minimum energy conformation, which is consequently similar for different chiralities. In maleimide derivatives however, the maleimide ring remains closed and stiffens the structure, consequently no flexibility is available (SMI, figure 1). The ring closure of the maleic anhydride, as is the case for the maleimides, creates a strong dependence of the relative position of the monomers along the polymer backbone as a function of chirality.

Because SMI is typically synthesized from SMA, the resulting polymer is therefore chirally random because of the initial randomness of SMA. [176,177,211] Two chiral sites exist in SMI polymers. Site 1 is located at the carbon joining the styrene monomer to the maleimide, being described as R or S (Figure 5). Site 2 can be described by a Z (RS or SR) or E (RR or SS) configuration of the polymer around the maleimide rings.

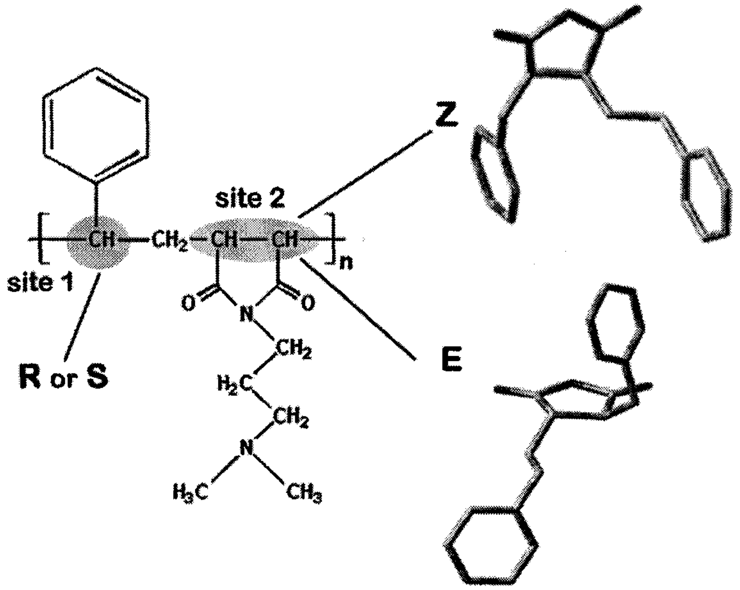

Figure 5: Chiral sites in SMI polymers. Site 1 has an R or S chirality, while site 2 has a possible E or Z chirality. In SMA, site 2 does not restrict the linear conformation of the chain or the relative distribution of styrene monomers, but this is not the case for maleimide copolymers.

### 1.4. Effect of chiral sequences on polymer structure

Linear polymers were found for totally symmetric chiralities, isotactic polymers: sites 1 and 2 having [E(SS) and S] or [E(RR) and R]. The isotactic case was first studied, providing a reference point to evaluate the effects of chirality modifications. The styrene and maleimide monomers were found to be aligned with respect to each other, forming a cross with opposite ends being equivalent. This is similar to the case of isotactic poly(styrene-alt-carbon monoxide) (STCO), which adopts a similar conformation with almost identical geometry angles [149], even though maleimides are a different class of monomers than carbon monoxide. The geometry obtained by PM3 optimization of the isotactic hexamer in Figure 6. The angles between chains and styrene groups also agrees with the STCO polymer: 70° degrees for SMI, and slightly under 70° degrees for STCO.

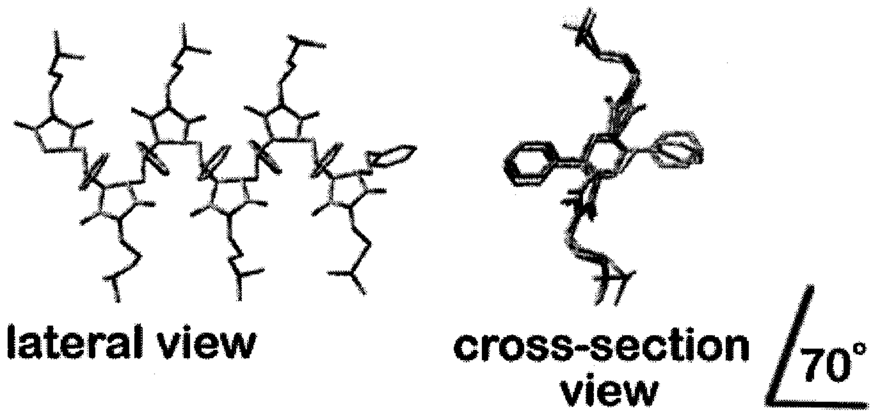

Figure 6: PM3 optimized isotactic SMI hexamer: sites 1 = S, sites 2 = E(SS). (left) lateral view (right) cross section view. The styrene groups are organized in the isotactic polymer and can associate through π-stacking. The angles formed by the maleimide and styrene ring are 110° and 70°.

To simplify the calculations, the maleimide chains were removed and chirality changes evaluated; referred to as a NoChain Model (NCM). This NCM method also allows the results for the chirality effects to be extended to maleimides in general. To confirm that the first observations were still valid for the simplified NCM, the structures were reoptimized using the semi-empirical PM3 method described previously for the dimer, trimer and quadrimer. Figure 7 shows that the overall structure of the polymer is preserved for the SMI polymers with chains and without chains (NoChain model). This is because the chiral sites are preserved without the chains. STCO does not have any long chains but has a similar conformation. This supports the use of the NCM to study the effect of chirality changes.

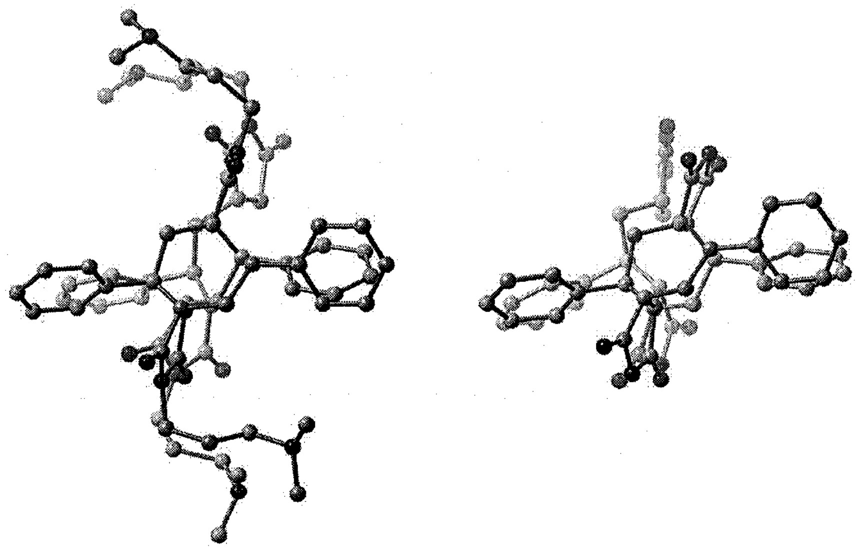

Figure 7: Visual representation of the NoChain model for a quadrimer (lighter atoms are further behind). Left, SMI quadrimer with chains, Right, SMI quadrimer without chains; NoChain Model. The styrene and maleimide monomers are slightly more disordered but the bulk of the structure is preserved without the chains.

The removal of the chain slightly increases the disorder between the styrene groups. However the longer maleimide chains in the SMI copolymer stiffen and order the polymer through chain-chain interactions. Therefore larger maleimide monomers reduce the flexibility of the chains. However, the bulk structure remains similar enough that the effects of chirality changes in sites 1 and 2 can be reliably predicted.

Using the NoChain Model, the second observation was that Z configurations in the polymer are unfavorable for obtaining regularly distributed styrene groups. Introducing a Z chirality at a terminal maleimide in the isotactic polymer (when sites 2 are all E) tilts the backbone by about 45 degree and the Z configuration of the maleimide rotates the relative position of the styrene group to which it is linked by 180 degrees. There is a double consequence of having terminal changes in maleimide chirality: the backbone is no longer linear and the ordering of styrene groups is disrupted. The effect of modifying the end chirality of a totally symmetric optimized quadrimer (all E(SS) and S) in the NoChain model and observing the changes by geometry optimizations using PM3 is shown in Figure 8.

If the chains are reintroduced in the model the geometry changes slightly, but the general trend is still that the ordering of styrene and maleimide groups is randomized. In addition, the stiffness of the backbone does not allow much flexibility and the polymer retains a relatively linear conformation with different chirality combinations. Modifying chiral sites 2, from E to Z along the polymer, showed that the polymer tends to remain relatively linear but the symmetrical distribution of monomers along the backbone is randomized, with maleimide monomers intercalated between the styrene monomers (Figure 8).

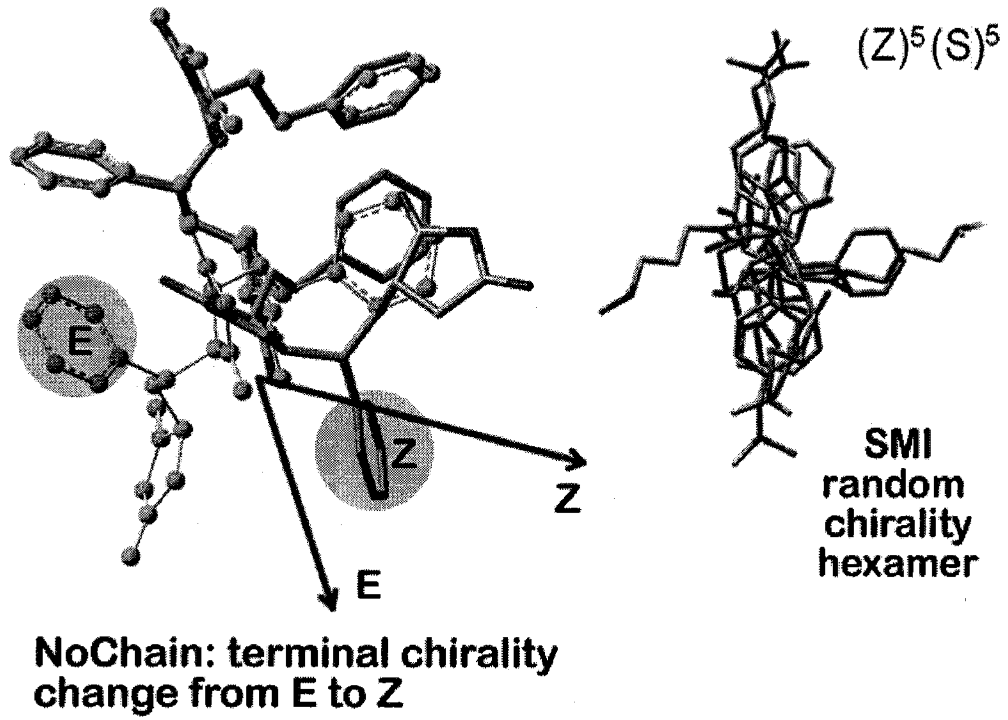

Figure 8: Left: The chiral sequence in "balls and bond" model, is for an isotactic quadrimer with a chiral sequence $Z(SS)^3 S^3$. In the "tube" model, the end chirality is changed from E to Z, showing $E(SS)^2 S^2$ Z(RS) S chiral sequence. Terminal styrene monomer is rotated by 180° (circles E to Z) and the polymer backbone tilts by 45° (arrows). Right: A random chiral sequence for an hexamer, showing a linear configuration but no symmetry, styrene monomers overlap maleimide monomers in this cross-section view.

The third observation using the NoChain Model is that changes in the chiral site 1, chirality R or S of the carbon linking the styrene monomer to the maleimide, must be identical to the chirality of the E conformations, i.e. if E is SS, the carbon of the styrene must be S. If this is not the case, the deformation destroys the alignment of the styrene monomers. The polymers remain fairly linear, but the styrene groups are disordered (Figure 9). Site 1 chirality changes rotate the monomer by 45°, 90° or 180° with respect to its original position.

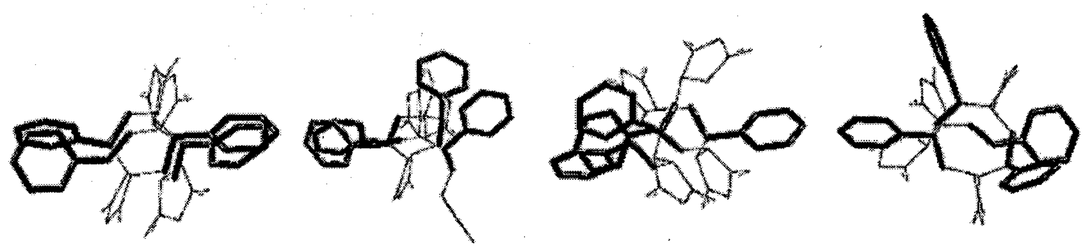

Figure 9: Cases were the chirality for site 1 was reversed for centre and terminal styrene monomers in a NoChain SMI quadrimer. (a) isotactic quadrimer: $E(SS)^3$ SSS (b) First centre chirality reversed: $E(SS)^4$ RSS (c) Second centre chirality reversed: $E(SS)^3$ SRS (d) Terminal chirality reversed: $E(SS)^3$ SSR. Chiralities are described starting from the alternating monomer with a terminal styrene. The styrene monomers are left in bold, while the rest of the polymer is left in sticks to emphasize the changes in orientation of the styrene monomers.

## 2. π-stacking association between maleimide and styrene alternating copolymers

It was shown that the isotactic alternating copolymers of styrene and maleimide are linear and have an ordered distribution of monomers along the polymer backbone. The ordered distribution of styrene monomers allows them to associate through π-stacking more efficiently. However, polymers which are not isotactic, as previously defined, cannot form strong associations.

The theoretical study of the association was focused on the association between isotactic polymers. SMI polymers were positioned such that the styrene monomers can interact through π-stacking and two types of association geometries were found (Figure 10). A maleimide polymer with chains was used to show that maleimides in general, when copolymerized with styrene to form an isotactic polymer, can form complexes and offer a more general description of the association than studying short chain maleimides, which follow a similar behaviour. If the polymers have identical orientations, the association is termed Head-to-Tail. On the other hand, if they are facing in opposite orientations, the association is Head-to-Head.

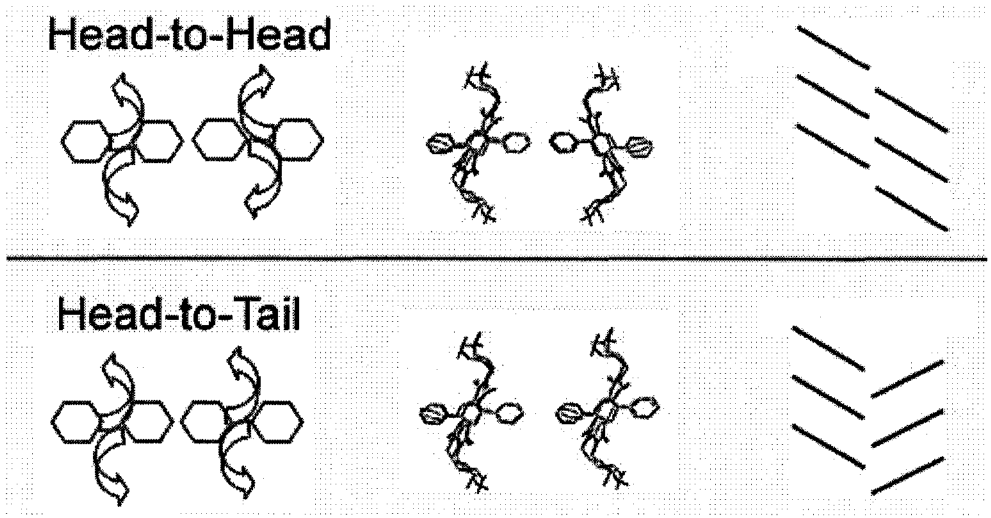

Figure 10: Association geometries between isotactic SMI hexamers. From left to right: shown are the cartoons of cross-section views, the tube models along with the herringbone arrangements of the styrene monomers for each association geometry.

To determine the optimal association geometry and the strength of the association, a method was developed to handle the large system. The study of the association was done using SMI hexamers because they are sufficiently large to model the behaviour of larger polymers and also because the hexamer has enough styrene monomer to decrease the number of possible π-stacking geometries, making the study more computationally challenging but simpler because it limits the associations to linear ones. Regular geometry optimizations, performed on the polymer structure, could not be done for the association complex because of the large degrees of freedom for free molecules in space. Hence, a computational scheme was developed to guide the optimization towards the optimal geometry.

Semi-empirical PM3 calculations were used to study the association because of its reliability in predicting the geometry of SMI polymers. To determine the relative energies of $\pi$-stacking, PM3 also had to be used because of the large size of the system. Although parametrized Molecular Mechanic force fields such as AMBER and Hartree-Fock calculations using Moller-Plesset (MP2) methods with basis sets including diffused polarization functions are best suited to study $\pi$-stacking energies [151,163,164], semi-empirical methods have been shown to provide results which parallel AMBER and MP2, although the energy is not accurate. The PM3 results consistently overestimate the contribution from electrostatics but predict the changes in stabilization energies from changes in conformations. Because our interest is not in determining accurately the energy of association, but rather determining how strong the association is, PM3 was chosen to search for the optimal association conformation and the relative changes in energy were studied, with the knowledge that they do not provide accurate energy values.

For each association geometry, all the atomic cartesian coordinates were frozen and the polymer backbones were separated by a distance, the inter-polymer distance (*r*). Constrained optimizations were performed by releasing only the coordinates of the styrene monomers which could then interact and the system was left to optimize to a minimum energy. The inter-polymer distance was varied from 10 to 14 Å by increments of 0.5 Å: from overlapping styrene monomers to beyond the range of strong interactions. Constrained optimizations were carried out at each step. The initial geometry of the complex, spacing between styrene monomers and polymer separation, was chosen based on experimental data from x-ray scattering of benzene dimer arrangements in phenylalanine [15,16] and x-ray crystal structures of styrene based polymers [149,160]. The method employed is similar to the calculations described in Chapter II for the minimum energy association search between SMA polymers.

The stability of the complex was evaluated by calculating the stabilization energy, Eq. 1. The energy of the association geometry at a specified distance is given by $E(r)$, while the energy of the unassociated complex is given by $E(r \rightarrow \infty)$, where $r$=40 Å, beyond the range for any interactions between polymers. Subtracting both of these values provides a value for the stability of the association: negative values indicate a stabilized association, while positive values indicate a destabilizing association.

$$E_{stabilization}(r) = E(r \rightarrow \infty) - E(r) \qquad r \rightarrow \infty, r = 40\text{ Å} \qquad (1)$$

To compare the minimum inter-polymer distances for different association geometries, the distance between the centres of the aligned styrene monomers was measured, the inter-phenyl distance ($r'$). Evaluating the stabilization energy as a function of $r'$ allows the comparison between the Head-to-Head and the Head-to-Tail associations. Results (Table 1) show an inter-phenyl distance of 4.5 and 5.2 Å for the minimum energy geometry (Figure 11). The styrene monomers take on a herringbone configuration in both associations, [15,161] expected when styrene monomers are closely packed.

**Table 1**: Energies of the Head-to-Head and Head-to-Tail geometries at different inter-phenyl distances using the constrained optimization method described in the text.

**HEAD-TO-TAIL**

| Inter-phenyl distance (Å) | Total energy for Hexamer association (kJ/mol) | Stabilization energy per π-stacking pair (kJ/mol) | Energy after relaxation of constraints (kJ/mol) |
|---|---|---|---|
| 3.6 | -3451.0 | -4.99 | - |
| 4.1 | -3457.1 | -7.02 | - |
| 4.7 | -3465.9 | -9.92 | - |
| 5.2 | -3467.0 | -10.3 | -13.6 |
| 5.7 | -3439.4 | -1.10 | - |
| 6.2 | -3438.4 | -0.76 | - |
| 40.0 | -3436.0 | 0.00 | - |

**HEAD-TO-HEAD**

| Inter-phenyl distance (Å) | Total energy for Hexamer association (kJ/mol) | Stabilization energy per π-stacking pair (kJ/mol) | Energy after relaxation of constraints (kJ/mol) |
|---|---|---|---|
| 4.0 | -3453.8 | -2.43 | - |
| 4.5 | -3468.1 | -7.21 | -12.6 |
| 5.5 | -3458.7 | -4.09 | - |
| 6.3 | -3449.9 | -1.13 | - |
| 8.8 | -3446.4 | 0.01 | - |
| 40.0 | -3436.0 | 0.00 | - |

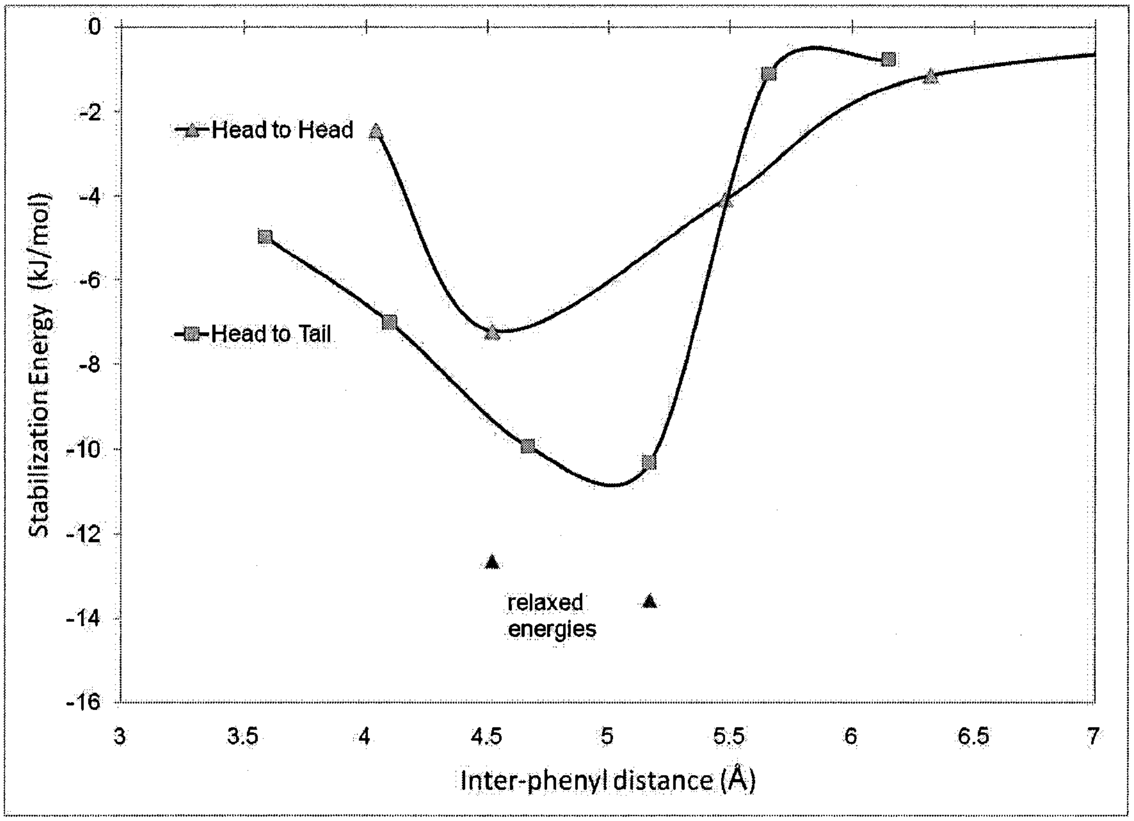

Figure 11: The stabilization energies per π-stacking phenyl pair, from the constrained geometry optimizations, are shown as a function of inter-phenyl distance (*r'*). The stabilization energies obtained when the constraints were removed are identified by the single triangles.

Experimental data predict stabilization energies of 12-25 kJ/mol and *r'* values between 3-6 Å, similar to the distances obtained for the minimum energy geometries. Upon releasing the constraints imposed on the remainder of the molecule, but keeping them at the same minimum energy distance, and re-optimization using PM3, the energy for both geometries were comparable. The Head-to-Head association had a stabilization energy of -12.6 kJ/mol, while the Head-to-Tail association had a stabilization energy of -13.6 kJ/mol. The difference in energy is small enough that both can be considered equally stable.

The result is expected to be similar for shorter maleimide chains. However, chain-chain interactions can also stabilize the complex, as described in the next Chapter. If both chain-Chain and π-stacking interactions are present in an association complex, as would be the case for bent association geometries, the complex would be more stable than linear associations because of the extra stabilizing Van de Waals forces (chain-chain), not present in linear associations. In the limit where maleimide chains are shorter, the stabilization energy is not expected to change much between the different association geometries. The complex becomes invariable to changes in the association angle. Preliminary results show that at least two carbons are required on the maleimide chain to significantly lower the stabilization energy. However, the lack of proximity between chains in linear association geometries for long chain maleimides, or generally in short chain maleimides, would limit the stabilization to π-stacking only.

To confirm the validity of the PM3 calculations used to search for the minimum energy association between SMI polymers, a fragment of the optimized structure was used to perform HF PM2 single point energy calculations using 6-31G* basis set. The fragment is composed of 3 styrene monomers and 3 maleimide monomers without chains (Figure 12) taken from the optimized Head-to-Tail conformation. Energy calculations at 5.2 Å and 20 Å provided a stabilization energy that can be compared to experimental values. The difference in energy obtained using Eq. 1 shows a 15.5 kJ/mol of stabilization energy. Therefore, both the distances obtained from the PM3 calculations and the energy obtained from the MP2 calculations show agreement with known experimental values.

The staggered herringbone geometry of the association geometries shows the importance of the electrostatic attraction between the aromatic groups of the styrene monomers, which originates from the quadrupole moment of benzene. The electrostatic attraction between the styrene monomers can also be seen in both the electrostatic potential surface and in the Delocalized Molecular Orbitals (DLMO) of the fragment studied using MP2 (Figure 12). The electrostatic attraction between the negatively charged delocalized p orbitals and the positively charged C-H bonds of the styrene monomers describes why the staggered herringbone association is more stable. About 20% of DLMO show overlap of wavefunctions between two or all three the styrene monomers. Most DLMO which show this characteristic had s-s and s-π character but there are also DLMO of higher energy with π-π character.

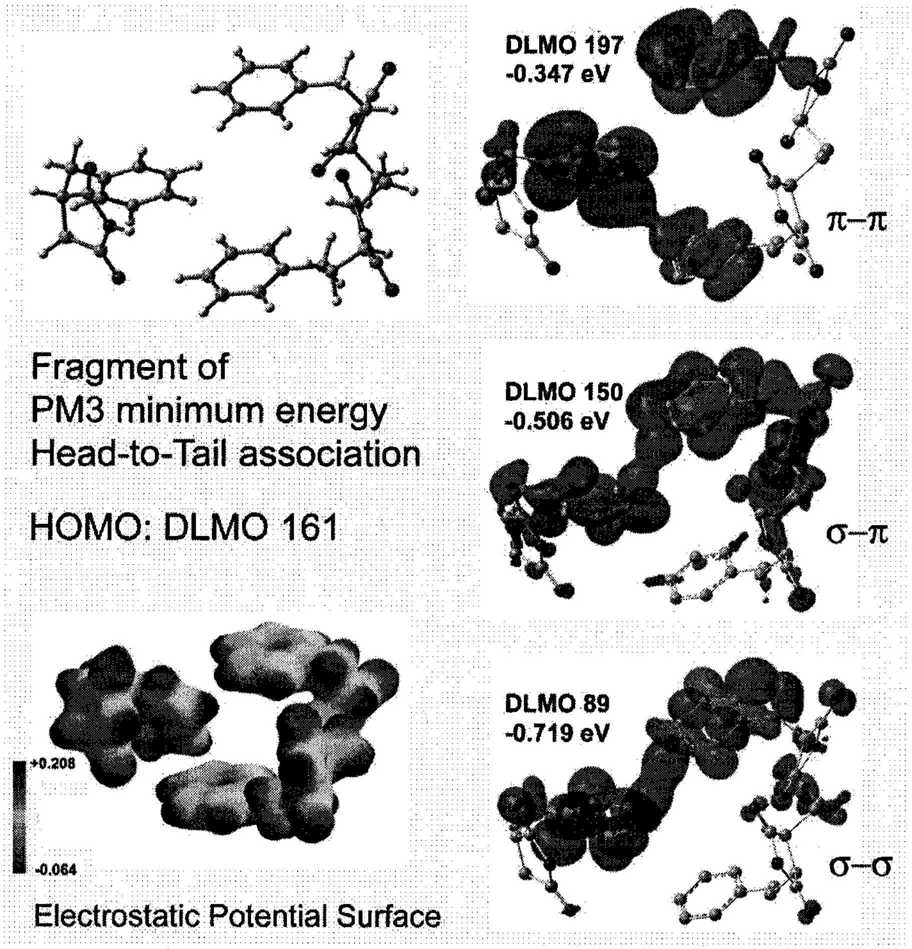

Figure 12: Fragment of the PM3 minimum energy Head-to-Tail association used to perform MP2 single point energy calculation using HF 631G* basis set and the corresponding DLMO which show wavefunction overlap between aromatic groups. Also shown, is the electrostatic potential surface generated to show that the interaction between styrene monomers is electrostatic.

## Concluding remarks

If alternating copolymers of styrene and maleimide are to self-associate through $\pi$-stacking, they must be isotactic. When isotactic, these polymers are linear and the styrene and maleimide monomers are symmetrically distributed along the polymer backbone, which allows them to associate through $\pi$-stacking. The present study can be summarized as follows:

1. To obtain associated polymers, the styrene and maleimide alternating copolymer must be isotactic, all chiral sites 2, located at the maleimide ring, must be of the same chirality as the chiral site 1, located at the carbon linking to the Styrene monomer: all E(SS)S monomers or all E(RR)R monomers.

2. Changing the chirality from E to Z bends the polymer backbone while a mixture of E and Z gives a linear polymer, but with an asymmetric distribution of styrene and maleimide monomers. The resulting polymer cannot strongly associate through π-stacking interactions.

When polymers associate, the energy of the complex is lower. The inter-phenyl distances and geometries are comparable with known experimental and theoretical data. This survey does not exclude the possibility that certain specific chiral sequences might also be linear and have an ordered distribution of styrene monomers. However, making such specific sequences might pose more of synthetic challenge that the preparation of an isotactic polymer would. For this reason, all chirality sequences were not studied, given that their synthesis is not possible with current methods. The case of an isotactic polymer is in principle achievable with the proper stereospecific catalysts for use with polar monomers, although these are still under development [212].

# Nanotube self-assembly of isotactic poly(styrene-alt-maleimide) polymers: theory and experiment

## Chapter VI

## Abstract

The different association geometries between poly(styrene-alt-dimethyl-N,N-propylamide) (SMI) isotactic polymers were studied in greater detail to explain how SMI polymer can form nanotubes. For each of the Head-to-Head and Head-to-Tail associations, bent and linear association geometries are possible. While all associations were stabilized by π-stacking of the styrene monomers, the bent geometries were further stabilized by van der Walls interactions between maleimide chains. Similarly to poly(styrene-alt-maleic anhydride) (SMA), the association between many polymers leads to sheets of polymers that associate along the length of the polymer. The association between polymers occurs with a bent geometry, which the most stable. The polymer sheets can bend with minimal loss of entropy and form more stable closed sheet structures, which are polymer nanotubes. The nanotubes predicted were observed using Atomic Force Microscopy (AFM) and Transmission Electron Microscopy (TEM) and the sizes measured agreed with the theoretical dimensions.

## Introduction

In this chapter, the use of a different styrene based alternating copolymer to produce other shape and size nanotubes was investigated. Poly(styrene-alt-dimethyl-N,N-propylamide) (SMI) was studied in a similar to was SMA in Chapter II. Styrene is important for π-stacking interactions, which form the nanotubes in SMA. Therefore, in this alternating copolymer, the maleic anhydride monomer is functionalized to a maleimide with a short carbon chain, while retaining the styrene monomers. Modifications to the preparation conditions of SMA nanotubes can be carried out to control the size of and the aggregation properties of the nanostructures. This was briefly investigated in Chapter II. The above ideas are summarized in Figure 1.

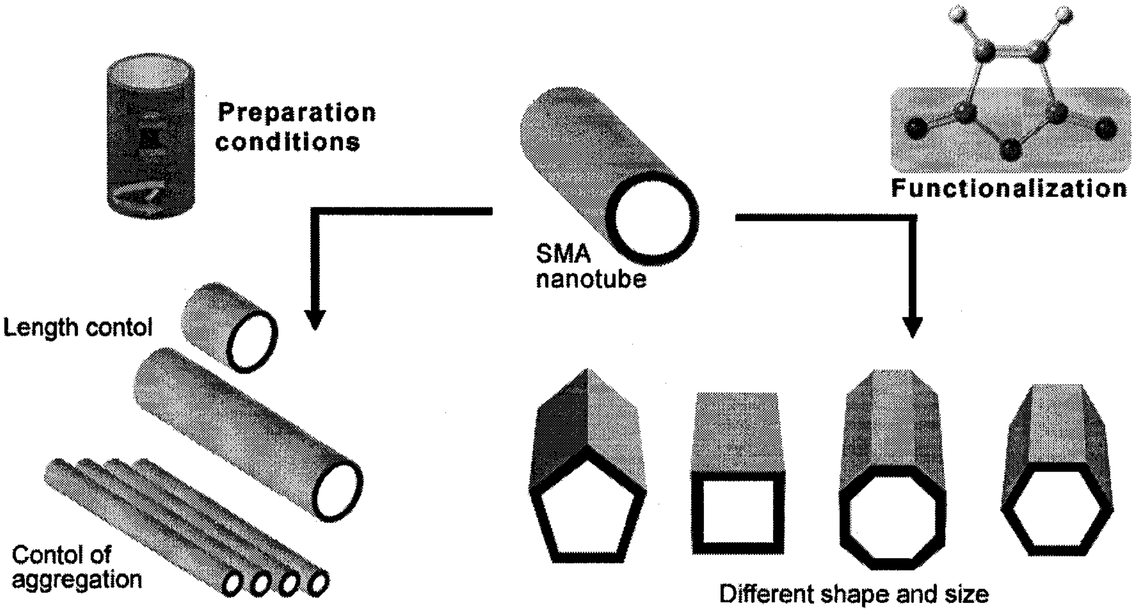

Figure 1: Summary of the different paths to control the size, shape and length of styrene based alternating copolymers. The topic of this chapter is to study the effects of the functionalization of maleic anhydride.

## 1. Association between many SMI polymers

SMI polymer aggregation is caused by hydrophobic forces, which originate from π-stacking interactions between styrene monomers and van der Waals forces between maleimide chains. However, to obtain ordered SMI polymers aggregates, the basic building blocks, the SMI polymers, need to have an ordered structure, as shown in Chapter V. Only isotactic polymers are capable of such association to form nanotubes.

As it was shown in Chapter V, the association between SMI polymers is stabilized when joining two SMI polymers such that the styrene monomers interact through π-stacking. The two possible types of association geometries are Head-to-Tail, in which the polymers are in identical orientations, and Head-to-Head, in which the polymers are facing in opposite orientations. Furthermore, they can join with different association angles. These were not investigated in Chapter V (Figure 2).

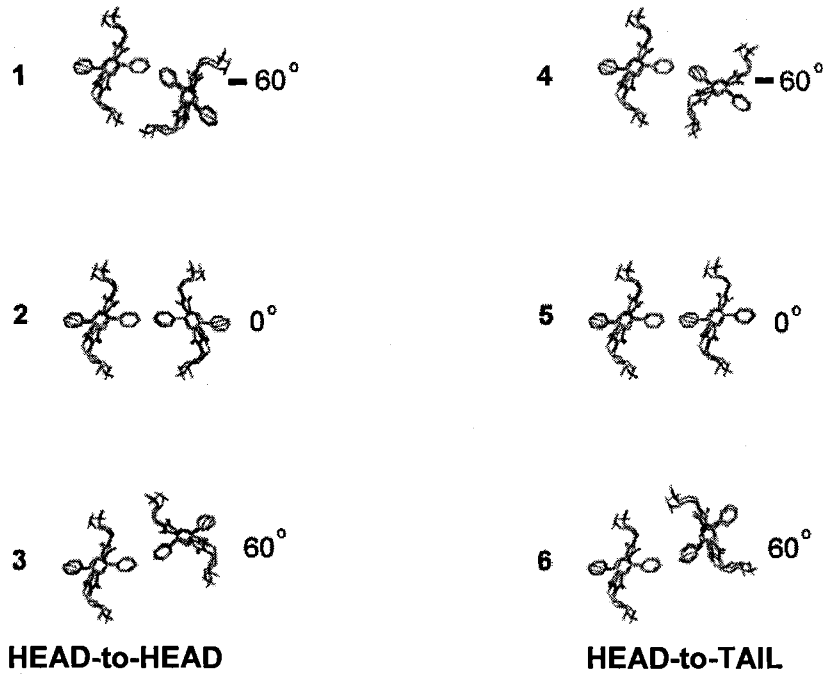

Figure 2: Summary of the six association geometries studied for the Head-to-Head and Head-to-Tail conformations. Associations 4 and 6 are equivalent and were not computed twice.

To determine the optimal geometries and stabilization energies of the six possible association geometries, the method presented in Chapter V was used. For each of the Head-to-Head and the Head-to-Tail geometries, three limiting geometries exist: when the there is no rotation between polymers (linear) and two limiting cases where the rotation is ±60° (bent). In total, 5 different geometries were optimized because geometries 4 and 6 are equivalent.

The study of the three Head-to-Head association with different association angles and varying inter-polymer distances is shown in Figure 3. The same treatment was performed on the Head-to-Tail association. The stabilization energies are given for three pairs of styrene monomers (two associated hexamers). Full calculation details are given in Chapter V, where associations 2 and 5 were originally compared. The variation in the stabilization energy as a function of inter-polymer distance is similar to the behaviour of interacting coulomb molecular charges.

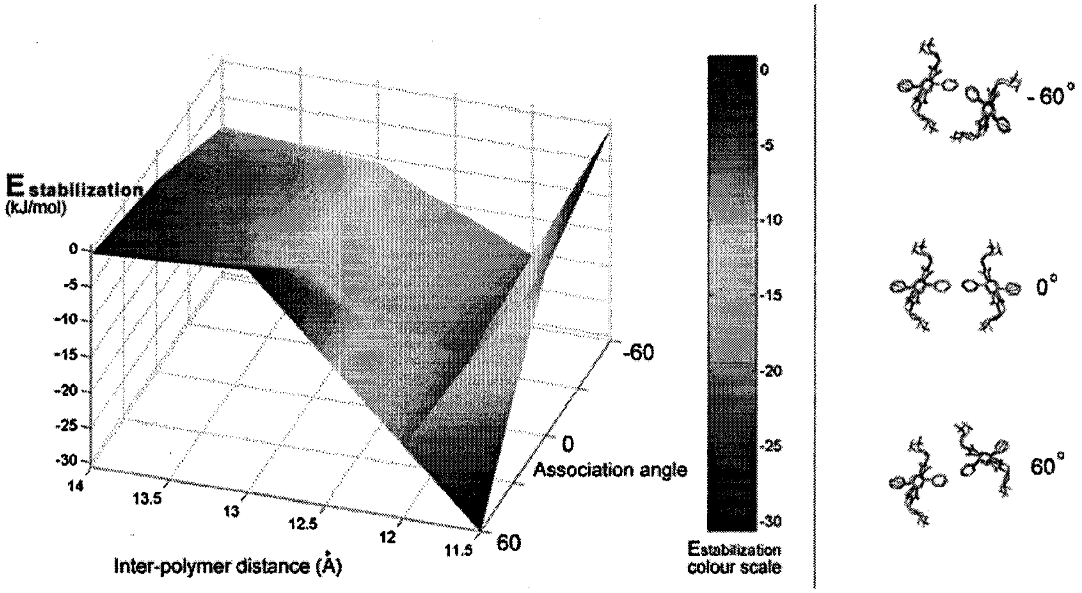

Figure 3: Stabilization energy, plotted as a function of inter-polymer distance (A) and association angle for the <u>Head-to-Head</u> association between SMI polymers. The minimum association differs slightly for different angles due to chain-chain interactions and is about 12-13 angstroms.

To compare the minimum inter-polymer distances for different association geometries, the distance between the centres of the aligned styrene monomers in Figure 2 was measured, to give the inter-phenyl distance (*r'* ). Evaluating the stabilization energy $E_{stabilization}$ as a function of *r'* allows comparing all six associations, Figure 4. It is important to note that the stabilization energies are given for 3 $\pi$-stacking pairs, because two hexamers interact, with three styrene groups each. An average inter-phenyl distance of between 4.5 and 5.5 Å was found. The most stable constrained association (# 3, Figure 2) has a greater contact area between the maleimide chains, but a larger inter-phenyl distance. The other remaining association geometries have similar inter-phenyl distances but comparable weak maleimide chain interactions. In all cases, the aromatic rings of the styrene monomers take on a herringbone configuration[160], expected when the styrene monomers are closely packed.

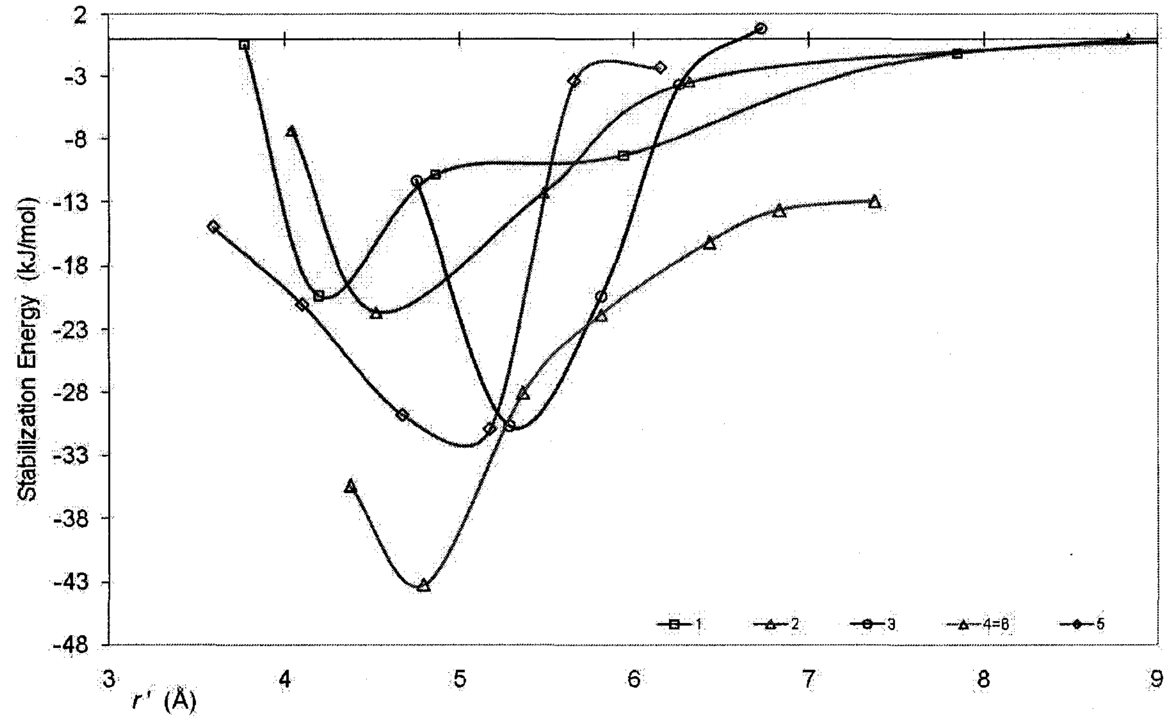

Figure 4: The stabilization energy is shown as a function of inter-phenyl distance ($r'$), a measurement which allows the different geometries of association to be compared between each other. (for 3 $\pi$-stacking pairs)

Releasing the constraints imposed on the remainder of the molecule and re-optimizing using PM3, the Head-to-Head associations 1 and 3 were the most stable, with approximately 21 kJ/mol of $E_{stabilization}$ for each $\pi$-stacking pair. Table 1, summarizes the PM3 results obtained when the constraints were released. The stabilization energy per styrene monomer pair, which occurs only from $\pi$-stacking interactions, can be evaluated from the value of the stabilization energy of the linear association complexes, 2 and 5 in figure 2. A value of about 12 kJ/mol from PM3 calculations was found in both cases. The increase in stabilization energy in the bent associations comes from chain-chain stabilizing interactions of the maleimide monomers and contribute about 8 kJ/mol to $E_{stabilization}$.

**Table 1**: Energies of the optimized minimum energy association geometries with constraints and after their release and re-optimization using PM3.

| SMI association # | Stabilization Energy per $\pi$-stacking pair With constraints (kJ/mol) | Stabilization Energy per $\pi$-stacking pair With constraints (kJ/mol) |
|---|---|---|
| **1** | 6.80 | 21.2 |
| **2** | 7.21 | 12.6 |
| **3** | 10.2 | 20.2 |
| **4=6** | 14.4 | 17.7 |
| **5** | 10.3 | 13.6 |

Because the relative energies using the PM3 method parallel experimental values, they can be reliably compared to each other. It can be concluded that lower steric hindrance from the maleimide chains allows stronger π-stacking. However, chain-chain interactions can also stabilize the complex. If both of these interactions are present in an association complex, as is the case for the bent association geometries, the complex is more stable because of chain-chain stabilizing interactions. However, the lack of proximity between chains in linear association geometries limits the stabilization to π-stacking only.

In the limit where maleimide chains are shorter, the stabilization energy for the non-linear association geometries does not change much between the different geometries. The complex becomes insensitive to changes in the association angle because of the lack of chain-chain interactions. Preliminary results show that at least two carbons are required on for the maleimide chain to significantly lower the stabilization energy.

## 2. Higher order association between SMI polymers

Having determined the lowest energy association geometries for the association between two SMI polymers, the association between more than two polymers was investigated. Systems beyond two hexamers (about 500 atoms) could not be investigated computationally. The optimal inter-phenyl distances and association angles from the lowest energy association geometries were used to reproduce the conformation expected for higher order associations. The conformations 1 and 3, Figure 2, were the lowest energy associations with inter-phenyl distances of 5.2 and 5.3 A and angles of –60° and +60° respectively.

Each polymer-polymer association is stabilizing. Addition of polymer chains in their minimum energy association geometries, along the styrene monomers of isotactic SMI polymers can occur and form sheet structures, Figure 5 shows different sheet arrangement from a cross-section view. Because the association geometries of the bent structures (1, 3, 4=6) are energetically equivalent, they are equally probable. Sheets can be formed from these different combinations of association geometries and can grow by addition of further isotactic polymers.

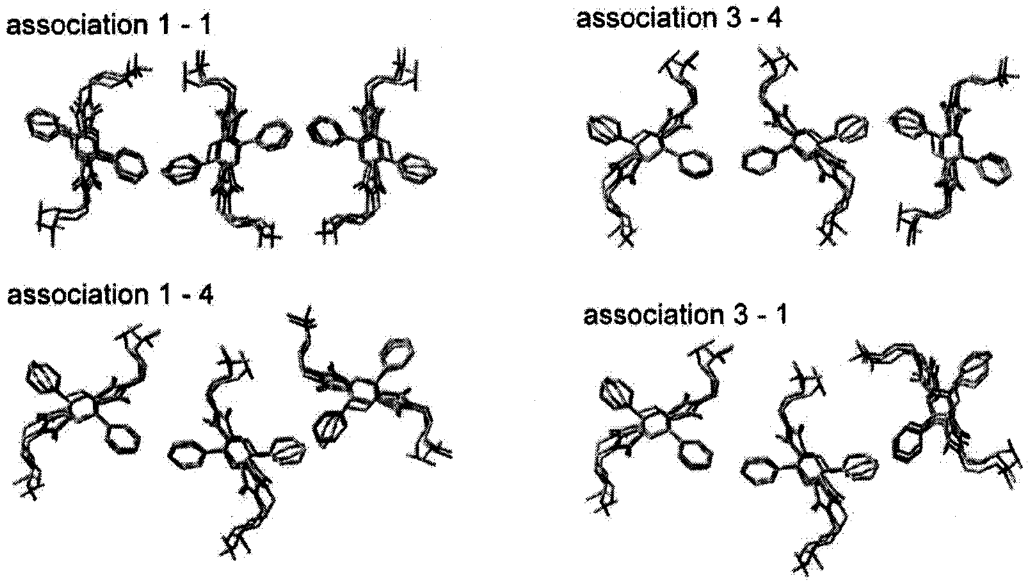

association 1 - 1

association 3 - 4

association 1 - 4

association 3 - 1

Figure 5: Sheet structures from 3 isotactic SMI hexamers, all are energetically equivalent. Bent association geometries (1, 3, 4=6) are energetically equivalent and can form sheet structures with different combinations between them. Shown are examples of these combinations. Cross section views, along the axis of the linear polymers are shown.

Additionally, the gain in stabilization energy from two polymers associating is not negligible and the system gains in energy by associating more polymers. As sheets grow there are free styrene ends at the edges. The system can reach a more stable configuration by avoiding these free styrene ends by associating these. The curvature required for the sheet to form a closed tube does not have any steric constraints because bent associations are more stable. If the sheets form a closed loop structure, the hydrophobic groups, the styrene monomers and maleimide chains are no longer in contact with the hydrophilic solvent but interact within a more hydrophobic environment, inside the nanotube walls. This leads to a closed octagonal structure consisting of 8 SMI polymers, which is a short segment of a polymer nanotube, Figure 6 shows how a sheet structures from 8 SMI polymers, in the Head-to-Head conformation, associated with the $\pi$-stacking of the terminal aromatic groups of the sheet; inter-phenyl distances and association angles were taken from the optimized values found. Measurements of the inner diameter and outer diameter using different reference points in the structure gave an outer diameter of (4.8 ± 0.2) nm, and the inner diameter of (1.7 ± 0.2) nm. The equivalent structure is also possible for the SMI polymer associating in a Head-to-Tail conformation and also a mixture of the two types of association. Stabilization energies, inter-phenyl distances and association angles are comparable between both Head-to-Head and Head-to-Tail conformations. Therefore, this closed structure can form from isotactic SMI polymers, irregardless of the self-associating association geometries.

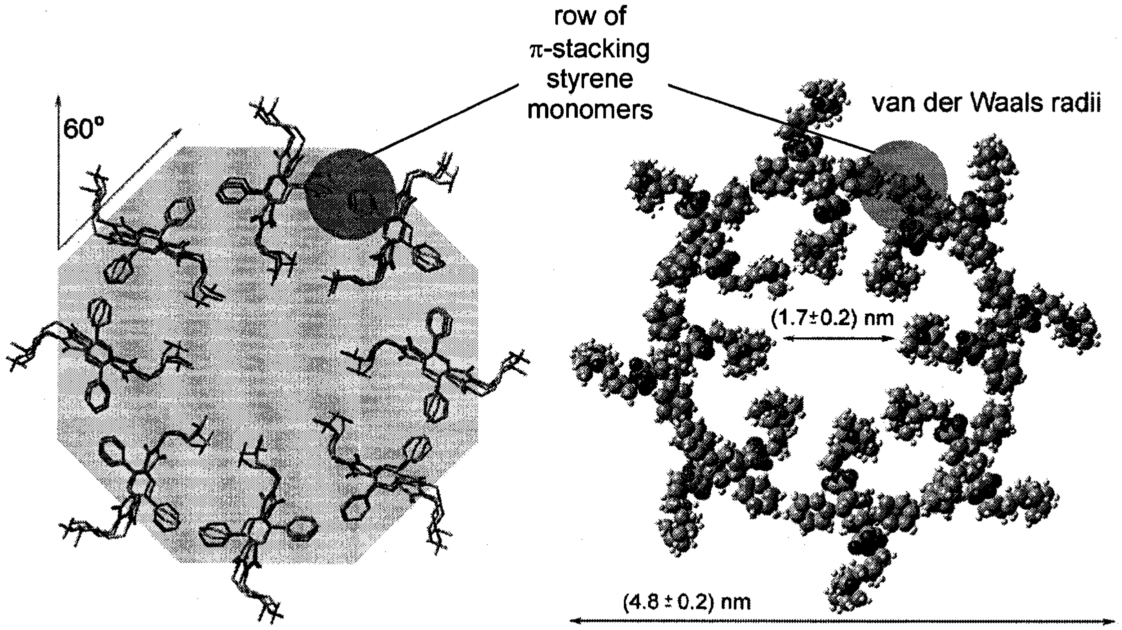

Figure 6: Organization of a sheet of SMI polymers into a nanotube structure. This structure offers the highest stabilization energy for the association between SMI polymers, forming a closed system between hydrophobic ends. (a) The nanotube has an octagon shape, made from 8 isotactic SMI polymer in the Head-to-Head conformation. (b) SMI nanotube shown with van der Waals radii, used to approximate the outer and inner diameter.

Because the polymers are polydisperse and the π-stacking is rarely perfect between associated polymers, the short closed segment can grow linearly by addition of further polymers to the free styrene monomers located at each extremity of the short polymer nanotube; the tube grows linearly (Figure 7). SMI nanotubes are not expected to associate between each other, as was the case for SMA nanotubes, and remain as individual nanotubes because the all the styrene monomers π–stack inside the walls of the nanotubes and are therefore shielded from any further interactions. This conformation reduces unfavourable solvent-styrene monomer interactions. It is interesting that with SMI polymers, the modification of the maleic anhydride monomer in SMA changes the shape of the nanotube. For SMA, the tubular structure was assembled from a minimum of 8 SMA polymers associating in a square shape with inner diameter of 2.5 nm and outer diameter of 4.1 nm. SMI nanotubes are also formed from a minimum of 8 polymers associating into an octagonal shape with smaller inner diameter, 1.7 nm, and larger outer diameter, 4.8 nm.

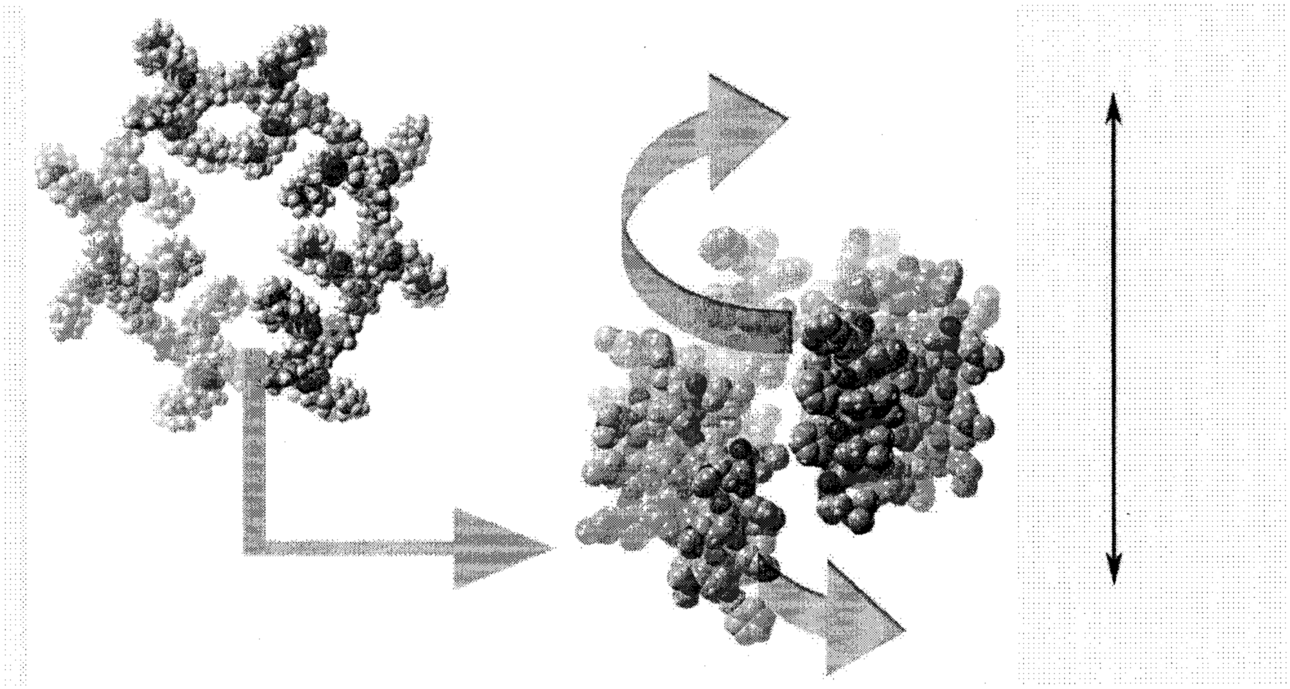

Figure 7: proposed growth mechanism for SMI nanotubes. SMI polymers can self-assemble at the edges of an initially closed structure and gain in stabilization energy from the ordered association because free styrene monomers are available for π-stacking. The nanotube grows in a spiral. (lighter colour atoms are further behind the plane of view)

## 3. SMI nanotubes characterization

### 3.1. SMI nanotube preparation

SMI nanotubes were prepared from low molecular weight SMI 1001 purchased from Sartomer Inc. This alternating copolymer is prepared by reaction of low molecular weight SMA polymer ($M_w$ 1600) with N,N-dimethylpropyl amine. The polymer resin was dispersed in deionized water, which was filtered using 0.2 μm PTFE filters, at a concentration of 1% wt. The suspension was brought to pH 3 by addition of HCl until the polymer was dissolved and the solution was transparent.

As discussed in the results from Chapter V, only isotactic polymers can self-assemble and each monomer has 3 chiral centres. Yields are therefore expected to be low and this was indeed observed. The nanotubes could still be observed because the nanostructures are much larger than unassociated polymer and therefore are easier to identify. The SMI sample used is approximately an octamer with a contour length of 4 nm. The probability of obtaining an isotactic polymer can be calculated. Each chiral site can be assumed to be either R or S with equal probability, and each monomer has three chiral centres. Therefore the probability of obtaining an isotactic monomer (SSS or RRR) is $2(½)^3 = 2/8$. For an octamer, the probability of obtaining an isotactic polymer would be $2(1/8)^8$. This corresponds to about a 0.00002% of the polymer being isotactic if there is no chiral preference. The fraction is small, but if the concentration is high (1% wt.) and only the isotactic polymers aggregate, it is possible to observe these nanotubes. The general formula to calculate the percentage of isotactic polymer, assuming all sites have equal probability of being S or R and are independent, is given by Eq (1).

$$\%_{isotactic} = 2\left(\frac{1}{2}\right)^{3n} * 100 \tag{1}$$

where $n$ *is the* number of monomers in the polymer and (1/2) is the probability of a chiral site being R or S.

### 3.2. Dynamic light scattering

Preliminary characterization of the SMI association in water was carried by Dynamic Light Scattering (DLS). All organic solvents were HPLC grade and filtered using 0.2 μm PTFE filters. Deionized water was filtered using 0.2 μm PTFE filters. The 1% wt. pH 3 solution was diluted and compared with similar concentration solutions of SMI dissolved in different organic solvents of varying dielectric constants, Figure 8. The Contin, multi-exponential and multi-exponential and the non-negative constrained least squares models gave similar particle size distributions. The hydrodynamic radius of the SMI polymer in aqueous solution shows that the aggregates formed are about 20x larger than the particles present in organic solvents. The hydrophobic forces described previously can explain the DLS results. Aggregation in other solvents is limited to small size particles, about 10 nm, consisting of a few polymers, at most, while water promotes π-stacking associations between polymers because π-stacking reduces unfavourable polymer-solvent interactions.

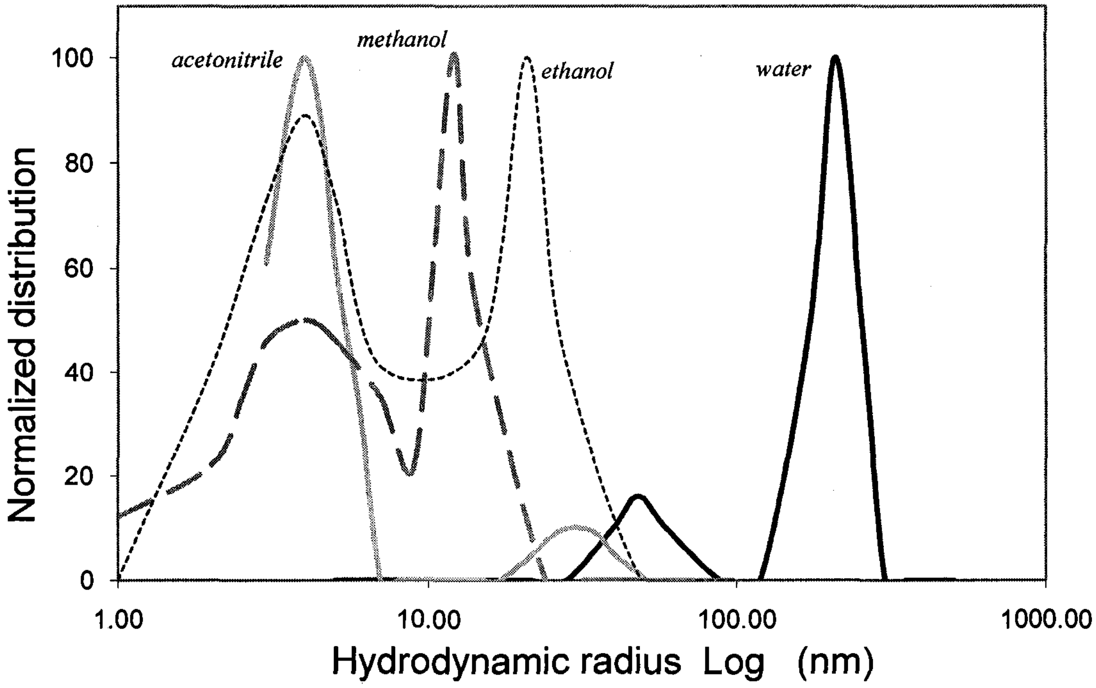

Figure 8: Particle size distributions determined by DLS using CONTIN model, for SMI polymer solutions (1% wt.) dissolved in different dielectic constant solvents.

SMI polymer exhibits similar solution properties to SMA. Large particles originated from ordered $\pi$-stacking interactions between linear polymer chains, leading to polymer nanotubes. Using DLS, the anisotropy of the particles was evaluated. Because the nanostructures are polydisperse and unassociated polymer is in excess, an exact value for the axis ratio could not be determined. It was however possible to determine if the aggregates were spherical or anisotropic. The autocorrelation function of the scattered light intensity-time fluctuations $g(\tau)$ provides the characteristic width of the intensity spectra ($\Gamma$). For rigid rods, the normalized heterodyne autocorrelation function, where the incident and scattered light are vertically polarized is given by[213]:

$$g_{VV}^{(1)}(\tau) = \sum_{l=0}^{\infty} B_l e^{-l(l+1)D_R\tau}\, e^{-D_T q^2 \tau} \tag{2}$$

where $D_T$ and $D_R$ are the translational and rotational diffusion coefficients and $B_l$ are functions[130] of the scattering angle and $q$ is the scattering vector defined below as a function of the refractive index ($n$) of the solution, the wavelength of the incident light ($\lambda_0$) and the scattering angle ($\theta_s$).

$$q = \frac{4\pi n}{\lambda_0} \sin\left(\frac{\theta_s}{2}\right) \tag{3}$$

The equivalent homodyne autocorrelation function can be obtained from the Siegert relationship[130].

$$g_{VV}^{(2)}(\tau) = 1 + \left[g_{VV}^{(1)}(\tau)\right]^2 \tag{4}$$

For particles of relatively large radii, the expansion in Eq. (5), only needs to be carried out to $l=4$ [130]. The force fitted decay frequency ($\Gamma$) as a multiple exponential relation to the square of the scattering vector and does not follow a single exponential decay as described in the introduction for spherical particles.

$$g_{VV}^{(2)}(\tau) = 1 + \left[B_0 \mathrm{e}^{-D_T q^2 \tau} + B_2 \mathrm{e}^{-(2D_T q^2 - 6D_R)\tau} + B_4 \mathrm{e}^{-(D_T q^2 - 20D_R)\tau}\right]^2 \tag{5}$$

$$\Gamma \propto Dq^2 + \textstyle\sum_{l=0}^{\infty} \beta_l \tag{6}$$

where, $\beta_l$ are functions of the scattering vector and of both the rotational and translational diffusion coefficients. However, for scattering angles below 45°, only the first term is important[130] and the relation reverts to the case of a single exponential decay. Therefore, at low scattering angles, a linear relation of $\Gamma$ as a function of $q^2$ should be observed, Eq. (7), and a deviation is expected above a value of 45°.

$$\Gamma \propto Dq^2 \tag{7}$$

For spherical particles, the auto-correlation function decays as the $e^{-2\Gamma\tau}$ and $\Gamma$ is equal to the product of the translational diffusion coefficient ($D_T$) and the square of the scattering vector ($q$), Eq. (7). However, anisotropic particles have a non-zero rotational diffusion coefficient ($D_R$). In the auto-correlation function, $D_R$ appears in an exponential term along with $D_T$. When anisotropic particles are present[130,214], the value of Gamma is no longer linear with respect to $q^2$, but has an exponential dependence.

The data required to analyze the SMI polymer in solution was collected by measuring $\Gamma$ at detection angles varying from 20° up to 80°. A standard of 100 nm particles of latex suspended in water, from Duke Scientific, was measured at the same angles. The $R^2$ value for a linear fit ($\Gamma \propto q^2$), Eq. (7), for the latex standard was 0.993, while the linear fit for the SMI data was of 0.925. When fitting the SMI data to an exponential curve ($\Gamma \propto e^{q^2}$), the value of $R^2$ increased to 0.975. The increase in $R^2$ indicates that a certain fraction of the particles in solution are anisotropic; the remaining fraction is most likely isotropic polymer aggregates.

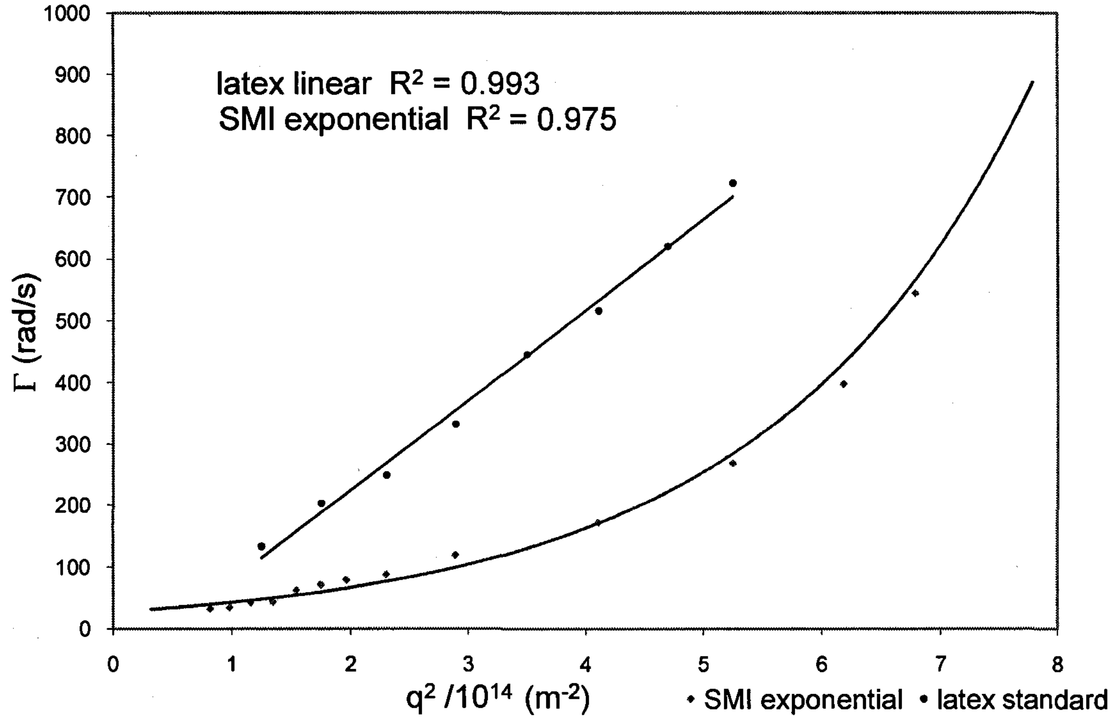

Figure 9: Low angle DLS measurements of both a standard of 100 nm spherical latex particles and SMI pH 3 solution. The exponential fit of the SMI data indicates that a fraction of the particles are anisotropic.

### 3.3 Atomic force microscopy

Non-contact mode AFM studies were performed on mica surfaces to characterize the anisotropic nanostructures. To prepare the samples for imaging, 200 μl of pyrrole were added to 10 ml of the SMI solution and left to simultaneously diffuse inside the nanostructures and polymerize. Addition of pyrrole was used to stabilize the SMA nanotubes by providing a hydrophobic core, making it possible to observe them[207]. The hydrophobic forces holding the nanotube together are disrupted by drying and the presence of pyrrole inside the tube reduces drastically the loss of structures upon drying. The same approach taken for SMA was used to stabilize the SMI nanostructures. These were observed with and without pyrrole using both AFM and TEM. To image the sample, mica was used as a surface because the structures being observed are the nm scale and mica has an atomically flat surface. The SMI polymer pH 3 solution was deposited on the slide, the drop was left for 5 minutes and the excess liquid removed by tilting the surface onto a filter paper. The sample was rinsed with a drop of water while the slide was tilted. For TEM imaging, the samples at pH 3 were deposited on carbon coated grids, left to rest for 5 min. and the excess liquid adsorbed using a filter paper.

AFM results showed that much of the polymer had an amorphous structure. However, a fair amount of the investigated areas on the mica surface presented worm-like to rod-like features, which originates from ordered non-rigid self-association of SMI polymers and were not present in the control solution containing the same amount of pyrrole at the same pH. These are the expected nanotubes, with dimensions corresponding to the predicted theoretical results. The average height of the rods was measured by scanning across the nanotube and was found to be between 4.5-5 nm, (Figure 10). The nanotube lengths are approximately 50x greater than the polymer contour length. The branching observed is a result of defects in the self-assembly of the SMI polymers, where tubes continue to grow in different directions. The mica surface was rarely visible and covered by unassociated polymer that deposits due to the electrostatic attraction with the surface and appears as a *soft* surface when scanned (Figure 10).

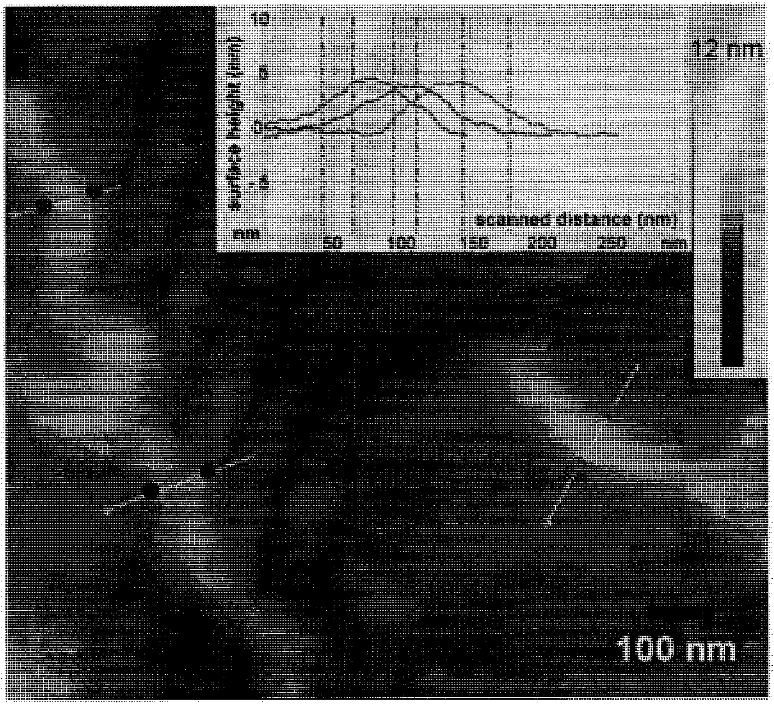

Figure 10: AFM scans of SMI polymer deposited on a mica surface. The large amorphous particles are disordered polymer aggregates. The scan on the right is a close up of the left scan. Inset are three different height profiles taken along 100-250 nm distances showing the height of the nanotubes. The linear features correspond to the non-rigid SMI nanotubes. Average height of about 4.5 nm, corresponding to the diameter of the nanotubes.

### 3.4 Transmission electron microscopy

The TEM investigation revealed short polymer rods and was carried out without pyrrole due to difficulty of differentiating the polypyrrole from the polymer. The nanotubes observed had a shorter length than the ones observed in AFM, probably due to the absence of pyrrole which helps stabilize the structure. The nanorods had a similar cross-section diameter of 6.5 ± 1.5 nm and agree, within experimental error, with the theoretical nanotube dimensions (Figure 11).

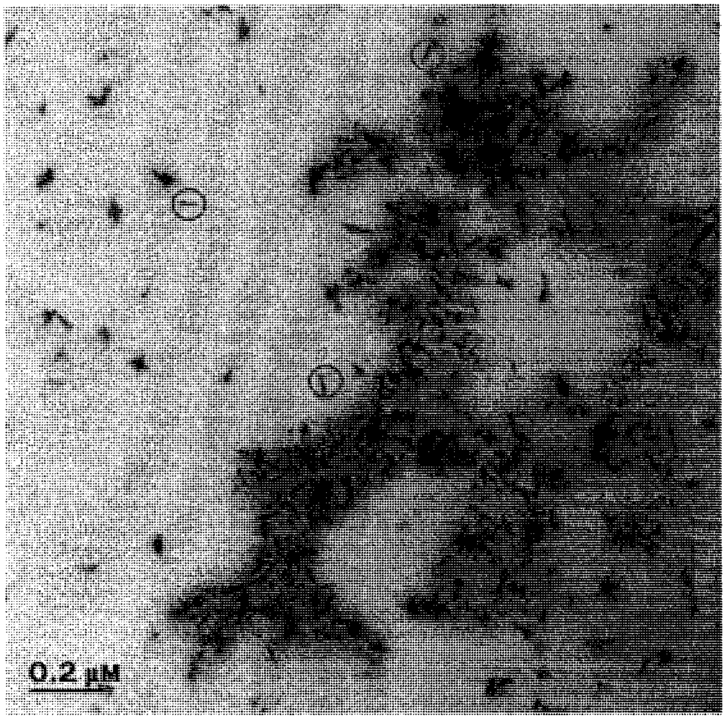

Figure 11: TEM scans of SMI polymer deposited on a commercial carbon coated grid. Pyrrole was not added to the solution to limit the number of artifacts, but its absence decreases the stability of the nanotubes. Needle structures (some which are circled) are observed with a comparable diameter observed with AFM, but shorter due to the absence of the stabilizing pyrrole core. The average cross-section diameter is 6.5 ± 1.5 nm.

## Concluding remarks

Association between isotactic polymers of SMI was investigated both in the present Chapter and in Chapter V. It was found that they can associate through $\pi$-stacking interactions. The constrained optimizations were performed using semi-empirical PM3 calculations. The bent association complexes with interacting maleimide chains were found to be more stable than linear associations, upon relaxation of the constraints. The additional stability of the bent associations can be explained by the long chain maleimides that further stabilize the association complexes through van der Waals interactions between the chains. Contribution to the stabilization energy from $\pi$-stacking only occurs in linear SMI associations. Maleimide chain-chain interactions contribute additional stabilization energy, about 1/3 of the $\pi$-stacking energy per pair to the stability of the complex.

Although the case of long maleimides has been studied in detail, the conclusions can also apply to other different styrene and maleimide copolymers. It was shown in Chapter V that removing the side chains did not affect the overall geometry of the polymer: the styrene monomers remain in the same position relative to each other and the maleimide groups also remain aligned with the same inclination, 70°. Association complexes can form between the copolymers, but without long enough maleimide chains, the bent and linear association complexes might not be significantly different in energy. Therefore, the bending of the polymer sheets into nanotubes may not be as energetically favored. Addition of chains onto the N of the maleimide can be either a stabilizing or a destabilizing factor, depending on the chemical structure of the chain. Adding hydrocarbon chains can stabilize the structure by van der Waals attractions, but adding chains with polar groups might destabilize the structure by electrostatic repulsions.

In this chapter, it was shown that by functionalizing the alternating copolymer, one can change the size and the shape of the nanotubes, and control the tertiary structure. Comparing SMA and SMI shows that the functionalization of SMA by reacting it with the primary amine changes the shape of the nanotubes from square to octagonal, increases the diameter, decreases the inner diameter and prevents aggregation between nanotubes due to additional self-assembly between nanotubes.

# Concluding remarks and future work

# Chapter VII

## 7.1. Thesis conclusions

The association behaviour of two styrene based alternating copolymers was studied. The origin of the association is $\pi$-stacking between styrene monomers. Poly(styrene-alt-maleic anhydride) (SMA) had already been shown to form nanotubes. The mechanism of association to explain nanotube formation was however lacking thermodynamic and geometrical detail, which were investigated in more detail. The polymer structure was re-investigated at a semi-empirical level and provided a description of the primary structure of SMA associated structure. SMA polymers are linear at neutral pH, 50% degree of protonation. The association between linear SMA polymers was described in terms of flexible and rigid associations. Rigid associations are more thermodynamically stable than flexible ones and form preferentially. Flexible associations then occur between rigid associations to form sheets of SMA polymers. From the folding of a sheet of 8 SMA polymers, a nanotube can be formed, which is thermodynamically more stable than a sheet. The association between SMA polymers describes the secondary structure of SMA polymer association. Further association between SMA nanotubes into stacks of nanotubes describes the tertiary structure of SMA polymer association.

The aqueous environment, in which the nanotubes were prepared, promotes the $\pi$-stacking because the styrene-styrene association minimizes the unfavourable solvent-styrene interactions. Experimentally, the fabrication of the SMA nanotubes was challenging. Previous experimental procedures simply did not produce any detectable yield of nanotubes. An improved method of fabricating the SMA nanotubes was developed. The technique involves completely hydrolyzing the maleic anhydride monomers of SMA at high pH with the addition of excess base and bringing down the pH slowly through dialysis against deionized water. The slow pH change from a random coil conformation to a linear polymer seems to promote ordered self-assembly, which was probably not the case when adding base directly and changing the pH rapidly. The experiments were carried out with a highly alternating SMA polymer synthesized with a $M_w$ of 12,000 Da and a commercial SMA sample with a $M_w$ of 50,000 Da. The nanotubes were shown to form between pH 6.5-8, where the degree of protonation is 50%. pH variations disrupt the association and no nanotubes were observed at pH>8 and pH<5. High molecular weight samples produced lower yields of nanotubes than with the lower molecular weight sample. Different bases used to hydrolyze SMA seem to affect the aggregation properties and length of the SMA nanotubes. This is not yet understood and merits further investigations.

The synthesized SMA polymer had part of the UV-sensitive initiator as a capping group, which was then converted to a disulphur. This reaction allowed the synthesis of silver and gold nanoparticles, stabilized with SMA polymer. Apart from spherical nanoparticles, other interesting structures were observed, which consisted of SMA nanotubes capped with SMA stabilized gold nanoparticles. In addition, when a slow reduction of silver ions dissolved in an SMA nanotube solution was performed, dense aligned rod-like structures were observed, similar to poly(pyrrole) filled nanotubes. These observations merit further investigation and may be useful to build systems making use of these self-assembly properties.

The dimensions of the nanotubes were changed by using a different styrene based alternating copolymer, poly(styrene-alt-N,N dimetylpropyl amide) (SMI). A conformational study of SMI showed that only isotactic polymers are ordered and have the potential to self-assemble. Investigations into the association of SMI dimers showed that the $\pi$-stacking association between styrene monomers is thermodynamically favourable and the stabilization energy and geometry values agree both with the values found for SMA dimers and literature for the $\pi$-stacking of styrenes.

Further studies on the association between many isotactic SMI dimers showed that similarly to SMA, both sheet structures and tubular structures were possible, with the tubular structure being lower in energy. The modeled nanotube dimensions were an outer diameter of 4.8 nm and an inner diameter of 1.7 nm. The linear growth mechanism of SMI nanotubes was similar than for SMA nanotubes. However, SMI nanotubes could not stack since the $\pi$-stacking styrene monomers lie inside the nanotube walls and are shielded from further interactions. This was experimentally observed using TEM and AFM. The dimensions of the observed individual rods agreed within experimental error with the theoretical dimensions of the nanotubes.

## 7.2. Suggested experiments for future research

Computationally, the study of different alternating copolymers should be performed. The aromatic π-stacking monomers could be changed to substituted styrene monomers or larger aromatic monomers such as DNA nucleotides or (Figure 1). The interaction between similar alternating copolymers having different quadrupolar moment aromatic monomers should be investigated because these could lead to stronger polymer-polymer association. Changing the shape of the aromatic groups can also modify the size of the nanotube. If the aromatic monomers are longer, the alternating copolymer association may lead to larger diameter nanotubes. Studying the π-stacking association between the isotactic polymers, poly(styrene-alt-maleimide) and isotactic poly(hexafluorostyrene-alt-maleimide), should reveal stronger association interactions (see Chapter I). The advantage of such hybrid systems is the increased stability of the nanotubes to changes in pH, solvent and ionic strength. DNA nucleotides are well known to assemble through π-stacking and their quadrupole moments should be different enough that the sideways association between the alternating copolymers of DNA base pairs and maleic anhydride can associate more selectively.

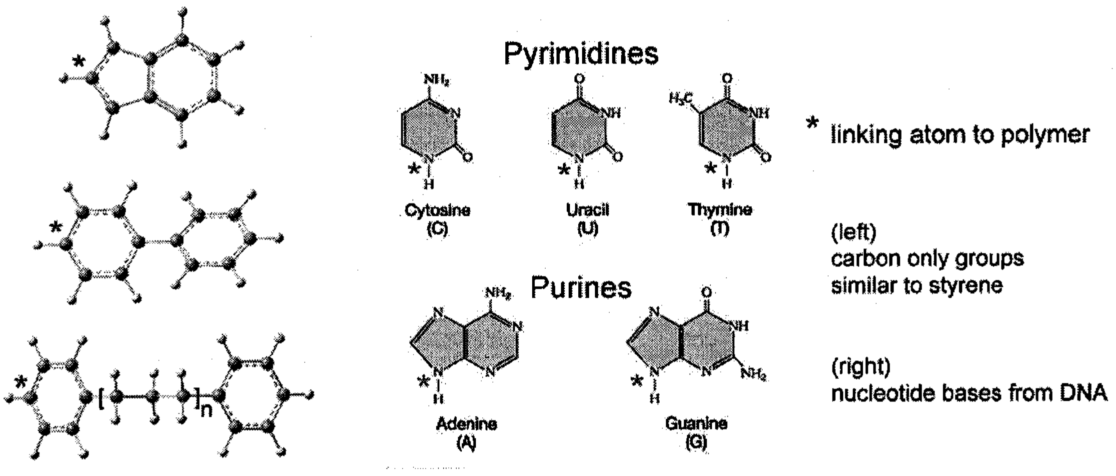

Figure 1: Example of potential aromatic groups that may be used to substituted styrene and provide more selected and stronger π-stacking.

The formation of nanotubes was investigated spectroscopically using TOCSY 1D $^1$H-NMR, 2D $^1$H-NMR and UV-VIS to observe if changes in the π-stacking of the styrene monomers was different at high and neutral pH. Unfornunately the results obtained were not conclusive. The results are shown in the appendix.

In UV-Visible studies, it was expected that a peak shift would be observed due to π-stacking, but no such shift was observed when tracking the nanotube formation from spectra taken at high pH until neutral pH was reached during dialysis. The problem may be that the styrene monomers follow a disordered π-stacking. Literature systems that exhibit a peak shift due to an increase in aromaticity, are based on aromatic π-stacking that is ordered (parallel), and in some cases conjugated systems involving opposite quadrupoles are involved. This is not the case for styrene-styrene interactions, which are between identical quadrupoles and does not give rise to ordered parallel structures. It would be valuable to find a spectroscopic technique to determine that SMA polymers self-assemble in ordered structures. The method could be used for other styrene (or aromatic monomer) based alternating copolymers. This would provide a stronger basis to the theory and could be used to study the stability and the kinetics of self-assembly in different experimental conditions. A spectroscopic method may also provide information on the yield of nanotubes obtained and would a more reliable and efficient tool than the microscopy techniques presented in Chapters II, IV and VI.

The stereoregularity of the SMA polymer studied was not controlled. It would be important to attempt the synthesis of an isotactic SMA polymer. This would simplify the theoretical work since only the modeling of an isotactic polymer is required to understand the experimental results. At the moment, calculations of the nanotube structure were only performed using isotactic SMA polymers, (SSS) chirality monomers. Additionally, an isotactic SMA polymer can be converted to an isotactic SMI polymer through an amination reaction with 3-(dimethylamino)-1-propylamine[205] and this polymer could be used to confirm the theoretical calculations performed on SMI polymers.

Different factors that would alter the SMA nanotube formation remain to be investigated. Solvent composition and salt effects were not investigated in detail. Furthermore, changing the base used changes the aggregation properties of SMA nanotubes, but this is not fully understood at the moment and merits further investigation using molecular modeling.

SMI nanotubes may be fabricated to be longer using a dialysis method similar to the preparation of SMA nanotubes. The SMI polymer could be suspended in water. The solution could then be dialyzed against acidified water to change the pH slowly and allow the polymer to self-assemble with a greater order. Using a higher $M_w$ cut-off membrane could also help concentrate the associated polymer, while leaving the unassociated polymer to diffuse out of the dialysis membrane.

A potential application of these styrene based alternating copolymer nanotubes is their use as polymerization templates; this was demonstrated with the polymerization of pyrrole inside the nanotubes. Monomers can be left to diffuse inside the nanotube, where the environment is more hydrophobic, and then polymerized using a radical initiator or a UV-initiated polymerization.

This would have the advantage of producing 2 nm wide fibres that would be up to 1 µm in length. The method would be extremely cost effective since SMA is not expensive, no organic solvents are needed, rather only water and base.

Another application of these polymer nanotubes would be their use to template surfaces. The chemistry studied in Chapter IV, which made use of thiol-gold chemistry would be of use to selectively pattern a surface with SMA. A method is suggested here where gold nanoparticle pillars are linked with SMA nanotubes (Figure 2). Silicon pillars of a few nanometers diameter and up to 500 nm in height can be produced using gold nanoparticles as a catalysts for their growth[193,195]. Gold nanoparticles with diameters of a few nanometers can be selectively deposited on a surface[215-220] (Figure 2(a)). The material surrounding the gold nanoparticles can then be removed using plasma etching, the Si is removed around the gold nanoparticles leaving a pillar terminated with a bare Au(0) nanoparticle (Figure 2(b)) [193,195]. The thiol terminated SMA polymer can then be brought into contact with the Au(0) surface in solution and a self-assembled monolayer (SAM) can form on the gold surface (Figure 2(c)). Because the polymer is polydisperse, it is reasonable to assume that there will be free polymer ends that are longer than the average thickness of the SAM. Therefore, free styrene monomers can protrude from the surface and initiate nanotube growth as is believed to occur in the SMA-Au composites discussed in Chapter IV. The surface would be rinsed many times and then the nanotubes could be either deposited on the surface to link with the free polymer on the SAMs or the nanotubes could be self-assembled in the presence of the surface with pillars (Figure 2(d)). The result would be pillars that could be linked with organic nanotubes, which could then be modified by filling the interior of the nanotube with quantum dots, metals by reduction of their salts, semi-conducting polymers by polymerization or simply using these as templates to build complex nano-architectures without the need for expensive methods such as ion beam etching[194].

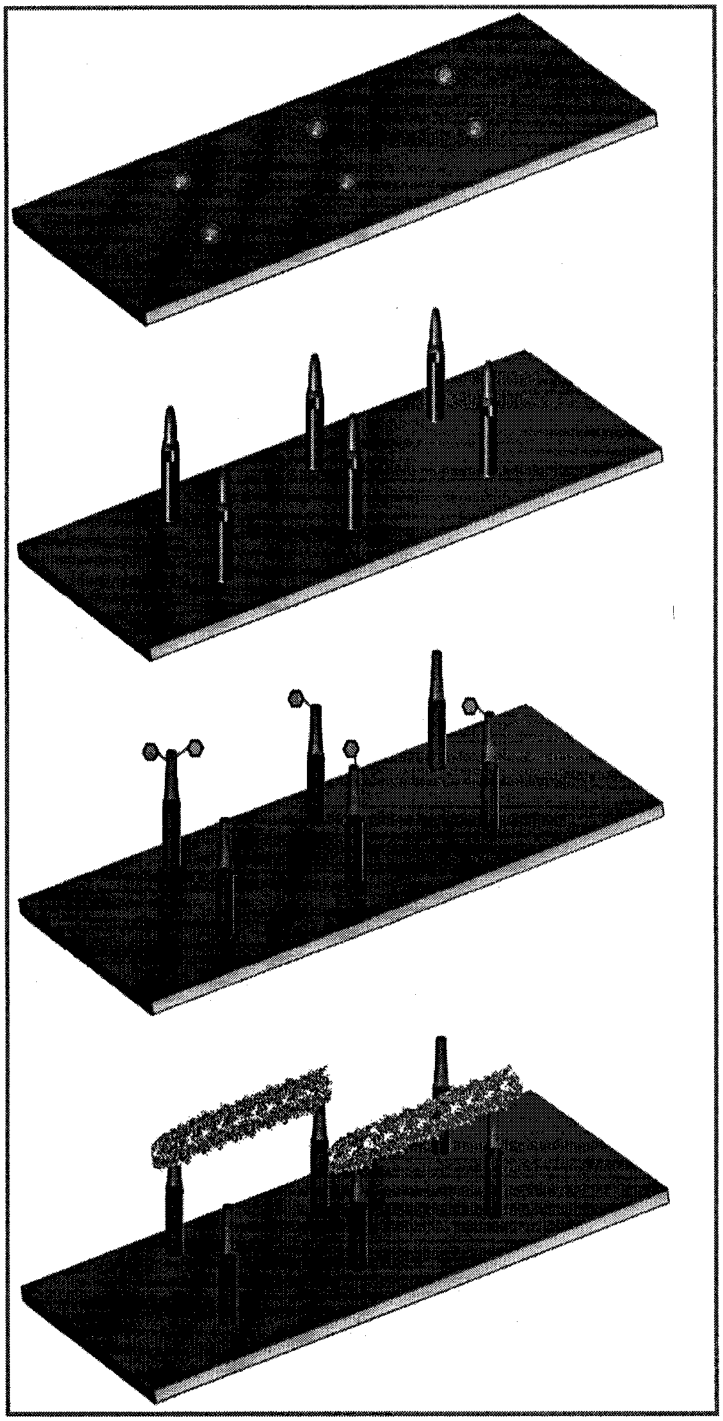

(a) Si surface with selectivery deposited stabilized gold nanoparticles.

(b) The Au nanoparticle covered Si surface is heated and the surface is uniformly etched using a plasma beam. The gold nanoparticles prevent the material underneath from being etched. The result is pillars with Au(0) nanoparticles.

(c) The Au(0) surface of the pillars can be stabilized by thiols. SMA-thiol terminated can be reacted in solution and form a SAM on the Au(0) substrate. Since the SMA is polydisperse, longer polymers can extend outside the SAM and act as nucleation points for nanotube growth by π–stacking.

(d) The cleaned surface can be reacted with non-thiol SMA and nanotubes can grow from the SAMs on the ends of the pillars. The flexible nanotubes can link two or more pillars together.

Figure 2: Schematic representation of a possible route to pattern silicon surfaces with SMA nanotubes.

Another relevant application of these nanotubes is their use in the fabrication of semi-conducting and conducting nanowires. Using electroless metallization techniques, metal ions or metal complexes can be reduced on the surface or in the interior of the polymer nanotubes. This could provide thin hybrid polymer-metal wires, which can find applications in areas such as electronics, nano-sensors and optical devices.

This method might also be used to separate isotactic SMI polymers from a mixture of random chirality SMI polymers. Because only isotactic SMI polymers can self-assemble into nanotubes, gold particles can be linked with isotactic SMI polymer nanotubes.

## 7.3. Original contributions to knowledge

The mechanism of association of SMA polymers into linear nanotubes, with an outer diameter of 4 nm and an inner diameter of 2.5 nm, was described in terms of mixtures of rigid and flexible associations originating from the π-stacking of styrene monomers along the length of the polymer backbones.

The association enthalpy was calculated using both semi-empirical methods (PM3) and perturbational Hartree-Fock (MP2) methods and agrees with known experimental values. The self-association was shown to be thermodynamically favourable.

An improved preparation technique to fabricate SMA nanotubes was established. Higher yields were obtained and the nanotubes can be reproduced reliably. The nanotubes were made from two different molecular weight SMA polymers, which were produced by two different polymerization methods (RAFT and radical polymerization). The synthesized polymer was chemically modified and SMA stabilized gold and silver nanoparticles were synthesized. Apart from the spherical nanoparticles observed, SMA nanotubes capped with gold nanoparticles were observed as well as SMA nanotubes with reduced silver. The combination of SMA nanotubes with metals may find potential applications in different nanotechnology fields.

A different styrene based alternating copolymer, SMI, was theoretically modeled and found to be capable of forming ordered associations only when the polymers are isotactic. SMI can also self-assemble into nanotubes and these have an outer diameters of 5 nm and an inner diameter of 1.7 nm. The geometry of the SMI nanotubes is different than for SMA, but the main association mechanism remain the π-stacking of the styrene monomers along the length of the polymers. The SMI nanotubes were experimentally characterized using TEM and AFM and the size measurements obtained from the experiments agreed with the theoretical prediction.

# Bibliography

1. Malardier-Jugroot C: **Novel self-assembly of an alternating copolymer into nanotubes: Theoretical investigation and experimental characterisation**: 2004.
2. Meikle JI: *American Plastic: a Cultural History*. New Brunswick, New Jersey: Rutgers University Press; 1997.
3. Kaminsky W: **Chapter 7**. In *Transition Metals and Organometallics as Catalysts for Olefin Polymerization*. Edited by: Spinger-Verlad; 1998.
4. Matyjaszewski K: **Chapter 2.** In *Advances in radical polymerization*. Edited by: A.C.S.; 2003.
5. Natta G, Danusso F: *Stereoregular Polymers and Stereospecific Polymerizations*, vol 1. Milano, Italy: Pergamon Press; 1967.
6. Natta G, Pino P, Mantica E, Danusso F, Mazzanti T, Peraldo M: **Stereospecific polymerization of alpha-olefins.** *Chimica e Industria*,(1956), **38**:124.
7. Alexandridis P, Lindman B: *Amphiphilic Block Copolymers: Self-Assembly and Applications*: Elsevier; 2000.
8. Sperling LH: *Introduction to Physical Polymer Science* edn 3rd. Hoboken, New Jersey: John Wiley & Sons; 2001.
9. Zhang Y, Keaton RJ, Sita LR: **Degenerative transfer living Ziegler-Natta polymerization: application to the synthesis of monomodal stereoblock polyolefins of narrow polydispersity and tunable block length.** *Journal of the American Chemical Society*,(2003), **125**:9062.
10. Kitayama T, Ute K, Yamamoto M, Fujimoto N, Hatada K: **Highly isotactic and living polymerization of ethyl methacrylate with tert-butylmagnesium bromide in toluene and the preparation of block and random copolymers with high stereoregularity.** *Polymer Journal*,(1990), **22**:386.
11. Morokuma K: **Why do molecules interact? The origin of electron donor-acceptor complexes, hydrogen bonding and proton affinity.** *Accounts of Chemical Research*,(1977), **10**:294.
12. Hehre W, Radom L, Schleyer P, Pople JA: *Ab-Initio Molecular Orbital Theory*. New york: John Wiley and Sons; 1986.
13. Hunter C: **Non-covalent interactions between aromatic molecules.** *From Simplicity to Complexity in Chemistry--and Beyond, [Lectures presented at a Workshop], Bielefeld, Ger., July 26-28, 1993*,(1996):113.
14. Hunter CA: **Meldola lecture. The role of aromatic interactions in molecular recognition.** *Chemical Society Reviews*,(1994), **23**:101.
15. Hunter CA, Lawson KR, Perkins J, Urch CJ: **Aromatic interactions.** *Journal of the Chemical Society, Perkin Transactions 2*,(2001):651.
16. Hunter CA, Sanders JKM: **The nature of p-p interactions.** *Journal of the American Chemical Society*,(1990), **112**:5525.
17. Cockroft SL, Perkins J, Zonta C, Adams H, Spey SE, Low CMR, Vinter JG, Lawson KR, Urch CJ, Hunter CA: **Substituent effects on aromatic stacking interactions.** *Organic & Biomolecular Chemistry*,(2007), **5**:1062.
18. Cockroft SL, Hunter CA, Lawson KR, Perkins J, Urch CJ: **Electrostatic Control of Aromatic Stacking Interactions.** *Journal of the American Chemical Society*,(2005), **127**:8594.
19. Ilhan F, Gray M, Blanchette K, Rotello VM: **Control of Polymer Solution Structure via Intra- and Intermolecular Aromatic Stacking.** *Macromolecules*,(1999), **32**:6159.
20. Newcomb LF, Gellman SH: **Aromatic Stacking Interactions in Aqueous Solution: Evidence That neither Classical Hydrophobic Effects nor Dispersion Forces Are Important.** *Journal of the American Chemical Society*,(1994), **116**:4993.
21. De Feyter S, De Schryver Frans C: **Two-dimensional supramolecular self-assembly probed by scanning tunneling microscopy.** *Chemical Society reviews*,(2003), **32**:139.
22. Wu J, Pisula W, Muellen K: **Graphenes as potential material for electronics.** *Chemical Reviews*,(2007), **107**:718.
23. Sponer J, Gabb HA, Leszczynski J, Hobza P: **Base-base and deoxyribose-base stacking interactions in B-DNA and Z-DNA: a quantum-chemical study.** *Biophysical Journal*,(1997), **73**:76.
24. Zhang J, Wang S-L, Liu J, chen GY: *Self-Assembled Nanostructures*. New York: Klumer Academic / Plenum Publishers; 2003.
25. Ludwigs S, Boeker A, Voronov A, Rehse N, Magerle R, Krausch G: **Self-assembly of functional nanostructures from ABC triblock copolymers.** *Nature Materials*,(2003), **2**:744.
26. Feng J, Ruckenstein E: **Self-assembling of ABC linear triblock copolymers in nanocylindrical tubes.** *Journal of Chemical Physics*,(2007), **126**:124902/1.
27. Zhang S: **Fabrication of novel biomaterials through molecular self-assembly.** *Nature Biotechnology*,(2003), **21**:1171.
28. Chaki NK, Vijayamohanan K: **Self-assembled monolayers as a tunable platform for biosensor applications.** *Biosensors & Bioelectronics*,(2002), **17**:1.
29. Schreiber F: **Structure and growth of self-assembling monolayers.** *Progress in Surface Science*,(2000), **65**:151.

30. Ulman A, Kang JF, Shnidman Y, Liao S, Jordan R, Choi G-Y, Zaccaro J, Myerson AS, Rafailovich M, Sokolov J, et al.: **Self-assembled monolayers of rigid thiols.** *Reviews in Molecular Biotechnology*,(2000), **74**:175.

31. Kariuki NN, Luo J, Hassan SA, Lim IIS, Wang L, Zhong CJ: **Assembly of Bimetallic Gold-Silver Nanoparticles via Selective Interparticle Dicarboxylate-Silver Linkages.** *Chemistry of Materials*,(2006), **18**:123.

32. Nath KG, Ivasenko O, Miwa JA, Dang H, Wuest JD, Nanci A, Perepichka DF, Rosei F: **Rational Modulation of the Periodicity in Linear Hydrogen-Bonded Assemblies of Trimesic Acid on Surfaces.** *Journal of the American Chemical Society*,(2006), **128**:4212.

33. Mu C, Zhao Q, Xu D, Zhuang Q, Shao Y: **Silicon Nanotube Array/Gold Electrode for Direct Electrochemistry of Cytochrome c.** *Journal of Physical Chemistry B*,(2007), **111**:1491.

34. Radushkevich LV, Luk'yanovich VM: **Structure of the carbon produced in the thermal decomposition of carbon monoxide on an iron catalyst.** *Zhumal Fizicheskoi Khimii*,(1952), **26**:88.

35. Iijima S: **Helical microtubules of graphitic carbon.** *Nature*,(1991), **354**:56.

36. Dekker C: **Carbon nanotubes as molecular quantum wires.** *Physics Today*,(1999), **52**:22.

37. Rochefort A: **Multi-Walled Carbon Nanotubes.**

38. Dai H: *Nanotube Growth and Characterization*. Berlin: Springer; 2001.

39. Bettinger HF, Dumitrica T, Scuseria GE, Yakobson BI: **Mechanically induced defects and strength of BN nanotubes.** *Physical Review B: Condensed Matter and Materials Physics*,(2002), **65**:041406/1.

40. Blase X, Rubio A, Louie SG, Cohen ML: **Stability and band gap constancy of boron nitride nanotubes.** *Europhysics Letters*,(1994), **28**:335.

41. Chopra NG, Zettl A: **Measurement of the elastic modulus of a multi-wall boron nitride nanotube.** *Solid State Communications*,(1998), **105**:297.

42. Cumings J, Zettl A: **Field emission and current-voltage properties of boron nitride nanotubes.** *Solid State Communications*,(2004), **129**:661.

43. Hernandez E, Goze C, Bernier P, Rubio A: **Elastic Properties of C and BxCyNz Composite Nanotubes.** *Physical Review Letters*,(1998), **80**:4502.

44. Kim Y-H, Chang KJ, Louie SG: **Electronic structure of radially deformed BN and BC3 nanotubes.** *Physical Review B: Condensed Matter and Materials Physics*,(2001), **63**:205408/1.

45. Rubio A, Corkill JL, Cohen ML: **Theory of graphitic boron nitride nanotubes.** *Physical Review B: Condensed Matter and Materials Physics*,(1994), **49**:5081.

46. Suryavanshi AP, Yu M-F, Wen J, Tang C, Bando Y: **Elastic modulus and resonance behavior of boron nitride nanotubes.** *Applied Physics Letters*,(2004), **84**:2527.

47. Bai X, Golberg D, Bando Y, Zhi C, Tang C, Mitome M, Kurashima K: **Deformation-driven electrical transport of individual boron nitride nanotubes.** *Nano letters*,(2007), **7**:632.

48. Cooper GM: *The Cell: A Molecular Approach* edn 2nd Ed. Sunderland, Missachusetts: Sinauer Associates Inc.; 2000.

49. Murphy GE, Leadbetter JR, Jensen GJ: **In situ structure of the complete Treponema primitia flagellar motor.** *Nature*,(2006), **442**:1062.

50. Bardy SL, Ng SYM, Jarrell KF: **Recent Advances in the Structure and Assembly of the Archaeal Flagellum.** *Journal of Molecular Microbiology and Biotechnology*,(2004), **7**:41.

51. Fedorov OV, Efimov AV: **Flagellin as an object for supramolecular engineering.** *Protein Engineering*,(1990), **3**:411.

52. Fagerstrom C, Wadsworth P: **Microtubules and Actin filaments in living cells.** *DEPARTMENT OF BIOLOGY, UNIVERSITY OF MASSACHUSETTS AMHERST*

53. Davidson MW: **Shematic representation of flagellum micro-structure.** *Florida State University*

54. Carloni P, Andreoni W, Parrinello M: **Self-assembled peptide nanotubes from first principles.** *Physical Review Letters*,(1997), **79**:761.

55. Guo Q, Xie Y, Wang X, Zhang S, Hou T, Lv S: **Synthesis of carbon nitride nanotubes with the C(3)N(4) stoichiometry via a benzene-thermal process at low temperatures.** *Chemical communications*,(2004):26.

56. Hartgerink JD, Clark TD, Ghadiri MR: **Peptide nanotubes and beyond.** *Chemistry-A European Journal*,(1998), **4**:1367.

57. Hartgerink JD, Granja JR, Milligan RA, Ghadiri MR: **Self-Assembling Peptide Nanotubes.** *Journal of the American Chemical Society*,(1996), **118**:43.

58. Horne WS, Stout CD, Ghadiri MR: **A Heterocyclic Peptide Nanotube.** *Journal of the American Chemical Society*,(2003), **125**:9372.

59. Kim HS, Hartgerink JD, Ghadiri MR: **Oriented Self-Assembly of Cyclic Peptide Nanotubes in Lipid Membranes.** *Journal of the American Chemical Society*,(1998), **120**:4417.

60. Matsui H, Douberly GE, Jr.: **Organization of Peptide Nanotubes into Macroscopic Bundles.** *Langmuir*,(2001), **17**:7918.

[61] Reches M, Gazit E: **Molecular self-assembly of peptide nanostructures: mechanism of association and potential uses.** *Current Nanoscience*,(2006), **2**:105.

[62] Vauthey S, Santoso S, Gong H, Watson N, Zhang S: **Molecular self-assembly of surfactant-like peptides to form nanotubes and nanovesicles.** *Proceedings of the National Academy of Sciences of the United States of America*,(2002), **99**:5355.

[63] Bong DT, Ghadiri MR: **Self-assembling cyclic peptide cylinders as nuclei for crystal engineering.** *Angewandte Chemie, International Edition*,(2001), **40**:2163.

[64] Rakotondradany F, Palmer A, Toader V, Chen B, Whitehead MA, Sleiman Hanadi F: **Hydrogen-bond self-assembly of DNA-analogues into hexameric rosettes.** *Chemical communications*,(2005):5441.

[65] Rakotondradany F, Whitehead MA, Lebuis A-M, Sleiman Hanadi F: **Photoresponsive supramolecular systems: self-assembly of azodibenzoic acid linear tapes and cyclic tetramers.** *Chemistry*,(2003), **9**:4771.

[66] Seebach D, Matthews JL, Meden A, Wessels T, Baerlocher C, McCusker LB: **Cyclo-beta -peptides. Structure and tubular stacking of cyclic tetramers of 3-aminobutanoic acid as determined from powder diffraction data.** *Helvetica Chimica Acta*,(1997), **80**:173.

[67] Ghadiri MR, Granja JR, Milligan RA, McRee DE, Khazanovich N: **Self-assembling organic nanotubes based on a cyclic peptide architecture.** *Nature*,(1993), **366**:324.

[68] Holmes TC, de Lacalle S, Su X, Liu G, Rich A, Zhang S: **Extensive neurite outgrowth and active synapse formation on self-assembling peptide scaffolds.** *Proceedings of the National Academy of Sciences of the United States of America*,(2000), **97**:6728.

[69] Banerjee IA, Yu L, Matsui H: **Cu nanocrystal growth on peptide nanotubes by biomineralization: Size control of Cu nanocrystals by tuning peptide conformation.** *Proceedings of the National Academy of Sciences of the United States of America*,(2003), **100**:14678.

[70] Yu L, Banerjee IA, Matsui H: **Direct Growth of Shape-Controlled Nanocrystals on Nanotubes via Biological Recognition.** *Journal of the American Chemical Society*,(2003), **125**:14837.

[71] Banerjee Ipsita A, Yu L, Matsui H: **Cu nanocrystal growth on peptide nanotubes by biomineralization: size control of Cu nanocrystals by tuning peptide conformation.** *Proceedings of the National Academy of Sciences of the United States of America*,(2003), **100**:14678.

[72] Djalali R, Chen Y-f, Matsui H: **Au nanocrystal growth on nanotubes controlled by conformations and charges of sequenced peptide templates.** *Journal of the American Chemical Society*,(2003), **125**:5873.

[73] Banerjee IA, Muniz G, Lee S-Y, Matsui H: **Mineralization of semiconductor nanocrystals on peptide-coated bionanotubes and their pH-dependent morphology changes.** *Journal of Nanoscience and Nanotechnology*,(2007), **7**:2287.

[74] Banerjee IA, Yu L, MacCuspie RI, Matsui H: **Thiolated Peptide Nanotube Assembly as Arrays on Patterned Au Substrates.** *Nano Letters*,(2004), **4**:2437.

[75] Djalali R, Chen Y-f, Matsui H: **Au nanowire fabrication from sequenced histidine-rich peptide.** *Journal of the American Chemical Society*,(2002), **124**:13660.

[76] Djalali R, Chen Y-f, Matsui H: **Au Nanocrystal Growth on Nanotubes Controlled by Conformations and Charges of Sequenced Peptide Templates.** *Journal of the American Chemical Society*,(2003), **125**:5873.

[77] Matsui H, Porrata P, Douberly GE, Jr.: **Protein Tubule Immobilization on Self-Assembled Monolayers on Au Substrates.** *Nano Letters*,(2001), **1**:461.

[78] Nuraje N, Su K, Samson J, Haboosheh A, MacCuspie RI, Matsui H: **Self-assembly of Au nanoparticle-containing peptide nanorings on surfaces.** *Supramolecular Chemistry*,(2006), **18**:429.

[79] Chun AL, Moralez JG, Fenniri H, Webster TJ: **Helical rosette nanotubes: A more effective orthopaedic implant material.** *Nanotechnology*,(2004), **15**:S234.

[80] Fenniri H, Deng B-L, Ribbe AE, Hallenga K, Jacob J, Thiyagarajan P: **Entropically driven self-assembly of multichannel rosette nanotubes.** *Proceedings of the National Academy of Sciences of the United States of America*,(2002), **99**:6487.

[81] Fenniri H, Mathivanan P, Vidale KL, Sherman DM, Hallenga K, Wood KV, Stowell JG: **Helical Rosette Nanotubes: Design, Self-Assembly, and Characterization.** *Journal of the American Chemical Society*,(2001), **123**:3854.

[82] Pantos GD, Pengo P, Sanders Jeremy KM: **Hydrogen-bonded helical organic nanotubes.** *Angewandte Chemie, International Edition*,(2007), **46**:194.

[83] Pantos GD, Pengo P, Sanders JKM: **Hydrogen-bonded helical organic nanotubes. [Erratum to document cited in CA146:251467].** *Angewandte Chemie, International Edition*,(2007), **46**:2138.

[84] Pantos GD, Wietor J-L, Sanders Jeremy KM: **Filling helical nanotubes with C60.** *Angewandte Chemie, International Edition*,(2007), **46**:2238.

[85] Grumelard J, Taubert A, Meier W: **Soft nanotubes from amphiphilic ABA triblock macromonomers.** *Chemical communications*,(2004):1462.

[86] Hamley IW: **Nanoshells and nanotubes from block copolymers.** *Soft Matter*,(2005), **1**:36.

[87] Liu G, Stewart S: **Hollow nanospheres and nanotubes from block copolymers.** *Polymeric Materials Science and Engineering*,(1999), **81**:10.

[88] Sun Y, Steinhart M, Zschech D, Adhikari R, Michler GH, Goesele U: **Diameter-dependence of the morphology of PS-b-PMMA nanorods alumina templates.** *Macromolecular Rapid Communications*,(2005), **26**:369.

[89] Yan X, Liu G, Li Z: **Preparation and phase segregation of block copolymer nanotube multiblocks.** *Journal of the American Chemical Society*,(2004), **126**:10059.

[90] Stewart S, Liu G: **Block copolymer nanotubes.** *Angewandte Chemie, International Edition*,(2000), **39**:340.

[91] Jofre A, Hutchison JB, Kishore R, Locascio LE, Helmerson K: **Amphiphilic Block Copolymer Nanotubes and Vesicles Stabilized by Photopolymerization.** *Journal of Physical Chemistry B*,(2007), **111**:5162.

[92] Yan X, Liu F, Li Z, Liu G: **Poly(acrylic acid)-Lined Nanotubes of Poly(butyl methacrylate)-block-poly(2-cinnamoyloxyethyl methacrylate).** *Macromolecules*,(2001), **34**:9112.

[93] Fuhrhop JH, Fritsch D: **Bolaamphiphiles form ultrathin, porous and unsymmetric monolayer lipid membranes.** *Accounts of Chemical Research*,(1986), **19**:130.

[94] Fuhrhop J-H, Wang T: **Bolaamphiphiles.** *Chemical Reviews*,(2004), **104**:2901.

[95] Masuda M, Shimizu T: **Lipid Nanotubes and Microtubes: Experimental Evidence for Unsymmetrical Monolayer Membrane Formation from Unsymmetrical Bolaamphiphiles.** *Langmuir*,(2004), **20**:5969.

[96] Schnur JM: **Lipid tubules: a paradigm for molecularly engineered structures.** *Science*,(1993), **262**:1669.

[97] Spector MS, Easwaran KRK, Jyothi G, Selinger JV, Singh A, Schnur JM: **Chiral molecular self-assembly of phospholipid tubules: a circular dichroism study.** *Proceedings of the National Academy of Sciences of the United States of America*,(1996), **93**:12943.

[98] Spector MS, Easwaran KRK, Selinger JV, Singh A, Schnur JM: **Circular dichroism studies of chiral packing in lipid tubules.** *Polymer Preprints*,(1996), **37**:482.

[99] She X, Song G, Li J, Han P: **Non-polar polymer nanotubes and nanorods fabricated by wetting of anodic aluminium oxide template.** *Xiandai Huagong*,(2006), **26**:37.

[100] Steinhart M, Goring P, Luo Y, Hofmeister H, Greiner A, Wendorff JH, Wehrspohn RB, Pippel E, Gosele U: **Nanotubes with complex wall architectures by template wetting.** *Abstracts of Papers, 227th ACS National Meeting, Anaheim, CA, United States, March 28-April 1, 2004 FIELD Full Journal Title:Abstracts of Papers, 227th ACS National Meeting, Anaheim, CA, United States, March 28-April 1, 2004*,(2004):PHYS.

[101] Steinhart M, Wehrspohn RB, Goesele U, Wendorff JH: **Nanotubes by template wetting: A modular assembly system.** *Angewandte Chemie, International Edition*,(2004), **43**:1334.

[102] Tao F, Guan M, Jiang Y, Zhu J, Xu Z, Xue Z: **An easy way to construct an ordered array of nickel nanotubes: the triblock-copolymer-assisted hard-template method.** *Advanced Materials*,(2006), **18**:2161.

[103] She X, Song G, Li J, Han P, Yang S, Peng Z: **Preparation and characterization of polyamide 66 nanotubes and nanowires on an anodic aluminum oxide template by a physical wetting method.** *Journal of Materials Research*,(2006), **21**:1209.

[104] Tian Y, He Q, Tao C, Cui Y, Ai S, Li J: **Fabrication of polyethyleneimine and poly(styrene-alt-maleic anhydride) nanotubes through covalent bond.** *Journal of Nanoscience and Nanotechnology*,(2006), **6**:2072.

[105] Steinhart M, Wendorff JH, Wehrspohn RB: **Nanotubes a la carte. Wetting of porous templates.** *ChemPhysChem*,(2003), **4**:1171.

[106] Williams DB, Carter CB: *Transmission Electron Microscopy : A Textbook for Materials Science* edn 1st. New York, New York: Spinger; 2004.

[107] Morita S, Wiesendanger R, Meyer E: *Noncontact Atomic Force Microscopy*. Edited by Avouris PDP. New York: Spinger-Verlag Berlin Heidelberg; 2002.

[108] Goldstein J, Newbury D, Joy D, Lyman C, Echlin P, Lifshin E, Sawyer L, Michael J: *Scanning Electron Microscopy and X-ray Microanalysis* edn 3rd. New York, New York: Springer; 2003.

[109] Malardier-Jugroot C, van de Ven TGM, Whitehead MA: **Characterization of a novel self-association of an alternating copolymer into nanotubes in solution.** *Molecular Simulation*,(2005), **31**:173.

[110] Malardier-Jugroot C, van de Ven TGM, Whitehead MA: **Linear conformation of poly(styrene-alt-maleic anhydride) capable of self-assembly: a result of chain stiffening by internal hydrogen bonds.** *The journal of physical chemistry. B, Condensed matter, materials, surfaces, interfaces & biophysical*,(2005), **109**:7022.

111. Brown DA: *Quantum Chemistry*. London: Penguin; 1972.
112. Parr RG: *The Quantum Theory of Molecular Electronic Structure*. New York: W.A. Benjamin; 1964.
113. on World Wide Web URL: http://fptchlx03.tu-graz.ac.at/tc_tutorial/tchcnE.html
114. Atkins PW: *Quanta – a handbook of concepts*. Oxford: Clarendon Press 1974.
115. Pariser R, Parr RG: **A semi-empirical theory of the electronic spectra and electronic structure of complex unsaturated molecules. I.** *Journal of Chemical Physics*,(1953), **21**:466.
116. Pople JA: **Electron interaction in unsaturated hydrocarbons.** *Transactions of the Faraday Society*,(1953), **49**:1375.
117. Pople JA, Santry DP, Segal GA: **Approximate self-consistent molecular orbital theory. I. Invariant procedures.** *Journal of Chemical Physics*,(1965), **43**:S129.
118. Pople JA, Segal GA: **Approximate self-consistent molecular orbital theory. II. Calculations with complete neglect of differential overlap.** *Journal of Chemical Physics*,(1965), **43**:S136.
119. Pople JA, Beveridge DL, Dobosh PA: **Approximate self-consistent molecular-orbital theory. V. Intermediate neglect of differential overlap.** *Journal of Chemical Physics*,(1967), **47**:2026.
120. Bingham RC, Dewar MJS, Lo DH: **Ground states of molecules. XXV. MINDO/3. Improved version of the MINDO semiempirical SCF-MO method.** *Journal of the American Chemical Society*,(1975), **97**:1285.
121. Dewar MJS, Thiel W: **A semiempirical model for the two-center repulsion integrals in the NDDO approximation.** *Theoretica Chimica Acta*,(1977), **46**:89.
122. Dewar MJS, Zoebisch EG, Healy EF, Stewart JJP: **Development and use of quantum mechanical molecular models. 76. AM1: a new general purpose quantum mechanical molecular model.** *Journal of the American Chemical Society*,(1985), **107**:3902.
123. Stewart JJP: **Optimization of parameters for semiempirical methods. II. Applications.** *Journal of Computational Chemistry*,(1989), **10**:221.
124. Stewart JJP: **Optimization of parameters for semiempirical methods. I. Method.** *Journal of Computational Chemistry*,(1989), **10**:209.
125. Kudin KN, Scuseria GE, Cances E: **A black-box self-consistent field convergence algorithm: One step closer.** *Journal of Chemical Physics*,(2002), **116**:8255.
126. Frisch eaMJ: **Gaussian 03W.** edn 6.0. Edited by. Pittsburgh: Gaussian Inc.; 2003.
127. Yager K, Barrett CJ: **Schematics of TEM apparatus.** *barrett-group.mcgill.ca*
128. Drechsler M: **TEM of bovine photoreceptor cells.** *http://www.mardre.com/homepage/mic/tem/samples/bio/ros/ret1.html*
129. Schmitz KS: *An Introduction to Dynamic Light Scattering by Macromolecules*. San Diego, CA Academic Press; 1990.
130. Pecora BJBaR: *Dynamic light scattering : with applications to chemistry, biology, and physics*. New York: Wiley; 1976.
131. Koppel DE: **Analysis of macromolecular polydispersity in intensity correlation spectroscopy. Method of cumulants.** *Journal of Chemical Physics*,(1972), **57**:4814.
132. Provencher SW, Hendrix J, De Maeyer L, Paulussen N: **Direct determination of molecular weight distributions of polystyrene in cyclohexane with photon correlation spectroscopy.** *Journal of Chemical Physics*,(1978), **69**:4273.
133. Provencher SW: **Inverse problems in polymer characterization: direct analysis of polydispersity with photon correlation spectroscopy.** *Makromolekulare Chemie*,(1979), **180**:201.
134. Chu B: *Laser Light scattering: Basic Principles and Practice* edn 2nd Ed.: Academic Press; 1992.
135. Huck WTS, Yan L, Stroock A, Haag R, Whitesides GM: **Patterned Polymer Multilayers as Etch Resists.** *Langmuir*,(1999), **15**:6862.
136. Blomberg S, Ostberg S, Harth E, Bosman AW, Van Horn B, Hawker CJ: **Production of crosslinked, hollow nanoparticles by surface-initiated living free-radical polymerization.** *Journal of Polymer Science, Part A: Polymer Chemistry*,(2002), **40**:1309.
137. Luo Y, Gu H: **Nanoencapsulation via interfacially confined reversible addition fragmentation transfer (RAFT) miniemulsion polymerization.** *Polymer*,(2007), **48**:3262.
138. Wang M, Braun H-G, Meyer E: **Patterning of Polymeric/Inorganic Nanocomposite and Nanoparticle Layers.** *Chemistry of Materials*,(2002), **14**:4812.
139. Wang SX, Wang MT, Lei Y, Zhang LD: **Mesoscopic self-assembling morphology of polymer based on emulsification.** *Materials Research Bulletin*,(2000), **35**:1625.
140. Zhu M-Q, Wei L-H, Du F-S, Li Z-C, Li F-M, Li M, Jiang L: **A unique synthesis of a well-defined block copolymer having alternating segments constituted by maleic anhydride and styrene and the self-assembly aggregating behavior thereof.** *Chemical Communications*,(2001):365.
141. Chen Y, Ji X, Jiang S, Sun Q, Jiang B: **Synthesis and characterization of CdS nanocrystals in poly(styrene-co-maleic anhydride) copolymer.** *Colloid and Polymer Science*,(2003), **281**:386.

[142] Harrisson S, Wooley KL: **Shell-crosslinked nanostructures from amphiphilic AB and ABA block copolymers of styrene-alt-(maleic anhydride) and styrene: polymerization, assembly and stabilization in one pot.** *Chemical Communications*,(2005):3259.

[143] Henry SM, El-Sayed MEH, Pirie CM, Hoffman AS, Stayton PS: **pH-Responsive Poly(styrene-alt-maleic anhydride) Alkylamide Copolymers for Intracellular Drug Delivery.** *Biomacromolecules*,(2006), **7**:2407.

[144] Hector HH, Ruegger UP: **Surface sizing [of paper] with styrene-maleic anhydride copolymers.** *Wochenblatt fuer Papierfabrikation*,(1973), **101**:781.

[145] Jin G, Shen Y: **Preparation and application of copolymer of styrene and maleic acid monoester as surface sizing agent.** *Zhongguo Zaozhi*,(2004), **23**:5.

[146] Fischer K: **New sizing agents on a SMA basis.** *Wochenblatt fuer Papierfabrikation*,(1999), **127**:586.

[147] Sajbel J: **Surface sizing additives.** *Sizing of Paper (3rd Edition)*,(2005):287.

[148] Sithole B, Ambayec B: **Identification and determination of surface sizing agents on sized papers.** *Pulp & Paper Canada*,(2000), **101**:53.

[149] De Rosa C: **Geometrical analysis and conformational and packing energy calculations on an isotactic alternating copolymer between carbon monoxide and styrene.** *Macromolecules*,(1997), **30**:5494.

[150] Drache M, Weber T, Schmidt-Naake G: **Conformation analysis of poly(styrene-alt-maleic anhydride) in solvents.** *Angewandte Makromolekulare Chemie*,(1999), **273**:69.

[151] Hobza P, Kabelac M, Sponer J, Mejzlik P, Vondrasek J: **Performance of empirical potentials (AMBER, CFF95, CVFF, CHARMM, OPLS, POLTEV), semiempirical quantum chemical methods (AM1, MNDO / M, PM3), and ab initio Hartree-Fock method for interaction of DNA bases: comparison with nonempirical beyond Hartree-Fock results.** *Journal of Computational Chemistry*,(1997), **18**:1136.

[152] Vetcher AA, Lushnikov AY, Navarra-Madsen J, Scharein RG, Lyubchenko YL, Darcy IK, Levene SD: **DNA Topology and Geometry in Flp and Cre Recombination.** *Journal of Molecular Biology*,(2006), **357**:1089.

[153] Reddy SY, Leclerc F, Karplus M: **DNA polymorphism: A comparison of force fields for nucleic acids.** *Biophysical Journal*,(2003), **84**:1421.

[154] Malardier-Jugroot C, van de Ven TGM, Cosgrove T, Richardson RM, Whitehead MA: **Novel Self-Assembly of Amphiphilic Copolymers into Nanotubes: Characterization by Small-Angle Neutron Scattering.** *Langmuir*,(2005), **21**:10179.

[155] Malardier-Jugroot C, van de Ven TGM, Whitehead MA: **Study of the water conformation around hydrophilic and hydrophobic parts of styrene-maleic anhydride.** *Theochem*,(2004), **679**:171.

[156] Garrett ER, Guile RL: **Potentiometric titrations of a polydicarboxylic acid: maleic acid-styrene copolymer.** *Journal of the American Chemical Society*,(1951), **73**:4533.

[157] Garnier G, Duskova-Smrckova M, Vyhnalkova R, van de Ven TGM, Revol J-F: **Association in Solution and Adsorption at an Air-Water Interface of Alternating Copolymers of Maleic Anhydride and Styrene.** *Langmuir*,(2000), **16**:3757.

[158] Anders E, Koch R, Freunscht P: **Optimization and application of lithium parameters for PM3.** *Journal of Computational Chemistry*,(1993), **14**:1301.

[159] Claracq J, Santos SFCR, Duhamel J, Dumousseaux C, Corpart J-M: **Rigid Interior of Styrene-Maleic Anhydride Copolymer Aggregates Probed by Fluorescence Spectroscopy.** *Langmuir*,(2002), **18**:3829.

[160] Trifuoggi M, De Rosa C, Auriemma F, Corradini P, Bruckner S: **Crystalline Structure of Some Alternate Copolymers between Carbon Monoxide and Styrene Derivatives.** *Macromolecules*,(1994), **27**:3553.

[161] Waters ML: **Aromatic interactions in model systems.** *Current Opinion in Chemical Biology*,(2002), **6**:736.

[162] Sponer J, Hobza P: **MP2 and CCSD(T) study on hydrogen bonding, aromatic stacking and nonaromatic stacking.** *Chemical Physics Letters*,(1997), **267**:263.

[163] Sponer J, Leszczynski J, Hobza P: **Structures and Energies of Hydrogen-Bonded DNA Base Pairs. A Nonempirical Study with Inclusion of Electron Correlation.** *Journal of Physical Chemistry*,(1996), **100**:1965.

[164] Sun S, Bernstein ER: **Aromatic van der Waals Clusters: Structure and Nonrigidity.** *Journal of Physical Chemistry*,(1996), **100**:13348.

[165] Ohno N, Nitta K, Makino S, Sugai S: **Conformational transition of the copolymer of maleic acid and styrene in aqueous solution.** *Journal of Polymer Science, Polymer Physics Edition*,(1973), **11**:413.

[166] Adams DJ, Butler MF, Weaver AC: **Effect of Block Length, Polydispersity, and Salt Concentration on PEO-PDEAMA Block Copolymer Structures in Dilute Solution.** *Langmuir*,(2006), **22**:4534.

167. Giacomelli C, Schmidt V, Borsali R: **Nanocontainers Formed by Self-Assembly of Poly(ethylene oxide)-b-poly(glycerol monomethacrylate)-Drug Conjugates.** *Macromolecules*,(2007), **40**:2148.

168. Reynhout IC, Cornelissen JJLM, Nolte RJM: **Self-Assembled Architectures from Biohybrid Triblock Copolymers.** *Journal of the American Chemical Society*,(2007), **129**:2327.

169. Sachl R, Uchman M, Matejicek P, Prochazka K, Stepanek M, Spirkova M: **Preparation and Characterization of Self-Assembled Nanoparticles Formed by Poly(ethylene oxide)-block-poly(e-caprolactone) Copolymers with Long Poly(e-caprolactone) Blocks in Aqueous Solutions.** *Langmuir*,(2007), **23**:3395.

170. Terreau O, Bartels C, Eisenberg A: **Effect of Poly(acrylic acid) Block Length Distribution on Polystyrene-b-poly(acrylic acid) Block Copolymer Aggregates in Solution. 2. A Partial Phase Diagram.** *Langmuir*,(2004), **20**:637.

171. Zhang J, Yu Z, Wan X, Chen X, Zhou Q: **Synthesis and characterization of helix-coil diblock copolymers with controlled supramolecular architectures in aqueous solution.** *Macromolecular Rapid Communications*,(2005), **26**:1241.

172. Zhang Y, Zhang Z, Wang Q, Xu C, Xie Z: **Multi-morphological complex aggregates formed from amphiphilic poly(ethylene oxide)-block-polydimethylsiloxane-block-poly(ethylene oxide) triblock copolymers.** *Macromolecular Rapid Communications*,(2006), **27**:1476.

173. Zhu R, Wang Y, He W: **Multiple morphological micelles formed from the self-assembly of poly(styrene)-b-poly(4-vinylpyridine) containing cobalt dodecyl benzene sulfonate.** *European Polymer Journal*,(2005), **41**:2088.

174. Wu D-C, Hong C-Y, Pan C-Y, He W-D: **Study on controlled radical alternating copolymerization of styrene with maleic anhydride under UV irradiation.** *Polymer International*,(2003), **52**:98.

175. Ha NTH, Fujimori K, Craven IE: **Relation between the alternating monomer unit sequence and the cis and trans linkage configurations at the cyclic maleic anhydride units in the copolymers of styrene and maleic anhydride prepared in carbon tetrachloride.** *Macromolecular Chemistry and Physics*,(1997), **198**:3507.

176. Rungaphinya W, Fujimori K, Craven IE, Tucker DJ: **Linkage configurations at the cyclic maleic anhydride units and sequence distribution in copolymers of p-chlorostyrene with maleic anhydride.** *Polymer International*,(1997), **42**:17.

177. Brown PG, Fujimori K, Tucker DJ: **Quantitative determination of the content of cis/trans configurations of maleic anhydride units in p-methoxystyrene-maleic anhydride copolymers by carbon-13 NMR DEPT experiments.** *Polymer Bulletin*,(1992), **27**:543.

178. Anslyn EV, Dougherty DA: *Modern Physical Organic Chemistry*. Sausalito, California: University Science Books; 2006.

179. Eliad L, Salitra G, Soffer A, Aurbach D: **Ion Sieving Effects in the Electrical Double Layer of Porous Carbon Electrodes: Estimating Effective Ion Size in Electrolytic Solutions.** *Journal of Physical Chemistry B*,(2001), **105**:6880.

180. Oh SG, Shah DO: **Effect of counterions on the interfacial tension and emulsion droplet size in the oil/water/dodecyl sulfate system.** *Journal of Physical Chemistry*,(1993), **97**:284.

181. Gilanyi T: **Fluctuating micelles: a theory of surfactant aggregation. 2. Ionic surfactants.** *Colloids and Surfaces, A: Physicochemical and Engineering Aspects*,(1995), **104**:119.

182. Gilanyi T, Varga I, Meszaros R: **Specific counterion effect on the adsorption of alkali decyl sulfate surfactants at air/solution interface.** *Physical Chemistry Chemical Physics*,(2004), **6**:4338.

183. Nguyen TT, Gopal A, Lee KYC, Witten TA: **Surface charge relaxation and the pearling instability of charged surfactant tubes.** *Physical Review E: Statistical, Nonlinear, and Soft Matter Physics*,(2005), **72**:051930/1.

184. Laredo T, Leitch J, Chen M, Burgess IJ, Dutcher JR, Lipkowski J: **Measurement of the Charge Number Per Adsorbed Molecule and Packing Densities of Self-Assembled Long-Chain Monolayers of Thiols.** *Langmuir*,(2007), **23**:6205.

185. Niklewski A, Azzam W, Strunskus T, Fischer RA, Woell C: **Fabrication of Self-Assembled Monolayers Exhibiting a Thiol-Terminated Surface.** *Langmuir*,(2004), **20**:8620.

186. Houston JE, Kim HI: **Adhesion, Friction, and Mechanical Properties of Functionalized Alkanethiol Self-Assembled Monolayers.** *Accounts of Chemical Research*,(2002), **35**:547.

187. Schlenoff JB, Li M, Ly H: **Stability and Self-Exchange in Alkanethiol Monolayers.** *Journal of the American Chemical Society*,(1995), **117**:12528.

188. Bain CD, Whitesides GM: **Modeling organic surfaces with self-assembled monolayers.** *Angewandte Chemie*,(1989), **101**:522.

189. Bucher J-P, Santesson L, Kern K: **Thermal Healing of Self-Assembled Organic Monolayers: Hexane- and Octadecanethiol on Au(111) and Ag(111).** *Langmuir*,(1994), **10**:979.

190. Slim M, Durisic N, Grutter P, Sleiman Hanadi F: **DNA-protein noncovalent cross-linking: ruthenium dipyridophenazine biotin complex for the assembly of proteins and gold nanoparticles on DNA templates.** *Chembiochem : a European journal of chemical biology*,(2007), **8**:804.

191. Aldaye FA, Sleiman HF: **Dynamic DNA Templates for Discrete Gold Nanoparticle Assemblies: Control of Geometry, Modularity, Write/Erase and Structural Switching.** *Journal of the American Chemical Society,*(2007), **129**:4130.

192. Aldaye FA, Sleiman HF: **Sequential self-assembly of a DNA hexagon as a template for the organization of gold nanoparticles.** *Angewandte Chemie, International Edition,*(2006), **45**:2204.

193. Lewis PA, Ahmed H, Sato T: **Silicon nanopillars formed with gold colloidal particle masking.** *Journal of Vacuum Science & Technology, B: Microelectronics and Nanometer Structures,*(1998), **16**:2938.

194. Ovchinnikov V, Malinin A, Novikov S, Tuovinen C: **Silicon nanopillars formed by reactive ion etching using a self-organized gold mask.** *Physica Scripta, T,*(1999), **T79**:263.

195. Parker AJ, Childs PA, Palmer RE: **Design and fabrication of colloid-based vertical nanoscale devices.** *Microelectronic Engineering,*(2002), **61-62**:681.

196. The moles of polymer are calculated assuming the polymer has a molecular weight of 12,000 Da

197. Bulaj G, Kortemme T, Goldenberg DP: **Ionization-Reactivity Relationships for Cysteine Thiols in Polypeptides.** *Biochemistry,*(1998), **37**:8965.

198. Ellman GL: **Tissue sulfhydryl groups.** *Archives of Biochemistry and Biophysics,*(1959), **82**:70.

199. Mock JJ, Barbic M, Smith DR, Schultz DA, Schultz S: **Shape effects in plasmon resonance of individual colloidal silver nanoparticles.** *Journal of Chemical Physics,*(2002), **116**:6755.

200. Kreibig U, Vollmer M: *Optical Properties of Metal Clusters.* Berlin: Springer; 1995.

201. Bohren CF, Huffman DR: **Absorption and Scattering of Light by Small Particles.** Edited by: Wiley; 1983.

202. Brust M, Walker M, Bethell D, Schiffrin DJ, Whyman R: **Synthesis of thiol-derivatized gold nanoparticles in a two-phase liquid-liquid system.** *Journal of the Chemical Society, Chemical Communications,*(1994):801.

203. Gordon JG, II, Swalen JD: **The effect of thin organic films on the surface plasma resonance on gold.** *Optics Communications,*(1977), **22**:374.

204. Halder S, Boettger U, Schneller T, Waser R, Baldus O, Jacobs P, Wehner M: **Laser annealing of BST thin films with reduced cracking at an elevated temperature.** *Materials Science & Engineering, B: Solid-State Materials for Advanced Technology,*(2006), **133**:235.

205. Liu H-Y, Cao K, Huang Y, Yao Z, Li B-G, Hu G-H: **Kinetics and simulation of the imidization of poly(styrene-co-maleic anhydride) with amines.** *Journal of Applied Polymer Science,*(2006), **100**:2744.

206. Gietzelt T: **Dependence of the contact angle on the molecular structure of poly(propene-alt-N-maleimide) and poly(styrene-alt-N-maleimide) copolymers.** *Journal of Materials Science,*(2001), **36**:2073.

207. Whitehead MA, Malardier-Jugroot C, van de Ven TGM, Lazzara TD: **Method for fabricating intrinsically conducting polymer nanorods.** US Patent 2005, 2005-CA833, 2005118688.

208. Spivey AC, Charbonneau P, Fekner T, Hochmuth DH, Maddaford A, Malardier-Jugroot C, Redgrave AJ, Whitehead MA: **Energy barriers to rotation in axially chiral analogues of 4-(dimethylamino)pyridine.** *The Journal of organic chemistry,*(2001), **66**:7394.

209. Villamagna F, Whitehead MA: **Comparison of complete conformational searching and the energy-optimized tree branch method in molecular mechanics calculations.** *Journal of the Chemical Society, Faraday Transactions,*(1994), **90**:47.

210. Malardier-Jugroot C, van de Ven TGM, Whitehead MA: **Linear conformation of poly(styrene-alt-maleic anhydride) capable of self-assembly: a result of chain stiffening by internal hydrogen bonds.** *J Phys Chem B Condens Matter Mater Surf Interfaces Biophys FIELD Full Journal Title:The journal of physical chemistry. B, Condensed matter, materials, surfaces, interfaces & biophysical,*(2005), **109**:7022.

211. Nguyen THH, Fujimori K, Tucker DJ: **Determination of monomer unit sequence distribution in the copolymers of styrene and maleic anhydride prepared in carbon tetrachloride and in N,N-dimethylformamide.** *Tap Chi Hoa Hoc,*(1997), **35**:89.

212. Brintzinger HH, Fischer D, Muelhaupt R, Rieger B, Waymouth RM: **Stereospecific olefin polymerization with chiral metallocene catalysts.** *Angewandte Chemie, International Edition* (1995), **34**:1143.

213. Cummins HZ, Carlson FD, Herbert TJ, Woods G: **Translational and rotational diffusion constants of tobacco mosaic virus from Rayleigh linewidths.** *Biophysical journal,*(1969), **9**:518.

214. Schumacher GA: **Light scattering studies on electrostatically stabilized colloidal particles.** Montreal: McGill University: 1990.

215. Xu H, Hong R, Wang X, Arvizo R, You C, Samanta B, Patra D, Tuominen MT, Rotello VM: **Controlled formation of patterned gold films via site-selective deposition of nanoparticles onto polymer-templated surfaces.** *Advanced Materials,*(2007), **19**:1383.

[216] Viallet B, Ressier L, Grisolia J, Peyrade JP, Podgajny R, Amiens C, van den Boogaart MAF, Brugger J: **Selective deposition of gold nanoparticles using Van der Waals interactions.** *Physica Status Solidi C: Current Topics in Solid State Physics*,(2007), **4**:276.

[217] Takahashi H, Niidome Y, Hisanabe H, Kuroiwa K, Kimizuka N, Yamada S: **Spatio-selective surface modification of glass assisted by laser-induced deposition of gold nanoparticles.** *Thin Solid Films*,(2006), **515**:1618.

[218] Lenggoro IW, Lee HM, Okuyama K: **Nanoparticle assembly on patterned "plus/minus" surfaces from electrospray of colloidal dispersion.** *Journal of Colloid and Interface Science*,(2006), **303**:124.

[219] Sheu J-T, Wu C-H, Chao T-S: **Selective deposition of gold particles on dip-pen nanolithography patterns on silicon dioxide surfaces.** *Japanese Journal of Applied Physics, Part 1: Regular Papers, Brief Communications & Review Papers*,(2006), **45**:3693.

[220] Akamatsu K, Terahata H, Hasegawa J, Nawafune H: **Site-selective deposition of gold on glass substrates using monolayer-protected gold nanoparticles.** *Hyomen Gijutsu*,(2005), **56**:427.

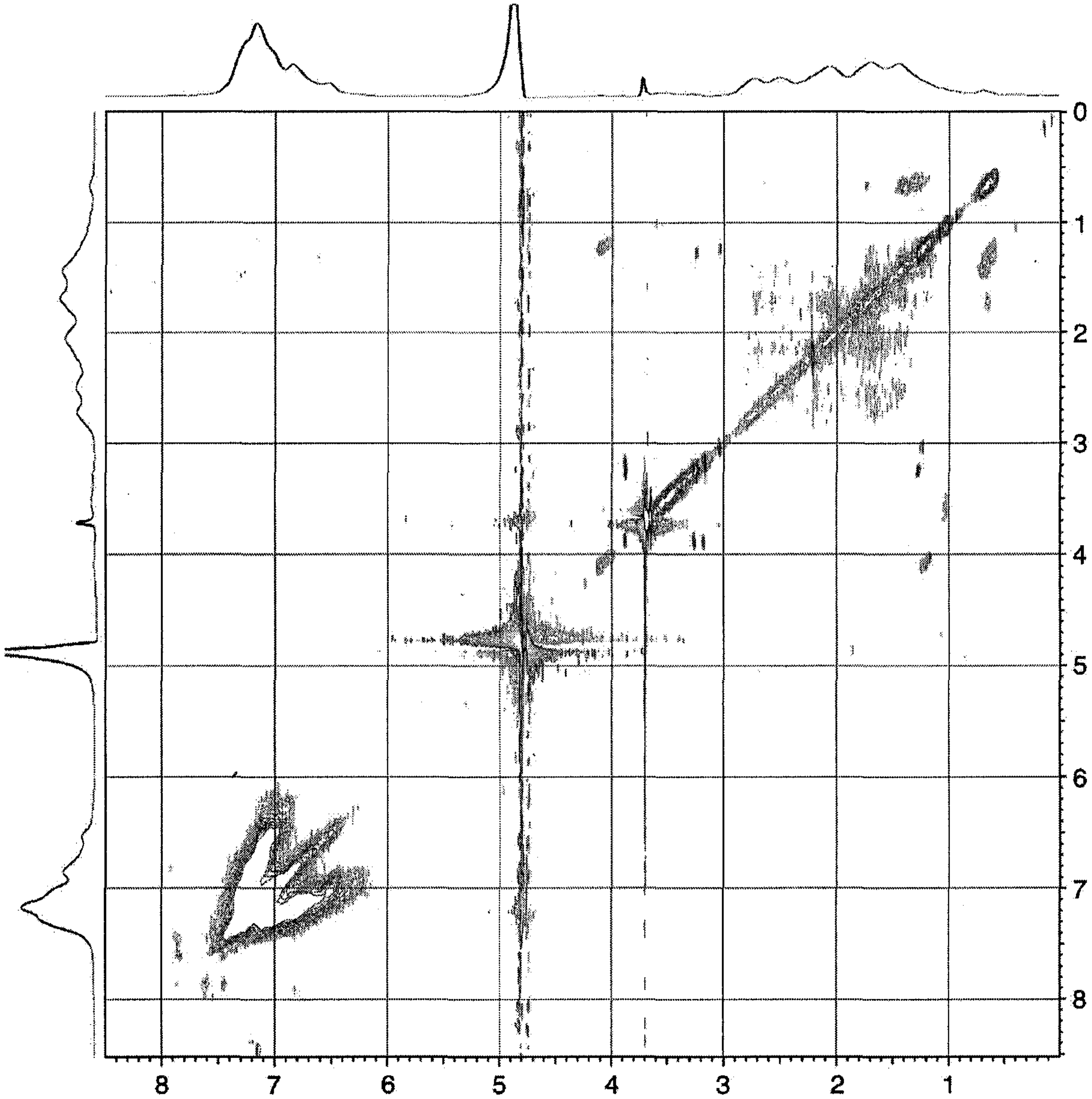

Figure I: 2D $^1$H NMR of SMA 12,000 Da in $D_2O$, concentration of 0.1% wt. and pH 7.5.

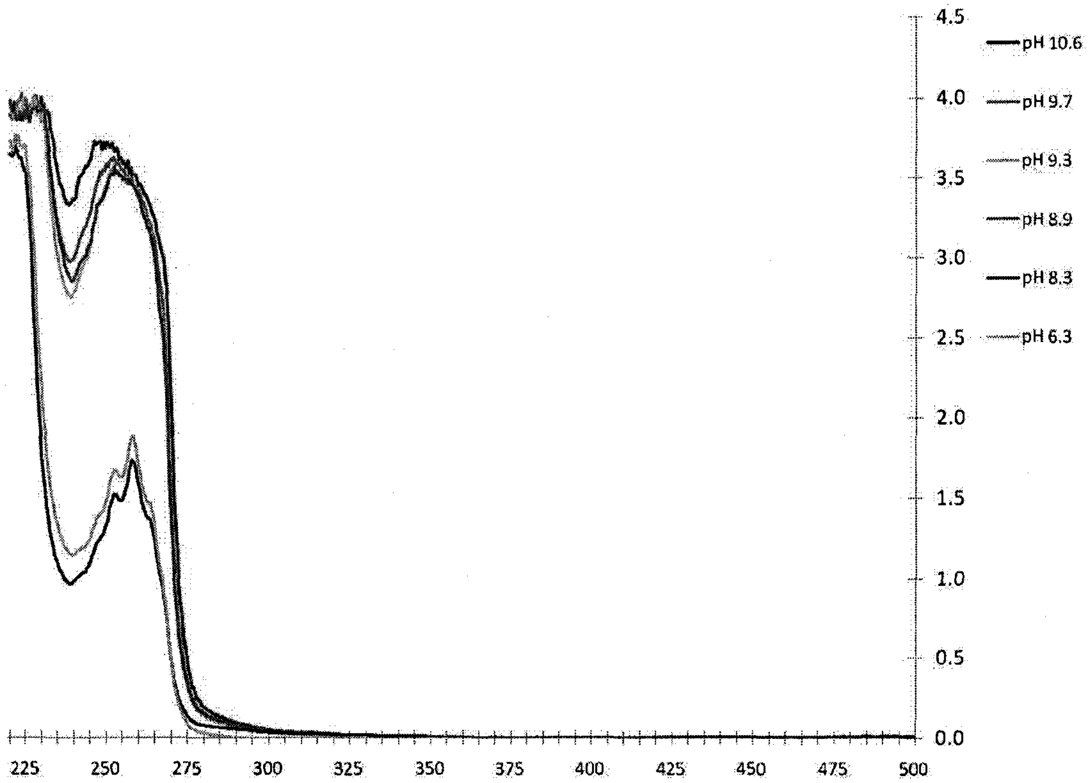

Figure 2: UV-Visible spectra of aqueous solution of 0.1% SMA, 12,000 Da $M_w$, taken at different pH values during dialysis. The dialysis procedure is explained in Chapter III, where the initial basic solution is lowered in pH by dialysis against deionized water.

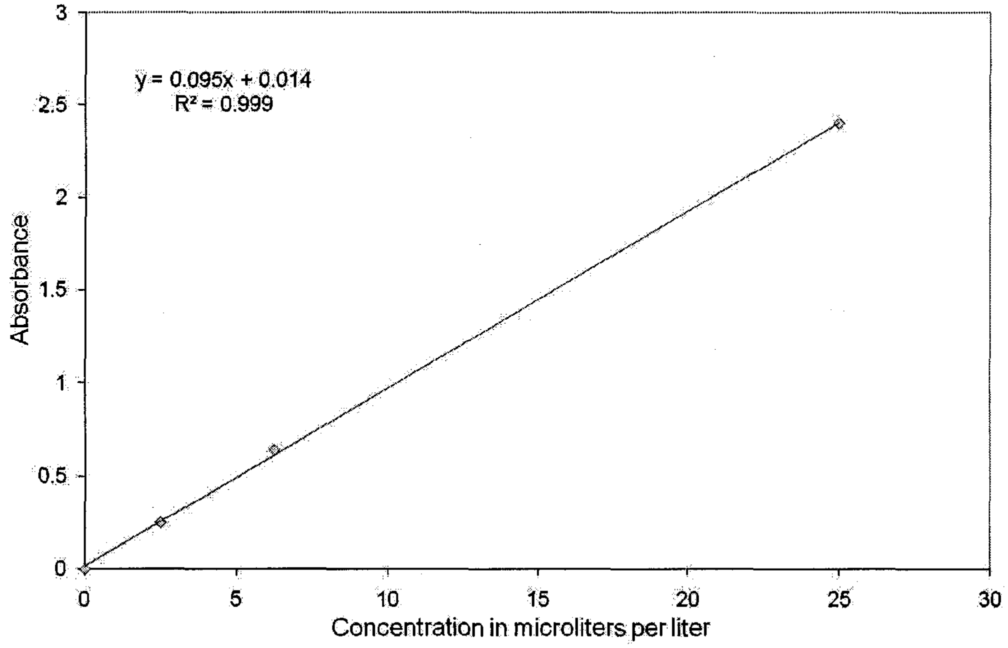

Figure 3: Calibration curve for the concentration of pyrrole dissolved in deionized water. The absorbance was taken in the highest absorbance region from 200-220 nm. The initial solution was prepared by pipetting 25 μL of pyrrole in 1 L volumetric flask and then diluting.

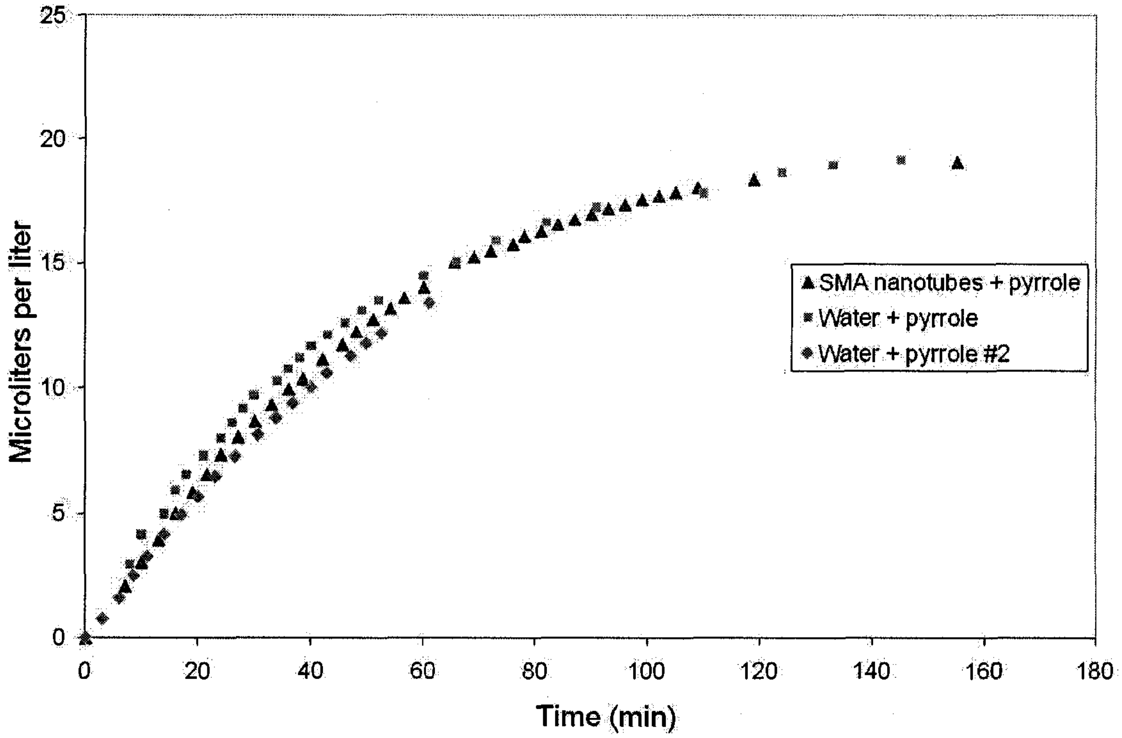

Figure 4: Pyrrole release experiments with water or SMA nanotube solution and 25 microliters of pyrrole. These were carried out to see if pyrrole loaded SMA nanotubes had a slower release of pyrrole. Pyrrole concentration in the water surrounding the dialysis bag was tracked and the calibration curve in Figure 3 was used to calculate the concentration. 0.05g of SMA polymer, 12,000 Da $M_w$, was dissolved in water, with 25 µL of pyrrole, for a total volume of 25ml inside dialysis bag. Three experiments were carried out, two control experiments with pyrrole in water and one with SMA nanotubes and pyrrole. The results are not conclusive because the diffusion was limited by the membrane diffusion, not for the diffusion of pyrrole outside the nanotubes.